



저작자표시-비영리-변경금지 2.0 대한민국

이용자는 아래의 조건을 따르는 경우에 한하여 자유롭게

- 이 저작물을 복제, 배포, 전송, 전시, 공연 및 방송할 수 있습니다.

다음과 같은 조건을 따라야 합니다:



저작자표시. 귀하는 원저작자를 표시하여야 합니다.



비영리. 귀하는 이 저작물을 영리 목적으로 이용할 수 없습니다.



변경금지. 귀하는 이 저작물을 개작, 변형 또는 가공할 수 없습니다.

- 귀하는, 이 저작물의 재이용이나 배포의 경우, 이 저작물에 적용된 이용허락조건을 명확하게 나타내어야 합니다.
- 저작권자로부터 별도의 허가를 받으면 이러한 조건들은 적용되지 않습니다.

저작권법에 따른 이용자의 권리는 위의 내용에 의하여 영향을 받지 않습니다.

이것은 [이용허락규약\(Legal Code\)](#)을 이해하기 쉽게 요약한 것입니다.

[Disclaimer](#)

A THESIS
FOR THE DEGREE OF DOCTOR OF PHILOSOPHY

Characterization of bioactive components from
***Ishige okamurae* and their biological activity**

Yun Fei Jiang

DEPARTMENT OF MARINE LIFE SCIENCES

GRADUATE SCHOOL

JEJU NATIONAL UNIVERSITY

June, 2020

**Characterization of bioactive components from
Ishige okamurae and their biological activity**

Yun Fei Jiang

(Supervised by Professor You-Jin Jeon)

A thesis submitted in partial fulfillment of the requirement
for the degree of DOCTOR OF PHILOSOPHY
2020. 06.

This thesis has been examined and approved by

이 승 현

Thesis director, Seungheon Lee, professor of Marine Life Science

BoMi Ryu

BoMi Ryu, Research Professor of Marine Life Science

김 영 상

Young-Sang Kim, Research Professor of Marine Science Institute

Jae-Young Oh

Jae-Young Oh, Research Professor of Marine Life Science

You-Jin Jeon

You-Jin Jeon, Professor of Marine Life Science

Date:2020.06

DEPARTMENT OF MARINE LIFE SCIENCES

GRADUATE SCHOOL

JEJU NATIONAL UNIVERSITY

CONTENTS

SUMMARY	i
LIST OF TABLES	iii
LIST OF FIGURES	iv
Background	1
Part I. Isolation and identification of polyphenols from <i>Ishige okamurae</i> and their uses	3
Section 1: Isolation and identification of polyphenols from <i>Ishige okamurae</i>	2
Abstract	3
1. Materials and methods	4
1.1. General methods	4
1.2. Materials and chemicals	4
1.3. Extraction and fractionation of <i>I. okamurae</i>	4
2. Result and Discussion	5
4. Conclusion	7
Section 2: Validation of DPFC by a HPLC method for the quality control of <i>Ishige okamurae</i>	27
Abstract	28
1. Introduction.....	29
2. Materials and methods	30
2.1. Chemicals	30
2.2. Analytical instruments and operation conditions.....	30
2.3. Sample preparation for HPLC analysis	30
2.4. Method validation.....	30
2.5. Statistical analysis.....	31
3. Results and discussion	32
4. Conclusion	35
Section 3: Anti-melanogenesis activity of Ishophloroglucin A (IPA) from <i>Ishige okamurae</i> in α-MSH-induced melanoma cells and zebrafish	37
Abstract.....	38

1. Introduction.....	39
2. Materials and methods	40
2.1. Chemical and reagents.....	40
2.2. Preparation of <i>Ishige okamurae</i> extract (IOE) and IPA.....	40
2.3. Molecular docking preparation.....	40
2.4. Cell assay.....	41
2.4.1. Determination of cell viability.....	41
2.4.2. Determination of melanin contents.....	41
2.4.3. Cellular Tyrosinase activity	42
2.5. In vivo assay	42
2.5.1. Origin and maintenance of parental zebrafish.....	42
2.5.2. Zebrafish pigmentation evaluating	43
2.6. Western blot analysis	43
2.7. Statistical Analysis.....	44
3. Results.....	45
3.1. Molecular Docking analysis of compounds IPA and DPHC	45
3.2. The effects of α -MSH, Arbutin, IOE and IPA on cell viability and melanin synthesis in B16F10 cells.....	45
3.3. Inhibitory effect of IOE and IPA on Tyrosinase activity and melanin synthesis in α -MSH-induced B16F10 cells	45
3.4. Western blotting analysis.....	49
3.4.1. IPA inhibits melanogenesis through downregulating the expressions of MITF, tyrosinase, TRP1, and TRP2 in α -MSH stimulated B16F10 cells.....	49
3.4.2. IPA inhibits melanogenesis through downregulating CREB-MITF pathway in α -MSH stimulated B16F10 cells.....	49
4. Discussion.....	54
5. Conclusion	55
Part II. Isolation and identification of α/β-adenosine from <i>I. okamurae</i> and its anti-angiogenesis activity.....	56
Abstract.....	57
1. Introduction.....	58
2. Materials and methods	59

2.1. Chemicals and reagents	59
2.2. Plant material.....	59
2.3. Extraction and isolation.....	59
2.3.1. Identification of α -adenosine and β -adenosine.....	60
2.4. Cell culture	66
2.4.1. Cell viability	66
2.4.2. Culture Inserts for the Cell Migration Assay.....	66
2.4.3. Tube formation assay.....	66
2.4.4. Western blot analysis	67
2.4.5. Treatments of PM in zebrafish transgenic (flk: EGFP) embryos	67
2.4.6. Treatments of α/β -adenosine and β -adenosine in zebrafish transgenic (flk: EGFP) embryos and vasodilation assay	68
2.5. Statistical Analysis.....	68
3. Results and discussion	69
3.1. Particulate matter (PM) induced angiogenesis in human endothelial cell line EA.hy926.....	69
3.2. Cell viability of the mixture of α/β -adenosine and β -adenosine on vascular endothelial cell line EA.hy926.....	73
3.3. Inhibitory effect of mixture α/β -adenosine and β -adenosine on PM induced cell migration.....	73
3.4. Effects of the mixture α/β -adenosine and β -adenosine on capillary formation in PM induced EA.hy926 Cells in Matrigel	77
3.5. Effects of the mixture α/β -adenosine on PI3K/Akt/eNOS Signal Pathway	77
3.6. Particulate matter-induced eyes vessel dilation in zebrafish embryo.....	77
3.7. Effects of the mixture α/β -adenosine and β -adenosine on PM-Treated Zebrafish Embryo	83
4. Conclusion	83
Part III. Isolation of fucoidan from <i>Ishige okamurae</i> and its anti-inflammatory activity.....	86
Abstract.....	87
1. Introduction.....	88
2. Materials and methods	88

2.1. Materials	88
2.2. Extraction of polysaccharides.....	89
2.3. Separation of the IOP by anion-exchange chromatography	89
2.4. FTIR characterization and monosaccharide analysis of subfraction from IOP.....	90
2.5. NMR analysis	90
2.6. Cell culture	90
2.7. Determination of the PGE ₂ expression and pro-inflammatory cytokines expression	90
2.8. Western bolt analysis	91
2.9. In vivo zebrafish experiment	91
2.9.1 Evaluation of the inhibition of NO production, and protective effects against cell death in LPS induced zebrafish embryo model	91
2.10. Statistical analysis.....	91
3. Results and discussion	92
3.1. Extraction, separation and monosaccharide analysis of IOP fractions.....	92
3.2. FT-IR spectroscopic and ¹ H NMR analysis of structural features of the polysaccharides.....	94
3.4. Cytotoxicity of each fraction from IOP in RAW 264.7 macrophages.....	98
3.5. The anti-inflammatory effect of F1-F4 fractions from IOP on the inhibition of NO in LPS stimulated RAW 264.7 macrophages.....	98
3.6. Pro-inflammatory cytokines production against F4 in LPS-stimulated RAW 264.7 macrophages	101
3.7. Effects of F4 on the mediation of iNOS, COX-2 in LPS-stimulated RAW 264.7 macrophages	101
3.8. In vivo evaluation of anti-inflammatory potential of F4 using zebrafish embryos .	105
4. Conclusion	105
References.....	106

SUMMARY

Seaweeds are one of the crucial marine living renewable resources as they are able to produce a great variety of secondary metabolites characterized by a broad spectrum of biological activities. *Ishige okamurae* (*I. okamurae*) is a member of the family *Ishige* as an edible brown alga, have attracted attention as various natural compounds with their biological activities.

In this study, new separation method was suggested to increase efficiency and improve the isolation performance using Pure C-850 FlashPrep system. In this study, Pure C-850 FlashPrep system was suggested to increase efficiency and improve the isolation of natural compounds from *I. okamurae*. A novel series of polyphenols, named as Ishophloroglucin; Ishophloroglucin A (IPA), Ishophloroglucin B (IPB), Ishophloroglucin C (IPC), and Ishophloroglucin D (IPD), and another two known compounds which is α/β -adenosine and Diphlorethohydroxycarmalol (DPHC) were isolated and identified. Their structure was elucidated by 1D- and 2D- Nuclear magnetic resonance (NMR), including ^1H , ^{13}C , HMBC, and COSY, as well as liquid chromatography-tandem mass spectrometry (LC-MS/MS).

As folk medicine, *I. okamurae* with various biological effects grows abundantly on the shores of Japan, north of China, and Korea where it is consumed as a part of daily diet. Appropriate quality control operations shall be employed to ensure that food having uniformed nutrients is suitable for human consumption. This study was conducted to establish an HPLC analysis method for determination of marker compounds as part of materials standardization for development of health functional food materials from *I. okamurae*. DPHC was selected as a marker compound due to it is more stable compared to IPA on the thermal stability analysis. The method was validated by system suitability, specificity, linearity, limits of detection (LOD), limits of quantification (LOQ), precision, and accuracy. The method showed high linearity of the calibration curve with a coefficient of correlation (R^2) of 0.9999, and LOD and LOQ was 0.144 $\mu\text{g/mL}$ and 0.435 $\mu\text{g/mL}$, respectively. Relative standard deviation values from precision was less than 0.622 %. Recovery rates of DPHC was 106.35 - 107.82 % within $100 \pm 20\%$. An optimized method for extraction of DPHC in *I. okamurae* was established through diverse extraction conditions, and the validation indicated that the method is accurate and sensitive for the determination of marker compounds in *I. okamurae* to develop a health functional food material.

Polyphenols, a group of phloroglucinol (1,3,5-trihydroxybenzene), are the dominant polyphenolic secondary metabolites found in marine brown algae. IPA as a dominant polyphenol in *I. okamurae*, was investigated their anti-melanogenesis effects. Through the comparative molecular docking analysis of IPA to tyrosinase (3NM8), IPA was further investigated their inhibitory effect against tyrosinase activity and melanin formation that causes an increase anti-melanogenesis effect in both murine melanoma cells *in-vitro* model and zebrafish *in-vivo* model.

The α/β -adenosine (1:1 ratio) was firstly identified from *I. okamurae*, which is known as a naturally occurring substance that relaxes and dilates blood vessels in angiogenesis. To characterize the vasodilation effect of α/β -adenosine in endothelial dysfunction of angiogenesis induced by Particulate matter (PM) exposure, commercial isomer β -adenosine was also investigated as well in human endothelial cell line EA.hy926 *in-vitro* model and transgenic zebrafish *in-vivo* model.

In the last study, fucoidan is an interesting group of bioactive sulfated polysaccharides in brown seaweeds. The current study highlights the enrichment and extraction of fucoidan from *I. okamurae* through enzyme-assistant extraction using Celluclast enzyme. The structural characterization of fucoidan was performed using FTIR and NMR spectroscopy, their monosaccharide compositions was analyzed by HPAE-PAD, the molecular weight distribution was performed by agarose gel electrophoresis and the sulfate content was analyzed as well. The purified fucoidan and its anti-inflammatory activity was investigated *in-vitro* and *in-vivo*.

In summary, this research suggested various natural compounds from *I. okamurae* isolated by a flash prepare system and their potential uses as marker compounds or pharmaceutical and nutraceutical agents. Therefore, the purpose of this research is to discuss the potential health benefits of *I. okamurae* to be used as a functional material in industries such as functional foods, nutraceuticals, and cosmeceuticals to utilize this precious natural resource for future generations.

LIST OF TABLES

Table 1. ^1H and ^{13}C NMR analysis data of DPHC (compound 1);

Table 2. ^1H , ^{13}C and HMQC Data of Ishophloroglucin A (compound 2)

Table 3. ^1H and ^{13}C NMR analysis data of Ishophloroglucin B (compound 3)

Table 4. ^1H and ^{13}C NMR analysis data of Ishophloroglucin C (compound 4)

Table 5. ^1H and ^{13}C NMR analysis data of Ishophloroglucin D (compound 5)

Table 6. Parameters value of system suitability for validation method.

Table 7. Linearity list of the developed high-performance liquid chromatography (HPLC) method for DPHC (n = 3).

Table 8. Results of precision for three analytes at three different concentrations.

Table 9. Accuracy of three recoveries with different concentrations of IOE.

Table 10. Chemical compositions of F1, F2, F3, and F4 from IOP of *I. okamurae*.

LIST OF FIGURES

Figure 1-1. Extraction and fractionation of *I. okamurae*. *I. okamurae* powder was extracted with 50% ethanol and fractionated with Hexane, Chloroform (CHCl₃), Ethyl acetate (EtOAc), and n-butanol (BuOH).

Figure 1-2. The structure of DPHC.

Figure 1-3. Liquid Chromatography-Mass Spectrometry (LC-MS/MS) analysis of DPHC, DPHC was obtained from ethyl acetate solvent fraction of 50% ethanol extract of brown seaweed *I. okamurae* after through FlashPrep system purification.

Figure 1-4. ¹H spectrum analysis of DPHC, DPHC was obtained from ethyl acetate solvent fraction of 50% ethanol extract of brown seaweed *I. okamurae* after through FlashPrep system purification.

Figure 1-5. ¹³C spectrum analysis of DPHC, DPHC was obtained from ethyl acetate solvent fraction of 50% ethanol extract of brown seaweed *I. okamurae* after through FlashPrep system purification.

Figure 1-6. Structure of Ishophloroglucin A (IPA).

Figure 1-7. Liquid Chromatography-Mass Spectrometry (LC-MS/MS) analysis of Ishophloroglucin A (IPA), IPA was obtained from ethyl acetate solvent fraction of 50% ethanol extract of brown seaweed *I. okamurae* after through FlashPrep system purification.

Figure 1-8. HMBC spectrum analysis of Ishophloroglucin A (IPA), IPA was obtained from ethyl acetate solvent fraction of 50% ethanol extract of brown seaweed *I. okamurae* after through FlashPrep system purification.

Figure 1-9. HMQC spectrum analysis of Ishophloroglucin A (IPA), IPA was obtained from ethyl acetate solvent fraction of 50% ethanol extract of brown seaweed *I. okamurae* after through FlashPrep system purification.

Figure 1-10. LC-MS/MS spectroscopy analysis of Ishophloroglucin A(IPA). fragments composition of IPA and the proposed fragmentations of IPA.

Figure 1-11. Structure of Ishophloroglucin B (IPB).

Figure 1-12. MS spectrum analysis of Ishophloroglucin B (IPB), IPB was obtained from ethyl acetate solvent fraction of 50% ethanol extract of brown seaweed *I. okamurae* after through FlashPrep system purification.

Figure 1-13. ^1H NMR spectroscopy analysis of Ishophloroglucin B (IPB), IPB was obtained from ethyl acetate solvent fraction of 50% ethanol extract of brown seaweed *I. okamurae* after through FlashPrep system purification.

Figure 1-14. ^{13}C NMR spectroscopy analysis of Ishophloroglucin B (IPB), IPB was obtained from ethyl acetate solvent fraction of 50% ethanol extract of brown seaweed *I. okamurae* after through FlashPrep system purification.

Figure 1-15. Structure of Ishophloroglucin C (IPC).

Figure 1-16. MS spectrum analysis of Ishophloroglucin C (IPC), IPC was obtained from ethyl acetate solvent fraction of 50% ethanol extract of brown seaweed *I. okamurae* after through FlashPrep system purification.

Figure 1-17. ^1H NMR spectroscopy analysis of Ishophloroglucin C (IPC), IPC was obtained from ethyl acetate solvent fraction of 50% ethanol extract of brown seaweed *I. okamurae* after through FlashPrep system purification.

Figure 1-18. ^{13}C NMR spectroscopy analysis of Ishophloroglucin C (IPC), IPC was obtained from ethyl acetate solvent fraction of 50% ethanol extract of brown seaweed *I. okamurae* after through FlashPrep system purification.

Figure 1-19. Structure of Ishophloroglucin D (IPD).

Figure 1-20. MS spectrum analysis of Ishophloroglucin D (IPD), IPC was obtained from ethyl acetate solvent fraction of 50% ethanol extract of brown seaweed *I. okamurae* after through FlashPrep system purification.

Figure 1-21. ^1H NMR spectroscopy analysis of Ishophloroglucin D (IPD), IPC was obtained from ethyl acetate solvent fraction of 50% ethanol extract of brown seaweed *I. okamurae* after through FlashPrep system purification.

Figure 1-22. ^{13}C NMR spectroscopy analysis of Ishophloroglucin D (IPD), IPD was obtained from ethyl acetate solvent fraction of 50% ethanol extract of brown seaweed *I. okamurae* after through FlashPrep system purification.

Figure 2-1. Comparison analysis of thermal stability of DPHC and IPA at different temperatures (25 °C and 40°C).

Figure 2-2. The chromatograms showing the specificity of HPLC chromatogram method for DPHC. blank (a), standard DPHC (b), and chromatogram of DPHC (c) in *I. okamurae* extract sample.

Figure 3-1. The effect of α -MSH, Arbutin, IOE, and IPA on cell viability (a, b, e, and f). Melanin synthesis in B16F10 cells (c, d, g, and h). Each data point represents the mean \pm SE (ns: not significant; * $p < 0.05$, ** $p < 0.01$ by One-Way ANOVA test in GraphPad Prism 8.3.0).

Figure 3-2. IOE and IPA ability for tyrosinase activity inhibition and melanin inhibition on α -MSH-induced B16F10 cells. Cells were treated with various concentrations of IOE and IPA and stimulated with α -MSH. Tyrosinase activity was analyzed using the L-DOPA oxidation assay (a, c). Melanin synthesis was assessed, melanin content is represented compared to the non-treated group as percentage value (b, d). Each data point represents the mean \pm SE (## $p < 0.01$, ### $p < 0.001$, * $p < 0.05$, ** $p < 0.01$, *** $p < 0.001$ by One-Way ANOVA test in GraphPad Prism 8.3.0).

Figure 3-3. IPA inhibits melanogenesis through downregulating the expressions of MITF, tyrosinase, TRP1, and TRP2 in α -MSH stimulated B16F10 cells (a), MITF (b), Tyrosinase (c), TRP1 (d), TRP2 (e). Each data point represents the mean \pm SE (## $p < 0.01$, ### $p < 0.001$, * $p < 0.05$, ** $p < 0.01$, *** $p < 0.001$ by One-Way ANOVA test in GraphPad Prism 8.3.0).

Figure 3-4. IPA inhibits melanogenesis through downregulating the CREB-MITF pathway in α -MSH stimulated B16F10 cells. Each data point represents the mean \pm SE (# $p < 0.01$, * $p < 0.05$, ** $p < 0.01$, *** $p < 0.001$ by One-Way ANOVA test in GraphPad Prism 8.3.0).

Figure 3-5. The survival rate of IOE and IPA in zebrafish; Inhibitory effect of IOE and IPA on melanin synthesis in zebrafish. (a) The survival rate of IOE and IPA in zebrafish; (b) Inhibitory effect of IOE and IPA on melanin synthesis in α -MSH induced zebrafish. Each data point represents the mean \pm SE (ns; not significant, ## $p < 0.01$, ** $p < 0.01$, *** $p < 0.001$, by One-Way ANOVA test in GraphPad Prism 8.3.0).

Figure 4-1. HPLC Chromatogram (A) of isomer compound B, and MS chromatogram (B) of the isomer compound B. Compound B was obtained from n-butanol solvent fraction of 50% ethanol extract of brown seaweed *I. okamurae* after through FlashPrep system purification.

Figure 4-2. ¹H NMR spectroscopy analysis of isomer compound B, compound B was obtained from n-butanol solvent fraction of 50% ethanol extract of brown seaweed *I. okamurae* after through FlashPrep system purification.

Figure 4-3. qNMR analysis of calculation for the relative percentage of isomer compound B, depending on the signal intensity of NMR, the ratio of isomer was calculated as 1:1.

Figure 4-4. ¹³C NMR spectroscopy analysis of compound B, compound B was obtained from n-butanol solvent fraction of 50% ethanol extract of brown seaweed *I. okamurae* after through FlashPrep system purification.

Figure 4-5. Cosy spectroscopy analysis of compound B, compound B was obtained from n-butanol solvent fraction of 50% ethanol extract of brown seaweed *I. okamurae* after through FlashPrep system purification.

Figure 4-6. The structures of α -adenosine and β -adenosine.

Figure 4-7. Cell viability of particulate matter (PM) in vascular endothelial cell EA.hy926. Cells were exposed to different concentrations of PM for 24 hours, the cell viability was determined by MTT assay. Each data point represents the mean \pm SE (ns: not significant, * $p < 0.05$, by One-Way ANOVA test in GraphPad Prism 8.3.0).

Figure 4-8. The effect of particulate matter induced cell migration on EA.hy926 cells. cells were exposed to PM for 6 hours, the cell photos were taken as records at the initial gap length (0h) and 6h. Cell migration was expressed as a percentage of gap closure. Each data point represents the mean \pm SE (ns: not significant, * $p < 0.05$, ** $p < 0.01$ by One-Way ANOVA test in GraphPad Prism 8.3.0).

Figure 4-9. The effect of particulate matter induced capillary formation on EA.hy926 cells. the harvest cells were divided into an equal number of cells (1×10^5) and suspended in different concentrations of PM. After 4h of incubation, each well was taken photos as record and analyzed using the plugin 'Angiogenesis Analyzer' of imageJ software. The angiogenic score was evaluated the angiogenesis. Each data point represents the mean \pm SE (ns: not significant, * $p < 0.05$, *** $p < 0.001$ by One-Way ANOVA test in GraphPad Prism 8.3.0).

Figure 4-10. Cell viability of the mixture α/β -adenosine and β -adenosine on EA.hy926. Each data point represents the mean \pm SE (* $p < 0.05$ by One-Way ANOVA test in GraphPad Prism 8.3.0).

Figure 4-11. The inhibitory cell migration effect of the mixture α/β adenosine on particulate matter-induced angiogenesis in EA.hy926 cells. Each data point represents the mean \pm SE (* $p < 0.05$, ** $p < 0.01$ by One-Way ANOVA test in GraphPad Prism 8.3.0).

Figure 4-12. The inhibitory cell migration effect of the β -adenosine on particulate matter-induced angiogenesis in EA.hy926 cells. Each data point represents the mean \pm SE (ns: not significant; ** $p < 0.01$ by One-Way ANOVA test in GraphPad Prism 8.3.0).

Figure 4-13. Vascular endothelial cells cultured in Matrigel, it can differentiate into capillary-like structures. The angiogenic score was determined for the quantitative evaluation of capillary formation. The inhibitory cell migration effect of the mixture α/β -adenosine on particulate matter-induced angiogenesis in EA.hy926 cells. Each data point represents the mean \pm SE (* $p < 0.05$, ** $p < 0.01$, *** $p < 0.001$ by One-Way ANOVA test in GraphPad Prism 8.3.0).

Figure 4-14. Vascular endothelial cells cultured in Matrigel, it can differentiate into capillary-like structures. The angiogenic score was determined for the quantitative evaluation of capillary formation. The inhibitory cell migration effect of β -adenosine on particulate matter-induced angiogenesis in EA.hy926 cells. Each data point represents the mean \pm SE (* $p < 0.05$, ** $p < 0.01$, *** $p < 0.001$ by One-Way ANOVA test in GraphPad Prism 8.3.0).

Figure 4-15. The effect of α/β adenosine on particulate matter downstream signaling pathway, b: p-PI3K/PI3K; c: phospho-protein kinase B (pAkt)/ protein kinase B (Akt); d: endothelial nitric oxide synthase (eNOS) were detected by Western blotting. Each data point represents the mean \pm SE (* $p < 0.05$, ** $p < 0.01$, *** $p < 0.001$ by One-Way ANOVA test in GraphPad Prism 8.3.0).

Figure 4-16. Effects of the mixture α/β -adenosine on PI3K/Akt/eNOS Signal Pathway in particulate matter-induced EA.hy926 cells.

Figure 4-17. *In vivo* evaluation of angiogenesis in PM induced transgenic zebrafish embryos. PM treated to zebrafish embryos at different concentrations, and fluorescence images were taken after 7 dpf. The survival rate of particulate matter in zebrafish (a); The effect of particulate matter induced eyes vasodilation in zebrafish (b). Vessel formation in retinal vessels

was evaluated by measuring the retinal vessel diameter of the images (10× magnification) amount of 15 different fishes, 10 times in different places using Gen 5 3.04 software. Each data point represents the mean ± SE (* $p < 0.05$, ** $p < 0.01$ by One-Way ANOVA test in GraphPad Prism8.3.0).

Figure 4-18. *In vivo* evaluation of anti-angiogenesis in PM-induced transgenic zebrafish embryos. the mixture of α/β -adenosine was treated to PM-induced transgenic zebrafish embryos at different concentrations, and fluorescence images were taken after 7 dpf. The mixture of α/β -adenosine inhibits particulate matter-induced eyes vasodilation in zebrafish. Vessel formation in retinal vessels was evaluated by measuring the retinal vessel diameter of the images (10× magnification) amount of 15 different fishes, 10 times in different places using Gen 5 3.04 software. Each data point represents the mean ± SE (* $p < 0.05$, ** $p < 0.01$ by One-Way ANOVA test in GraphPad Prism8.3.0).

Figure 4-19. *In vivo* evaluation of anti-angiogenesis in PM-induced transgenic zebrafish embryos. β -adenosine was treated to PM-induced transgenic zebrafish embryos at different concentrations, and fluorescence images were taken after 7 dpf. β -adenosine inhibits particulate matter-induced eyes vasodilation in zebrafish. Vessel formation in retinal vessels was evaluated by measuring the retinal vessel diameter of the images (10× magnification) amount of 15 different fishes, 10 times in different places using Gen 5 3.04 software. Each data point represents the mean ± SE (* $p < 0.05$, ** $p < 0.01$ by One-Way ANOVA test in GraphPad Prism8.3.0).

Figure 5-1. Isolation of IOP using DEAE-cellulose anion exchange chromatography. Column pre-equilibrated with 50.0 mM acetate buffer (pH 5.0). The increasing gradient of NaCl (0.0-1.3 M in the same buffer) was used as the mobile phase. The phenol-sulfuric method was used to measure the polysaccharide content.

Figure 5-2. FTIR spectra analysis was used for all subfractions (F1, F2, F3, F4) and commercial fucoidan.

Figure 5-3. ^1H NMR spectrum of the all subfractions (F1, F2, F3, F4) in D_2O solution-analyzed at 400 MHz.

Figure 5-4. HPAE-PAD spectrum of standard monosaccharide mixture. B: HPAE-PAD spectrum of all subfractions (F1, F2, F3, F4).

Figure 5-5. The cytotoxicity of each fraction (F1, F2, F3, and F4) on RAW 264.7 cells. Cells were treated with different sample concentrations, after 24h, MTT assay was determined for cytotoxicity. Each data point represents the mean \pm SE (* $p < 0.05$, ** $p < 0.01$ by One-Way ANOVA test in GraphPad Prism 8.3.0).

Figure 5-6. The inhibition of NO production and its protective effects against LPS induced cytotoxicity was evaluated in RAW 264.7 cells. cells were treated with LPS (1 $\mu\text{g/ml}$) and different concentrations of each fraction (F1, F2, F3, and F4). After 24h, the cytotoxicity was determined for cell viability (a), and culture media was used to analyze the NO production using Griess assay (b). Data points and bars represent the arithmetic means \pm SE (n = 3). Each data point represents the mean \pm SE (* $p < 0.05$, ** $p < 0.01$ by One-Way ANOVA test in GraphPad Prism 8.3.0).

Figure 5-7. Evaluation of the expression of PGE₂ and pro-inflammatory cytokines. PGE₂(a) and pro-inflammatory mediators including IL-6 (b); TNF- α (c); IL1- β (d) in LPS stimulated RAW 264.7 macrophages. RAW 264.7 cells were pretreated with different concentrations of F4 and co-treated with LPS (1 $\mu\text{g/ml}$). After 24 h, culture media was used to analyze the productions of PGE₂, TNF- α , IL1- β , and IL-6. Each data point represents the mean \pm SE (* $p < 0.05$, ** $p < 0.01$ by One-Way ANOVA test in GraphPad Prism 8.3.0).

Figure 5-8. Western blotting analysis of the expression of inflammatory regulators of COX-2 and i-NOS against F4 in RAW 264.7 macrophages induced by LPS. RAW 264.7 cells were pretreated with different concentrations of F4 and co-treated with LPS (1 $\mu\text{g/ml}$). After 24 h, cells were harvested to analyze the expression of COX-2 and i-NOS. Each data point represents the mean \pm SE (** $p < 0.01$, *** $p < 0.001$ by One-Way ANOVA test in GraphPad Prism 8.3.0).

Figure 5-9. *In vivo* evaluation of anti-inflammatory potential of F4 using zebrafish embryos. zebrafish embryos were treated with F4 and stimulated with LPS (10 $\mu\text{g/mL}$). After 168 hpf, Fluorescence images of the zebrafish embryos of NO production (a), and Cell death (b) were calculated according to the intensity of green fluorescence. Each data point represents the mean \pm SE (* $p < 0.05$, ** $p < 0.01$ by One-Way ANOVA test in GraphPad Prism 8.3.0)

Background

Marine macroalgae, known as seaweeds, it also refers to several species of macroscopic, multicellular, marine algae, seaweeds belong to a group of rather vaguely defined plants called algae, the term "seaweed" has no taxonomic value of its, but is a popular term used to describe the common large epiphyte marine algae, which include Rhodophyta (red algae), Phaeophyta (brown algae) and Chlorophyta (green algae) according to their pigmentation, respectively.

Since ancient times, seaweeds have constituted an important part of the traditional diet and medicine in Asia including Korea, China, Japan. it is the first organism in marine food chains and act as one of the largest producers of biomass in the marine environment, it is the source of producing biochemical components like polysaccharides, phlorotannins, dietary fibers, sterols, polyunsaturated fatty acids, vitamins, and minerals. Seaweeds have constituted an important part of the traditional diet and medicine in Asia including Korea, China, Japan. Compared to Europe, Asians have been using edible seaweed as food and medicine for a long time. In the traditional Korean diet, seaweed is used to make soups or dry products.

Polyphenol compounds are a diverse group of naturally occurring secondary metabolites. Over the years, dietary polyphenols from seaweeds have been widely studied on their biological activities including antioxidant activity, polyphenols can be found in marine organisms and contain multiple phenolic functionalities [1]. Besides the strong antioxidant properties, these naturally occurring polyphenols are known to have numerous biological activities such as anti-inflammation [2], anti-allergic [3], anti-bacterial, matrix metalloproteinase inhibition [4, 5] and anticancer [6].

Ishige okamurae (*Ishige*, Phaeophyta) is one of the most common edible brown seaweed with narrow fronds and acute apexes, grows on rocks in the upper and middle intertidal zones of coasts in Korea, Japan, and China [7]. Previous studies revealed that the enrichment of polyphenols and other chemical compositions present in *I. okamurae* [8]. It is composed of rich bioactive compounds, such as diphloretohydroxycarmalol [9], Ishigoside [10], Fucoxanthin [11], phloroglucinol and 6,6'-Bieckol [12], Methoxylated fatty acid [13]. *I.okamurae* is a very important material valued for its various biological activities. However, there are only few systematic studies of the chemical composition and its structure is not precisely known [14]. Column chromatographic purification has been widely used to purify natural products from various organisms. However, those methods are time-consuming and low yield, therefore, the

general purpose of this work is to suggest new separation method to increase efficiency and improve the isolation performance using Pure C-850 FlashPrep system.

**Part I. Isolation and identification of polyphenols
from *Ishige okamurae* and their uses**

**Section 1: Isolation and identification of polyphenols
from *Ishige okamurae***

Abstract

The edible seaweed of *Ishige okamurae* (*I.okamurae*), is a brown seaweed as a traditional health food and is a source of natural bioactive compounds. Polyphenols are main constituents in *I.okamurae* that have potential in functional food. In this study, five polyphenols were isolated from the ethyl acetate fraction of *I.okamurae* using Pure C-850 FlashPrep system equipped with reversed-phase preparative HPLC. A serial of novel polyphenols was identified from *I.okamurae*, they are Ishophloroglucin A, B, C, and D. One known polyphenol is Diphlorethohydroxycarmalol (DPHC). Their structures were identified and determined by 1D and 2D NMR (^1H , ^{13}C , HSQC, COSY, and HMBC) spectroscopy, and Mass Spectrometry (MS).

Keyword: *Ishige okamurae*; polyphenols; Ishophloroglucins

1. Materials and methods

1.1. General methods

All of ^1H , ^{13}C NMR spectra were recorded on BrukerBiospin Advance II NMR spectrometer; the chemical shifts were recorded as δ values. 2D NMR spectra include Correlation Spectroscopy (COSY), Heteronuclear Multiple Bond Correlation (HMBC) and Heteronuclear Singular Quantum Correlation (HSQC). Electrospray ionization mass spectrometry (ESI-MS) analyses were measured on Liquid chromatography-mass spectrometry SYNAPT G2-Si HDMS (Waters, Korea basic science institute, Seoul, South Korea). Pure C-850 Flash prep (BUCHI, Switzerland) equipped with flashpure column Ecoflex (C18, 50 μm spherical, 40 g) and HPLC column (YMC-Pack ODS-A, 250mm x 2.00 mmI.D. S-5 μm , 12nm) for isolation and purification of compounds. HPLC analysis was performed using an Agilent 1100 equipped with a UV detector and an Agilent poroshell 120 EC-C18column (4.6 mm x 100 mm, 4 μm).

1.2. Materials and chemicals

I. okamurae was collected in April 2018 from Seongsan along the Jeju coastline of South Korea. HPLC grade acetonitrile was obtained from Honeywell Burdick & Jackson (Muskegon, MI, USA). Analytical-grade formic acid was purchased from FlukaChemica (Buchs, Switzerland) and water was filtered by the Milli Q system (Millipore, Milford, MA, USA). Dimethyl sulfoxide-*d*₆ (DMSO-*d*₆) was obtained from Merck (Darmstadt, Germany). All other chemicals and solvents used in the current study were of analytical grade.

1.3. Extraction and fractionation of *I. okamurae*

The Samples were ground into powder after drying in a freeze dryer. The dried *I. okamurae* (500 g) was extracted three times with 3 L of 50% ethanol at room temperature for 24h. The obtained supernatant was concentrated to dryness powder by rotary evaporator concentrating under 37°C after centrifugation (revolutions per minute 12000, 10 mins, 4°C). The powder of 50% ethanol extract was suspended in distilled water and partitioned with hexane, chloroform, ethyl acetate, n-Butanol, respectively. The extraction procedure is summarized in Figure 1-1. The ethyl acetate fraction was evaporated to dryness powder under 37°C. And it was subjected to the ODS cartridge in FlashPrep system (C-850 FlashPrep, BUCHI, Switzerland). Fraction 1

and fraction 2 were obtained from ODS cartridge isolation, fraction 1 was further loaded into prep-YMS ODS HPLC column on FlashPrep system, 18% of acetonitrile was used as mobile phase. The compound 1 was obtained and purified by high-performance liquid chromatography and lyophilized to give the compound 1 (3.8 mg). Fraction 2 was loaded into the prep-YMS ODS HPLC column on the FlashPrep system, 30% of acetonitrile was used as a mobile phase. Four pure compounds were obtained, compound 2 (5.2 mg), compound 3 (2.1 mg), compound 4 (2.3 mg), and compound 5 (3.1 mg) were obtained. And the structures of five compounds were identified and elucidated by the ^1H and ^{13}C NMR data and LC-MS/MS, as well as the 2D NMR (HMBC) data.

2. Result and Discussion

Compound 1 was isolated as an amorphous powder. The molecular was established as $\text{C}_{24}\text{H}_{16}\text{O}_{13}$ by HR-ESI-MS, which showed a $[\text{M}-\text{H}]^-$ ion peak at m/z 511.0525, as shown in Figure 1-3, in addition to ^1H , ^{13}C NMR spectroscopic analysis (Figure 1-4, 1-5), the sixteen unsaturation degrees was calculated depending on the molecular formula. Seven aromatic protons at δ (ppm): 9.11-9.20 (9H, m), 6.05 (1H, s), 5.83 (1H, s), 5.81 (1H, s), 5.78 (1H, t, 2.0 Hz), 5.69 (1H, s), 5.678 (1H, d, 2.0 Hz), 5.675 (H, d, 2.0 Hz); which were supported by ^{13}C NMR spectral data, compound 1 showed spectral data in the literature [15], it was elucidated as Diphloretohydroxycarmalol (DPHC) (Figure 1-2). Its chemical shifts were arranged in Table 1.

Compound 2 was naturally obtained as light yellowish solid, The UPLC-MS spectrum showed its molecular formula as $\text{C}_{96}\text{H}_{66}\text{O}_{48}$ with a molecular weight at 1986.2630 as show in Figure 1-7. the unsaturated degree of it should be 64 from 16 aromatic rings (4 for each), respectively. Together with consideration of carbon signals in only three types at around 150, 120 and 90 ppm from the ^{13}C NMR spectrum, then it is obvious that the chemical structure of compound 2 should be polyphenol including 16 phenol homopolymers with maximum characteristic absorption at 230 nm (benzene ring sp^2 π bond) also. The linkages among these 16 phenols should be single bond without any rings and double bonds as well. Meanwhile, no any signals were found from 100 ppm to 150 ppm exception for some 120 ppm carbon atoms in the ^{13}C spectrum, it indicated that the linkage forms among 16 phenols should go to three types consisting of extraneous oxygen atoms binding to two aromatic carbon atoms directly (providing the chemical shifts at around 120 ppm), and the other linkages containing

endogenesis oxygen atoms from two phenolic hydroxyl groups of phenol units by dehydration, and linkages with oxygen bridge atoms from endogenesis phenol-OH directly bonded to the aromatic carbon atom. According to those data of ^1H , ^{13}C . HMQC and HMBC NMR spectra (Figure 1-8, 1-9), the proton signals from δ_{H} 8.92-9.07 ppm in ^1H NMR spectrum should be elucidated as proton atoms from free phenol hydroxyl groups and the other protons of 5.59-6.15 ppm should go to the free aromatic hydrogen atoms. It is proved by the ^{13}C NMR data with some finger-print signals considered as the aromatic carbons from 94.1-94.9 ppm. After the comprehensive analyses of all of these spectra data and SciFinder checking, the final structure of compound 2 was determined as a novel polyphenol named as Ishophloroglucin A (IPA) with unique complex linkages, together with a very high molecular weight up to 1986 which has been published in our previous paper [16] (see Figure 1-6 and Table 2). LC-MS/MS analysis was used to confirm the structure of Ishophloroglucin A (IPA), from MS/MS chromatogram Figure 1-10, all of the fragments (Y1-Y14) were matched with the structure fragments of IPA.

Compound 3 was naturally obtained as light yellowish solid, The UPLC-MS spectrum showed its molecular formula as $\text{C}_{78}\text{H}_{54}\text{O}_{39}$ with a molecular weight at m/z 806.1178, $[\text{M}-2\text{H}]^{2-}$ (1614.22 of MW) as shown in Figure 1-12. Compound 4 was naturally obtained as light yellowish solid, The UPLC-MS spectrum showed its molecular formula as $\text{C}_{90}\text{H}_{62}\text{O}_{45}$ with a molecular weight at m/z 930.1247, $[\text{M}-2\text{H}]^{2-}$ (1862.26 of MW) as shown in Figure 1-16. Compound 5 was naturally obtained as light yellowish solid, The UPLC-MS spectrum showed its molecular formula as $\text{C}_{114}\text{H}_{78}\text{O}_{57}$ with a molecular weight at m/z 1178.1546 $[\text{M}-2\text{H}]^{2-}$ (2358.30592 of MW) as shown in Figure 1-20.

Compounds 3, 4 and 5 were isolated from fraction 2 according to the intensity of peaks, an isocratic method was applied, further analysis of LC-MS/MS, ^1H and ^{13}C NMR, COSY, HSQC, and HMBC spectra shown that they are a serial of compounds with IPA, due to the unsaturation degree of compounds 3, 4 and 5 were 52, 60, and 76 from 13, 15, and 19 aromatic rings (4 for each) of compounds 3, 4, and 5, separately, besides the unsaturation degree of IPA is 16. Those four compounds (2, 3, 4, and 5) were observed in ^1H and ^{13}C NMR analysis and confirmed the polyphenolic structures as phlorotannins, seeing resonance signals were in the range of δ_{H} 5.47-6.17, 8.94-9.17, δ_{C} 93-95, 122-123 and 150-165, respectively, they are shown the same pattern each other. The quaternary carbons have characteristic resonances depending on the type of bonding. They are either involved in oxygen atoms-carbon bonding between phloroglucinol

units, in ether-linked phloroglucinol units or are attached to hydroxyl groups. Hence, compounds 2, 3, 4, and 5 were determined to be serial Ishophloroglucins, named as Ishophloroglucin A (IPA), Ishophloroglucin B (IPB), Ishophloroglucin C (IPC), and Ishophloroglucin D (IPD). All of the chemical shifts of IPB, IPC, and IPD were arranged in Tables 3, 4, and 5, separately.

4. Conclusion

I. okamurae is a kind of brown seed as a traditional health food in Korea and China, previous reaches have proven that exhibited excellent biological activities, the potential functional properties of this seaweed are ascribed to the presence of functional components. In this study, five polyphenols were isolated and identified as DPHC, and Ishophlorogucinols (IPA, IPB, IPC, and IPD). This basic research of chemical analysis deepens the knowledge about of functional components for exploring and developing functional products from *I. okamurae*.

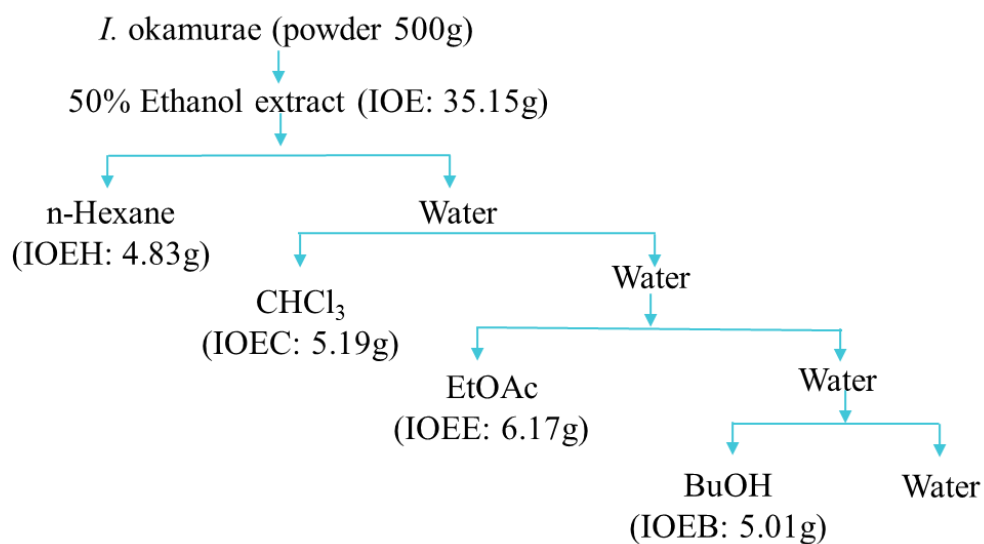


Figure 1-1. Extraction and fractionation of *I. okamurae*. *I. okamurae* powder was extracted with 50% ethanol and fractionated with Hexane, Chloroform (CHCl₃), Ethyl acetate (EtOAc), and n-butanol (BuOH).

Diphlorethohydroxycarmalol (Compound 1):

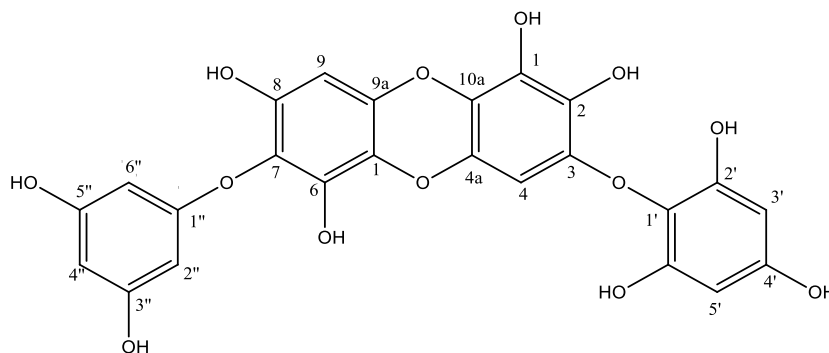


Figure 1-2. Structure of DPHC

Table 1. ^1H and ^{13}C NMR analysis data of Compound 1(DPHC)

No	δ_{H} (mult, J)	δ_{C} (mult)
1		159.9
2	5.81(1H,s)	95.9
3		154.6
4		125.5
5		154.6
6	5.81(1H,d)	95.9
7		158.7
8	6.05(1H,s)	94.1
9		138.6
10		135.1
11		139.4
12		132.8
13		142.9
14		145.8
15		158.7
16		142.9
17	5.83(1H,s)	93.5
18		139.4
19		164.9
20	5.68(1H,d, $J=2.4\text{Hz}$)	93.5
21		158.7
22	5.78(1H,t, $J=1.2\text{Hz}$)	94.7
23		158.7
24	5.67(1H,d, $J=2.4\text{Hz}$)	93.5
-OH*	9.02-9.30(m)	

Recorded in $\text{DMSO-}d_6$ at 400 MHz for ^1H NMR and 100 MHz for ^{13}C NMR; -OH*: all free phenol hydroxyl groups

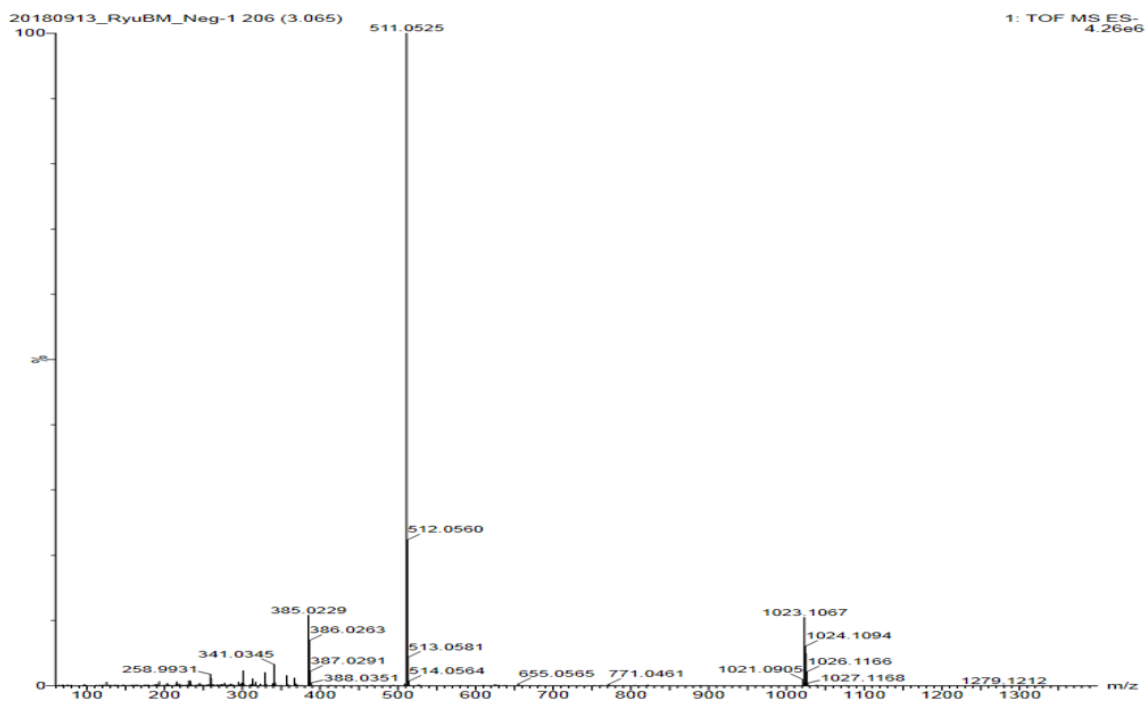


Figure 1-3. Liquid Chromatography-Mass Spectrometry (LC-MS/MS) analysis of DPHC, DPHC was obtained from ethyl acetate solvent fraction of 50% ethanol extract of brown seaweed *I. okamurae* after through FlashPrep system purification.

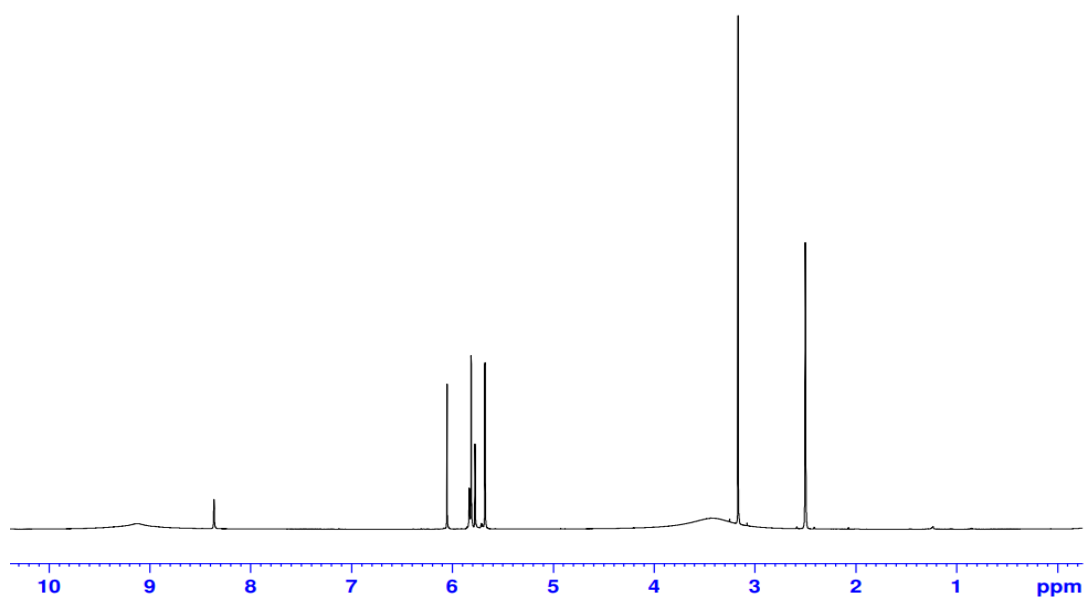


Figure 1-4. ^1H spectrum analysis of DPHC, DPHC was obtained from ethyl acetate solvent fraction of 50% ethanol extract of brown seaweed *I. okamurae* after through FlashPrep system purification.

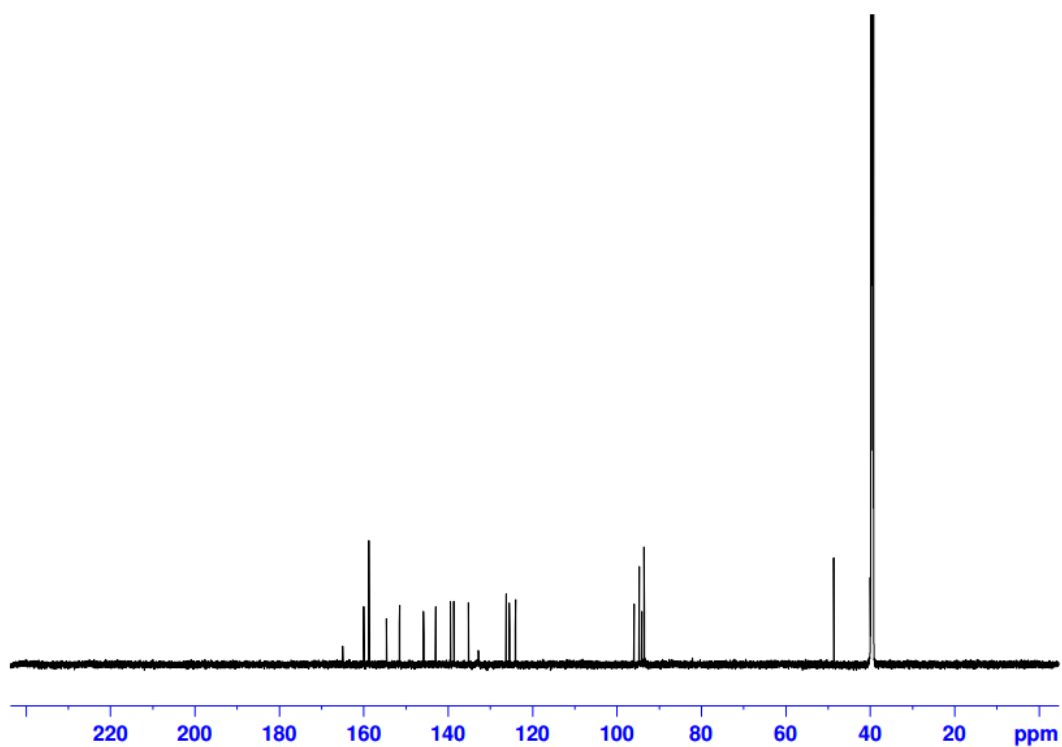


Figure 1-5. ^{13}C NMR spectrums analysis of DPHC, DPHC was obtained from ethyl acetate solvent fraction of 50% ethanol extract of brown seaweed *I. okamurae* after through FlashPrep system purification.

Ishophloroglucin A (Compound 2):

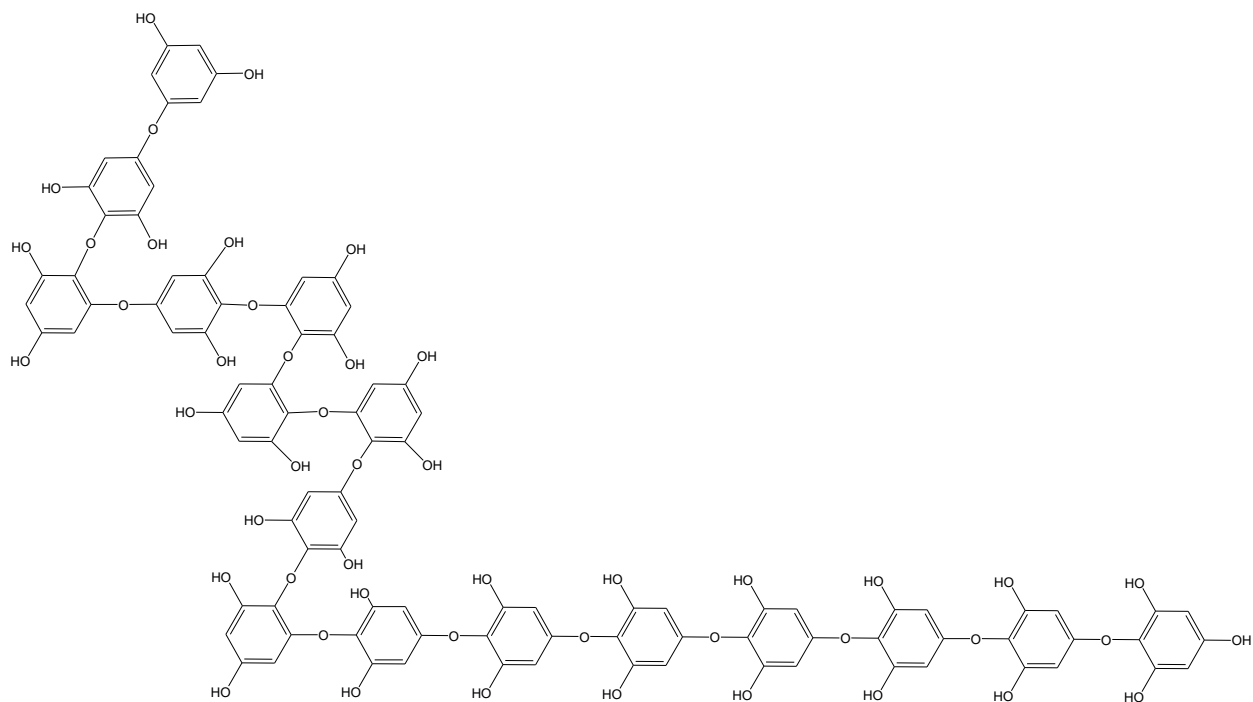


Figure 1-6. Structure of Ishophloroglucin A (IPA)

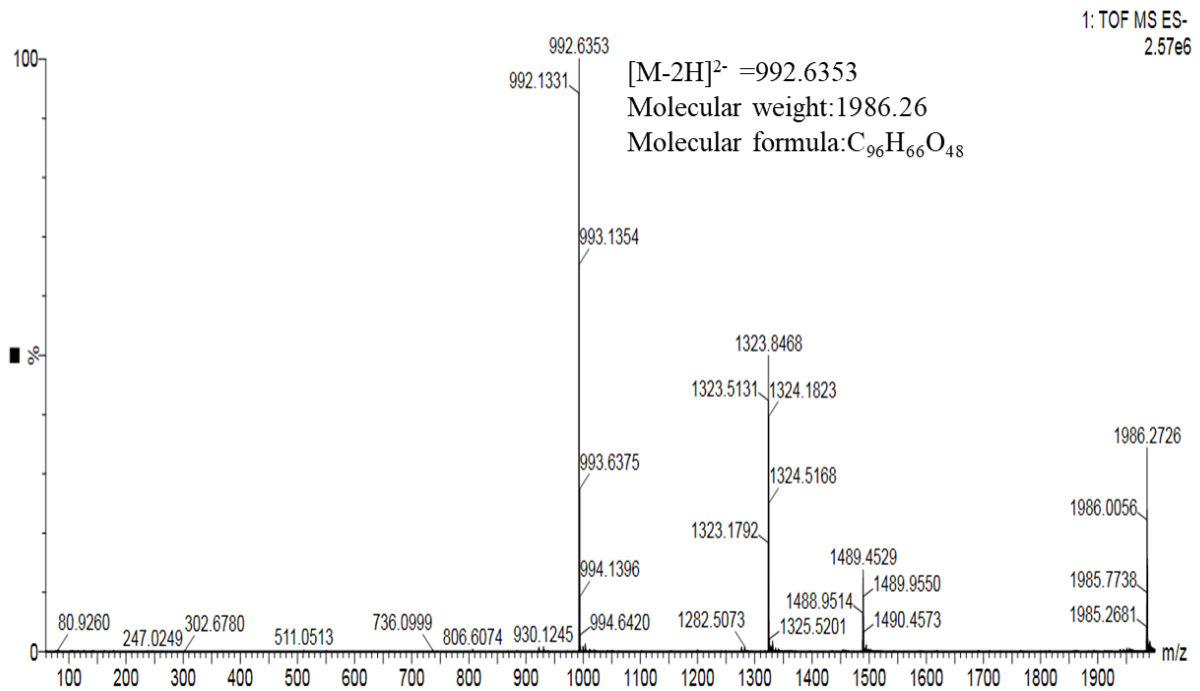


Figure 1-7. Liquid Chromatography-Mass Spectrometry (LC-MS/MS) analysis of Ishophloroglucin A (IPA), IPA was obtained from ethyl acetate solvent fraction of 50% ethanol extract of brown seaweed *I. okamurae* after through FlashPrep system purification.

Table 2. ¹H, ¹³C and HMQC Data of Ishphloroglucin A (compound 2)

No	δ_H (mult, J)	δ_C	No	δ_H (mult, J)	δ_C	No	δ_H (mult, J)	δ_C	No	δ_H (mult, J)	δ_C
1		156.2(s)	26	5.85(1H,s)	94.7(d)	51	5.85(1H,s)	94.7(d)	76		154.0(s)
2	5.95(1H,d, J = 1.6Hz)	94.2(d)	27		151.1(s)	52		154.0(s)	77	5.85(1H,s)	94.7(d)
3		151.1(s)	28		122.0(s)	53	5.85(1H,s)	94.7(d)	78		151.1(s)
4		122.0(s)	29		151.1(s)	54		151.1(s)	79		152.7(s)
5		151.1(s)	30	5.85(1H,s)	94.7(d)	55		123.4(s)	80		123.5(s)
6	5.95(1H,d, J = 1.6Hz)	94.2(d)	31		154.1(s)	56		150.8(s)	81		150.8(s)
7		154.0(s)	32	5.85(1H,s)	94.7(d)	57	5.60(1H,d, J = 1.6Hz)	94.1(d)	82	5.70(1H,d, J = 1.8Hz)	94.9(d)
8	5.85(1H,s)	94.7(d)	33		151.1(s)	58		153.0(s)	83		152.9(s)
9		151.1(s)	34		122.0(s)	59	5.75(1H,dd, J = 1.8, 1.6Hz)	94.7(d)	84	5.75(1H,dd, J = 1.8, 1.6Hz)	94.7(d)
10		122.0(s)	35		151.1(s)	60		152.7(s)	85		122.0(s)
11		151.1(s)	36	5.85(1H,s)	94.7(d)	61		123.4(s)	86		151.1(s)
12	5.85(1H,s)	94.7(d)	37		154.1(s)	62		152.7(s)	87	5.85(1H,s)	94.7(d)
13		154.1(s)	38	5.85(1H,s)	94.7(d)	63	5.75(1H,dd, J = 1.8, 1.6Hz)	94.7(d)	88		154.5(s)
14	5.85(1H,s)	94.7(d)	39		151.1(s)	64		153.0(s)	89	5.85(1H,s)	94.7(d)
15		151.1(s)	40		122.0(s)	65	5.60(1H,d, J = 1.6Hz)	94.1(d)	90		151.1(s)
16		122.0(s)	41		151.1(s)	66		150.8(s)	91		161.0(s)
17		151.1(s)	42	5.85(1H,s)	122.0(s)	67		123.4(s)	92	6.15(2H,d, J = 1.6Hz)	94.9(d)
18	5.85(1H,s)	94.7(d)	43		152.7(s)	68		150.8(s)	93		158.6(s)
19		154.1(s)	44		123.5(s)	69	5.60(1H,d, J = 1.6Hz)	94.1(d)	94	5.95(1H,d, J = 1.6Hz)	94.1(d)
20	5.85(1H,s)	94.7(d)	45		150.8(s)	70		153.0(s)	95		158.6(s)
21		151.1(s)	46	5.70(1H,d, J = 1.8Hz)	94.9(d)	71	5.75(1H,dd, J = 1.8, 1.6Hz)	94.7(d)	96	6.15(2H,d, J = 1.6Hz)	94.9(d)
22		122.0(s)	47		152.9(s)	72		152.7(s)	OH*	8.92-9.07 (33H,m)	
23		151.1(s)	48	5.75(1H,dd, J = 1.8, 1.6Hz)	94.7(d)	73		122.0(s)			
24	5.85(1H,s)	94.7(d)	49		122.0(s)	74		151.1(s)			
25		154.1(s)	50		151.1(s)	75	5.85(1H,s)	94.7(d)			

*Recorded in DMSO-*d*₆ at 400 MHz for ¹H NMR and 100 MHz for ¹³C NMR; -OH* : all free phenol hydroxyl groups

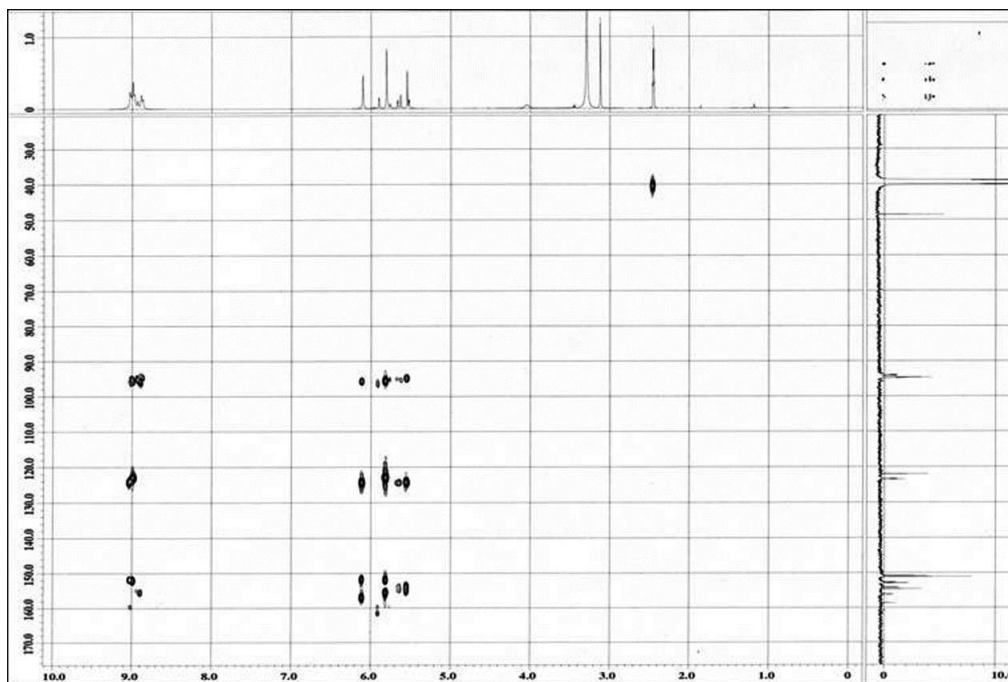


Figure 1-8. HMBC spectrum analysis of Ishophloroglucin A (IPA), IPA was obtained from ethyl acetate solvent fraction of 50% ethanol extract of brown seaweed *I. okamurae* after through FlashPrep system purification.

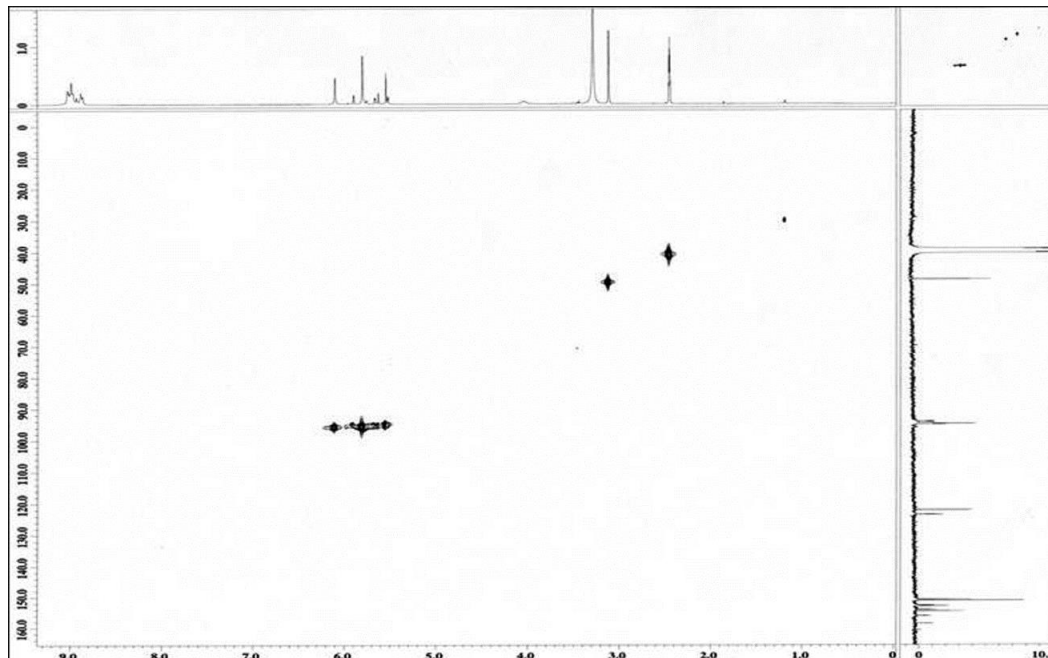


Figure 1-9. HMQC spectrum analysis of Ishophloroglucin A (IPA), IPA was obtained from ethyl acetate solvent fraction of 50% ethanol extract of brown seaweed *I. okamurae* after through FlashPrep system purification.

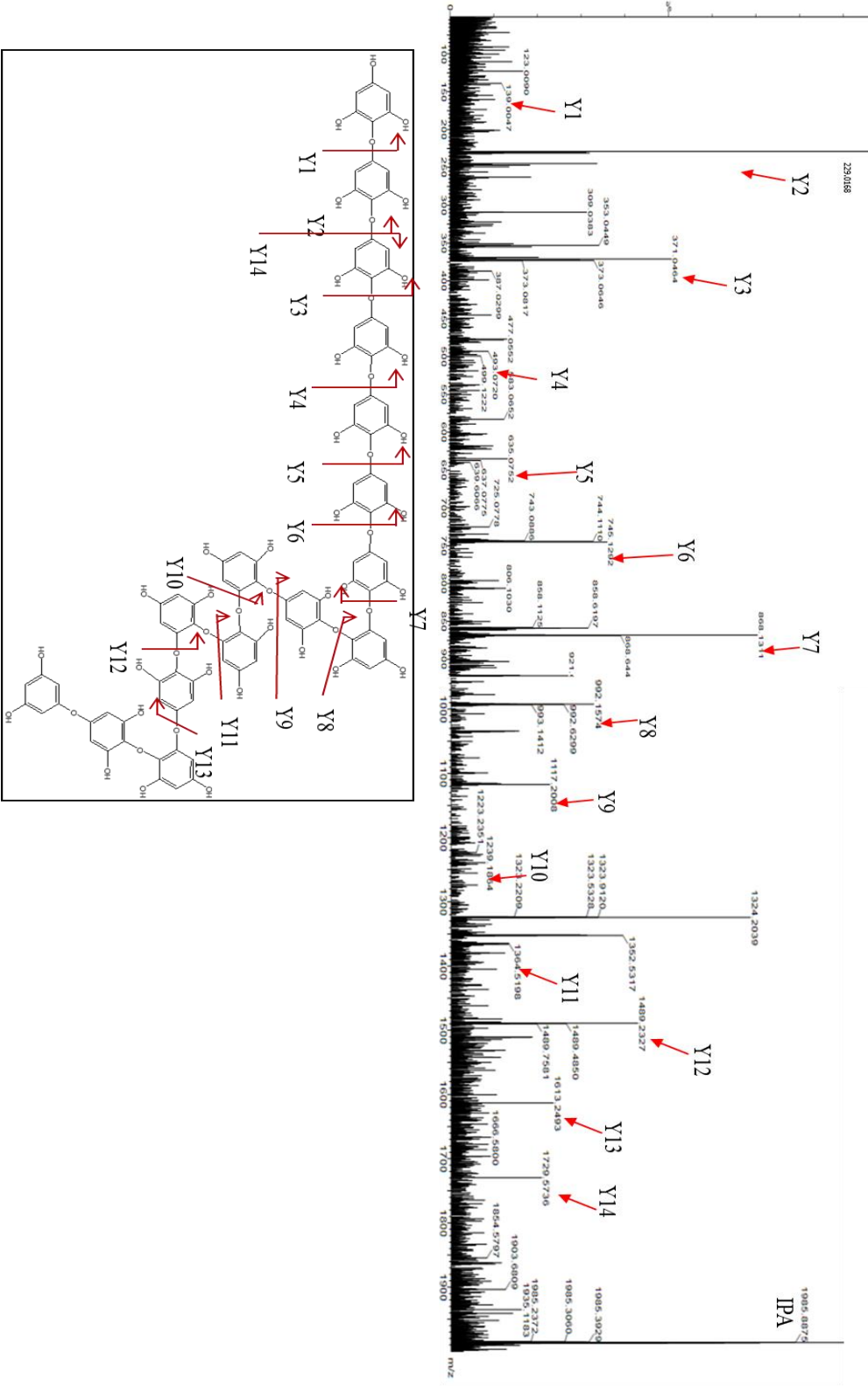


Figure 1-10. LC-MS/MS spectroscopy analysis of Ishophloroglucin A (IPA). fragments composition of IPA, MS/MS spectrum. The proposed fragmentations of IPA.

Ishophloroglucin B (Compound 3):

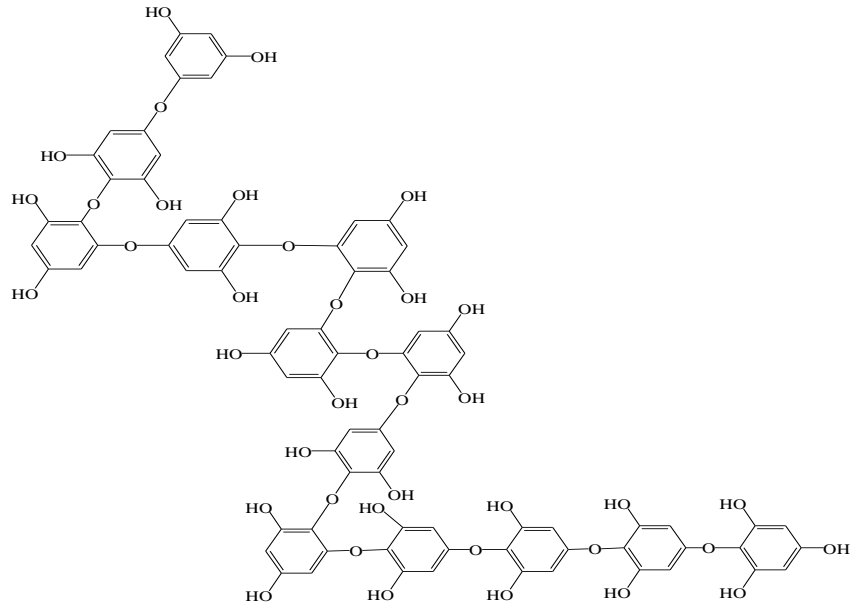


Figure 1-11. Structure of Ishophloroglucin B (IPB)

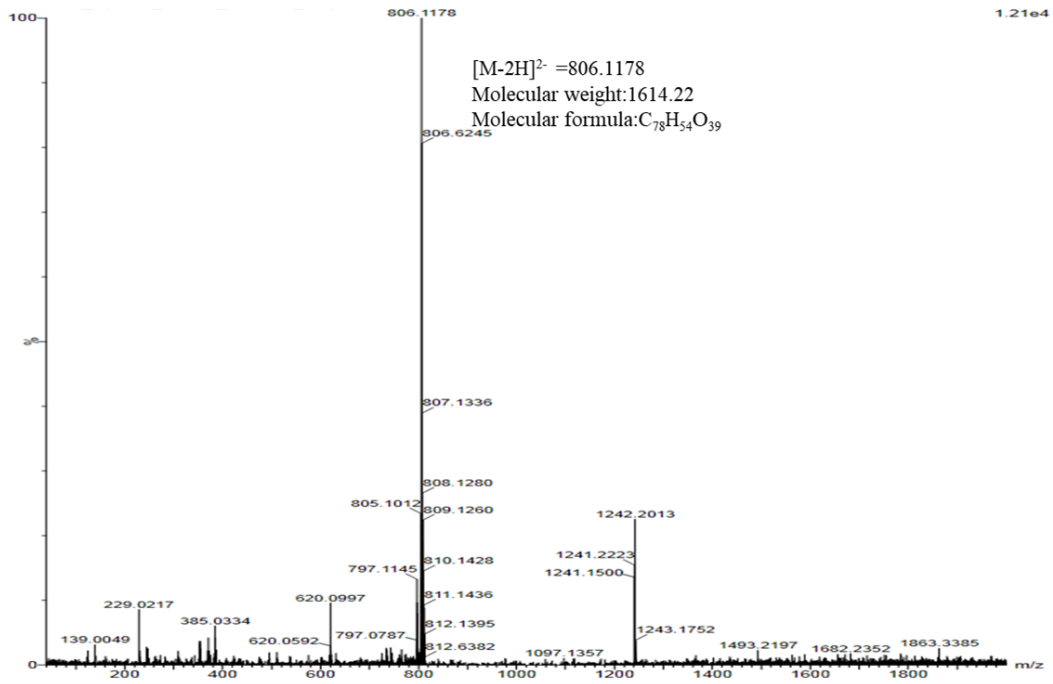


Figure 1-12. MS spectrum analysis of Ishophloroglucin B (IPB), IPB was obtained from ethyl acetate solvent fraction of 50% ethanol extract of brown seaweed *I. okamurae* after through FlashPrep system purification.

Table 3. ¹H, ¹³C and HMQC Data of Ishophloroglucin B (Compound 3)*

No	δ_H (mult, J)	δ_C (mult)	No	δ_H (mult, J)	δ_C (mult)	No	δ_H (mult, J)	δ_C (mult)	No	δ_H (mult, J)	δ_C (mult)
1		158.6(s)	26		123.5 (s)	51	5.68(1H,dd)	94.2(d)	76	6.16,(t, <i>J</i> =4.8Hz)	94.9(d)
2	5.60(1H,s)	94.0(d)	27		150.8(d)	52		152.8(d)	77		158.7(s)
3		151.2(s)	28	5.85(1H,s)	94.7(s)	53	5.85(1H,s)	94.7(s)	78	5.68(1H,dd)	94.2(d)
4		122.1(s)	29		152.9(s)	54		152.8(d)	OH*	8.95-9.17 (27H,m)	
5		151.2(s)	30	5.85(1H,s)	94.7(s)	55		123.5 (s)			
6	5.60(1H,s)	94.0(d)	31		122.1(s)	56		151.2(s)			
7		154.6(s)	32		151.2(s)	57	5.85(1H,s)	94.7(s)			
8	5.85(1H,s)	94.7(s)	33	5.85(1H,s)	94.7(s)	58		154.1(d)			
9		151.2(s)	34		154.1(s)	59	5.85(1H,s)	94.7(s)			
10		122.1(s)	35	5.85(1H,s)	94.7(s)	60		151.2(s)			
11		151.2(s)	36		151.2(s)	61		152.7(d)			
12	5.85(1H,s)	94.7(s)	37		123.47(d)	62		123.5(s)			
13		154.6(s)	38		150.8(d)	63		150.8(d)			
14	5.85(1H,s)	94.7(s)	39	5.68(1H,dd)	94.2(d)	64	6.16,(t, <i>J</i> =4.8Hz)	94.9(d)			
15		151.2(s)	40		152.8(d)	65		152.8(d)			
16		122.1(s)	41	5.85(1H,s)	94.7(s)	66	5.85(1H,s)	94.7(s)			
17		151.2(s)	42		152.8(s)	67		123.5 (s)			
18	5.85(1H,s)	94.7(s)	43		123.47(d)	68		150.8(s)			
19		154.6(s)	44		152.8(d)	69	5.85(1H,s)	94.7(s)			
20	5.85(1H,s)	94.7(s)	45	5.85(1H,s)	94.7(s)	70		154.6(s)			
21		151.2(s)	46		152.8(d)	71	5.85(1H,s)	95.8(d)			
22		122.1(s)	47	5.68(1H,dd)	94.2(d)	72		150.8(s)			
23		151.2(s)	48		150.8(d)	73		160.8(s)			
24	5.85(1H,s)	94.7(s)	49		123.47(d)	74	5.68(1H,dd)	94.2(d)			
25		152.9(s))	50		150.8(d)	75		158.7(s)			

*Recorded in DMSO-*d*₆ at 800 MHz for ¹H NMR and 200 MHz for ¹³C NMR; -OH*: all free phenol hydroxyl groups

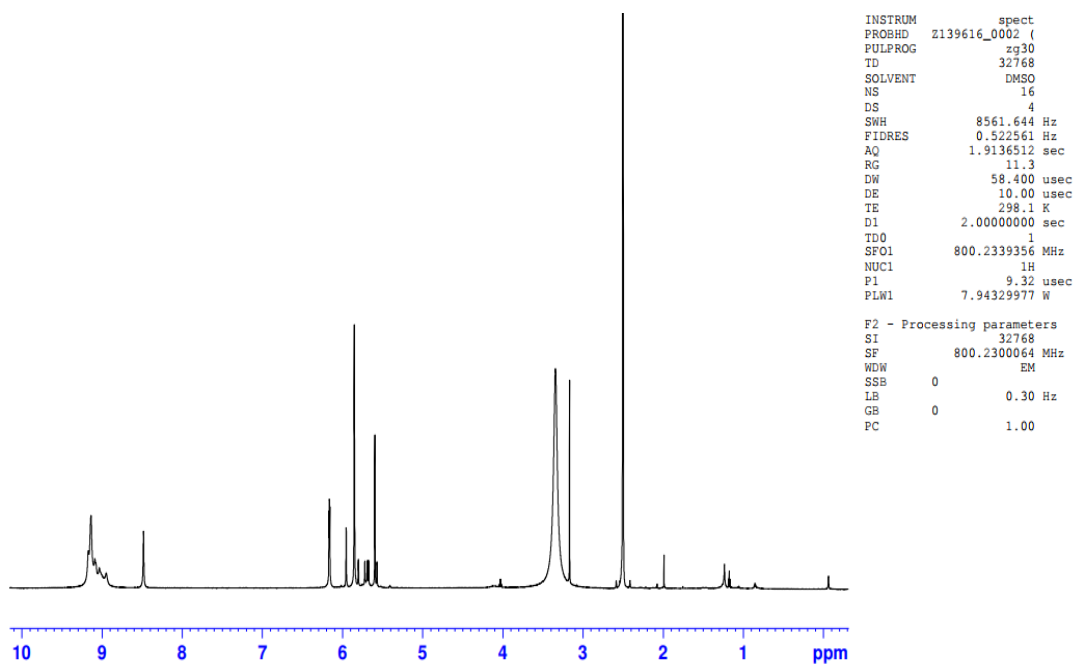


Figure 1-13. ^1H NMR spectroscopy analysis of Ishophloroglucin B (IPB), IPB was obtained from ethyl acetate solvent fraction of 50% ethanol extract of brown seaweed *I. okamurae* after through FlashPrep system purification.

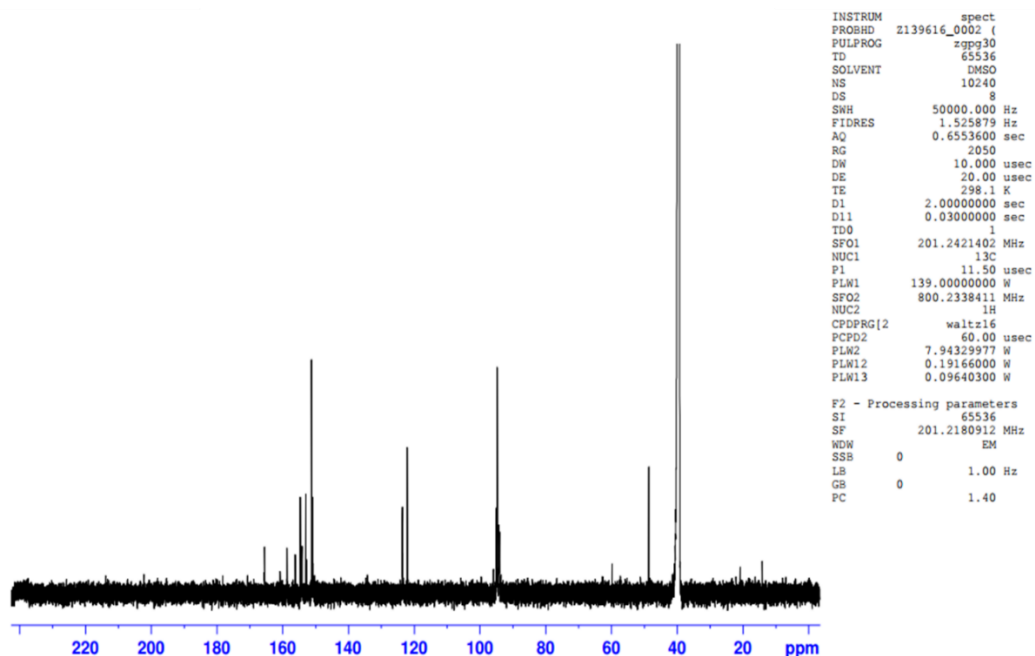


Figure 1-14. ^{13}C NMR spectroscopy analysis of Ishophloroglucin B (IPB), IPB was obtained from ethyl acetate solvent fraction of 50% ethanol extract of brown seaweed *I. okamurae* after through FlashPrep system purification.

Ishophloroglucin C (Compound 4):

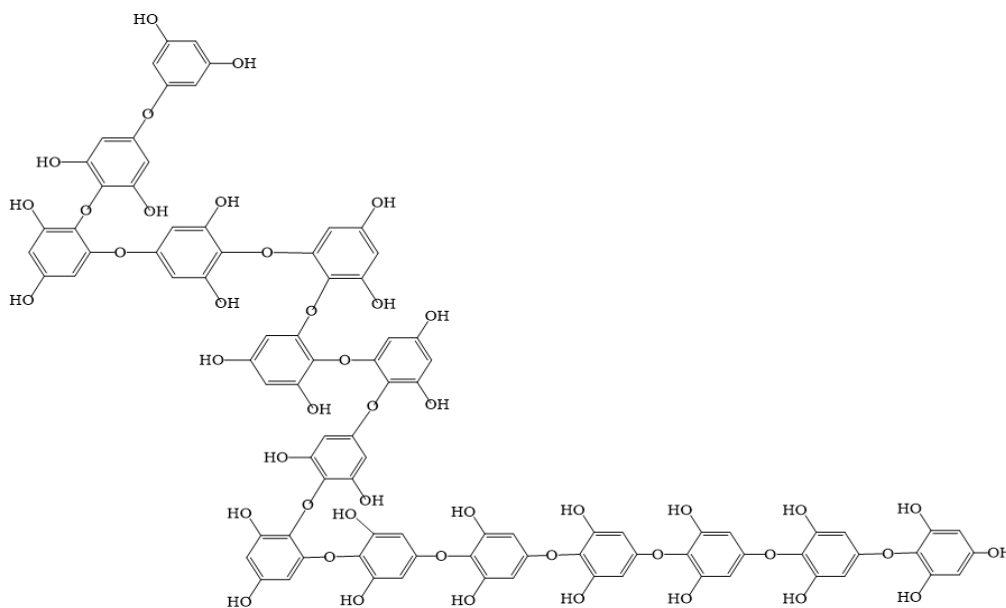


Figure 1-15. Structure of Ishophloroglucin C (IPC)

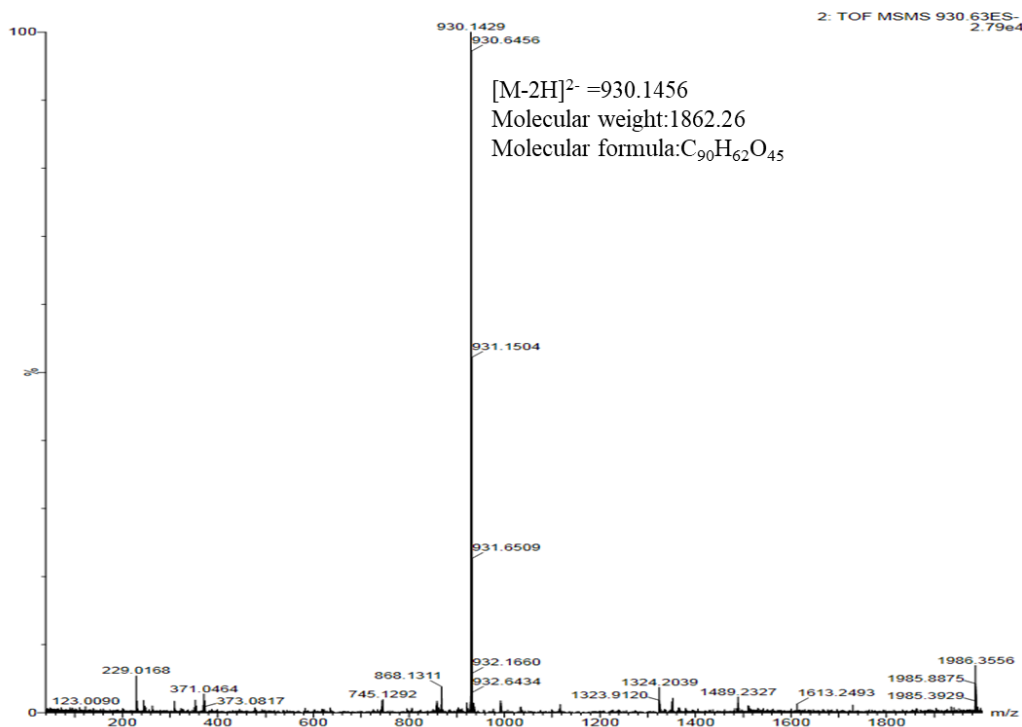


Figure 1-16. MS spectrum analysis of Ishophloroglucin C (IPC), IPC was obtained from ethyl acetate solvent fraction of 50% ethanol extract of brown seaweed *I. okamurae* after through FlashPrep system purification.

Table 4. ¹H, ¹³C and HMQC Data of Ishophloroglucin C (Compound 4)

No	δ_H (mult, J)	δ_C (mult)	No	δ_H (mult, J)	δ_C	No	δ_H (mult, J)	δ_C (mult)	No	δ_H (mult, J)	δ_C
1		156.2(s)	26	5.85(1H,s)	94.7(d)	51	5.85(1H,s)	94.7(d)	76		154.0(s)
2	5.95(1H,d)	94.2(d)	27		151.1(s)	52		154.0(s)	77	5.85(1H,s)	94.7(d)
3		151.1(s)	28		122.0(s)	53	5.85(1H,s)	94.7(d)	78		151.1(s)
4		122.0(s)	29		151.1(s)	54		151.1(s)	79		152.7(s)
5		151.1(s)	30	5.85(1H,s)	94.7(d)	55		123.4(s)	80		123.5(s)
6	5.95(1H,d)	94.2(d)	31		154.1(s)	56		150.8(s)	81		150.8(s)
7		154.0(s)	32	5.85(1H,s)	94.7(d)	57	5.60(1H,d, J = 1.6Hz)	94.1(d)	82	5.70(1H,d)	94.9(d)
8	5.85(1H,s)	94.7(d)	33		151.1(s)	58		153.0(s)	83		152.9(s)
9		151.1(s)	34		122.0(s)	59	5.75(1H,dd, J = 1.8, 1.6Hz)	94.7(d)	84	5.75(1H,d)	94.7(d)
10		122.0(s)	35		151.1(s)	60		152.7(s)	85		122.0(s)
11		151.1(s)	36	5.85(1H,s)	94.7(d)	61		123.4(s)	86		151.1(s)
12	5.85(1H,s)	94.7(d)	37		154.1(s)	62		152.7(s)	87	5.85(1H,s)	94.7(d)
13		154.1(s)	38	5.85(1H,s)	94.7(d)	63	5.75(1H,dd, J = 1.8, 1.6Hz)	94.7(d)	88		154.5(s)
14	5.85(1H,s)	94.7(d)	39		151.1(s)	64		153.0(s)	89	5.85(1H,s)	94.7(d)
15		151.1(s)	40		122.0(s)	65	5.60(1H,d, J = 1.6Hz)	94.1(d)	90		151.1(s)
16		122.0(s)	41		151.1(s)	66		150.8(s)	OH* 8.95-9.34 (31H,m)		
17		151.1(s)	42	5.85(1H,s)	122.0(s)	67		123.4(s)			
18	5.85(1H,s)	94.7(d)	43		152.7(s)	68		150.8(s)			
19		154.1(s)	44		123.5(s)	69	5.60(1H,d, J = 1.6Hz)	94.1(d)			
20	5.85(1H,s)	94.7(d)	45		150.8(s)	70		153.0(s)			
21		151.1(s)	46	5.70(1H,d)	94.9(d)	71	5.75(1H,dd, J = 1.8, 1.6Hz)	94.7(d)			
22		122.0(s)	47		152.9(s)	72		152.7(s)			
23		151.1(s)	48	5.75(1H,dd)	94.7(d)	73		122.0(s)			
24	5.85(1H,s)	94.7(d)	49		122.0(s)	74		151.1(s)			
25		154.1(s)	50		151.1(s)	75	5.85(1H,s)	94.7(d)			

*Recorded in DMSO-*d*₆ at 800 MHz for ¹H NMR and 200 MHz for ¹³C NMR; -OH* : all free phenol hydroxyl groups

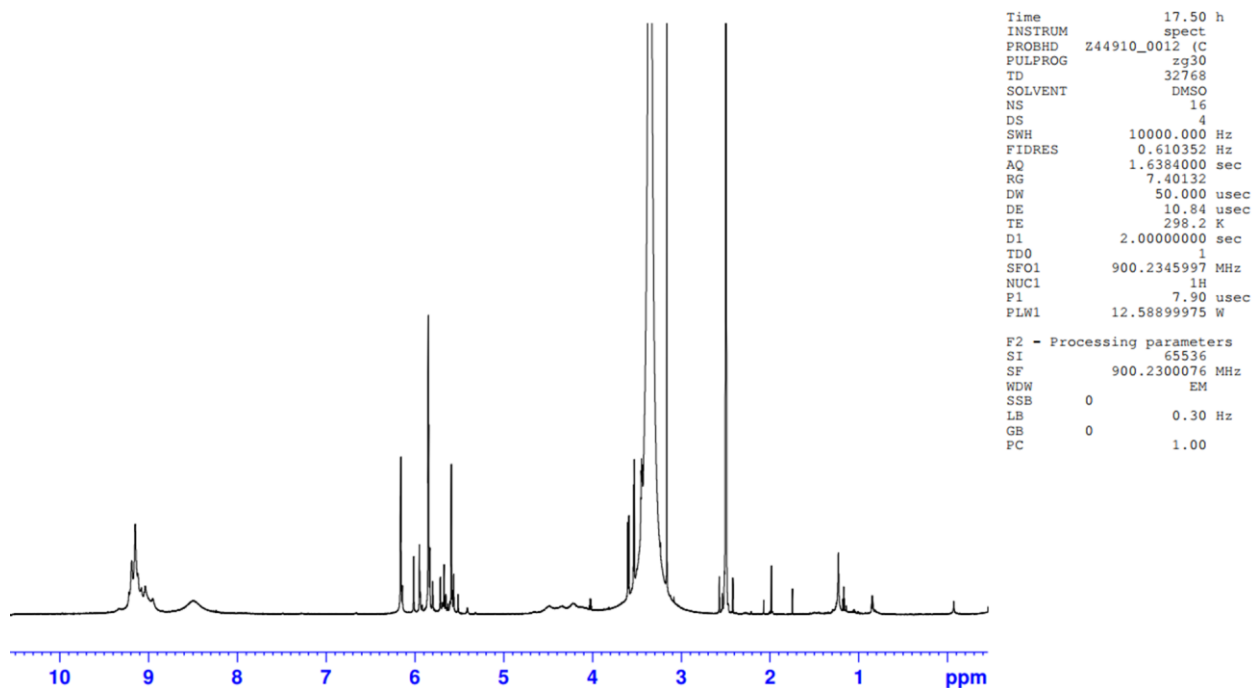


Figure 1-17. ^1H NMR spectroscopy analysis of Ishophloroglucin C (IPC), IPC was obtained from ethyl acetate solvent fraction of 50% ethanol extract of brown seaweed *I. okamurae* after through FlashPrep system purification.

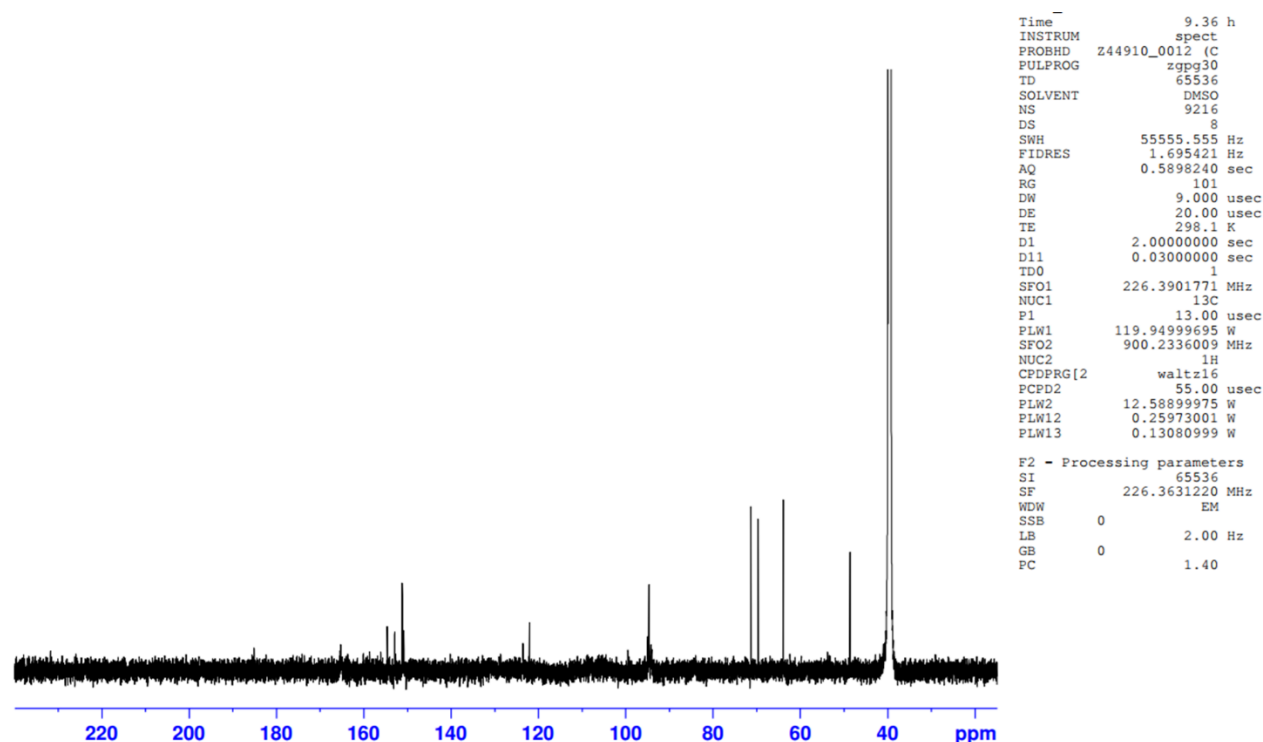


Figure 1-18. ^{13}C NMR spectroscopy analysis of Ishophloroglucin C (IPC), IPC was obtained from ethyl acetate solvent fraction of 50% ethanol extract of brown seaweed *I. okamurae* after through FlashPrep system purification.

Ishophloroglucin D (Compound 5):

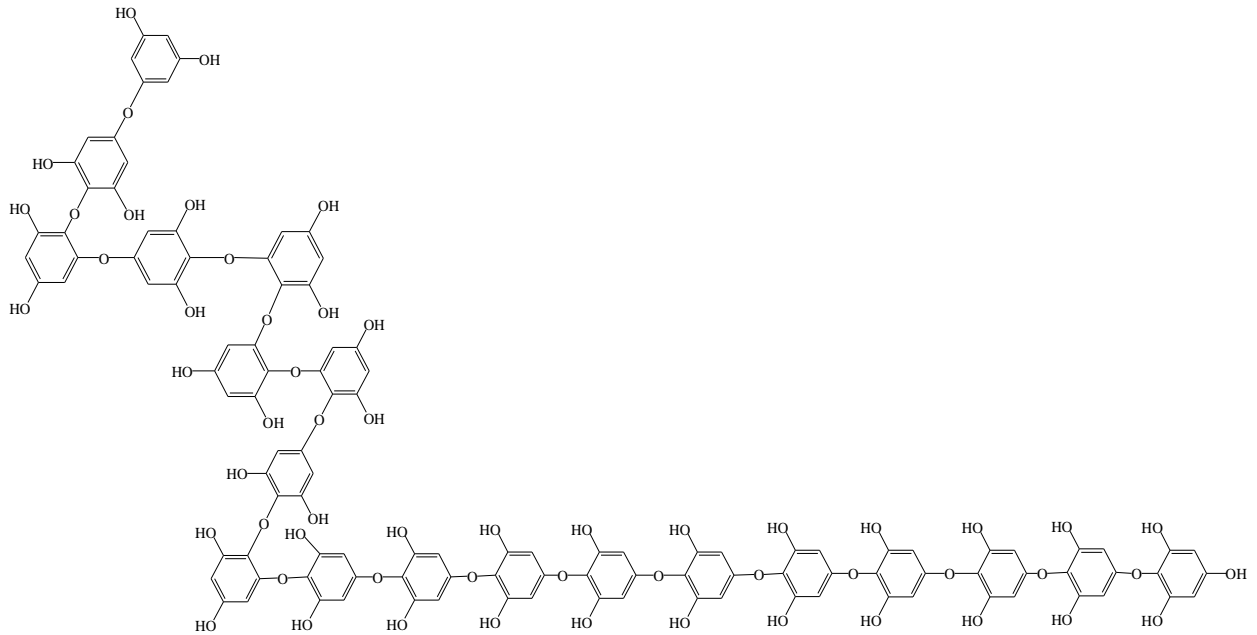


Figure 1-19. Structure of Ishophloroglucin D (IPD)

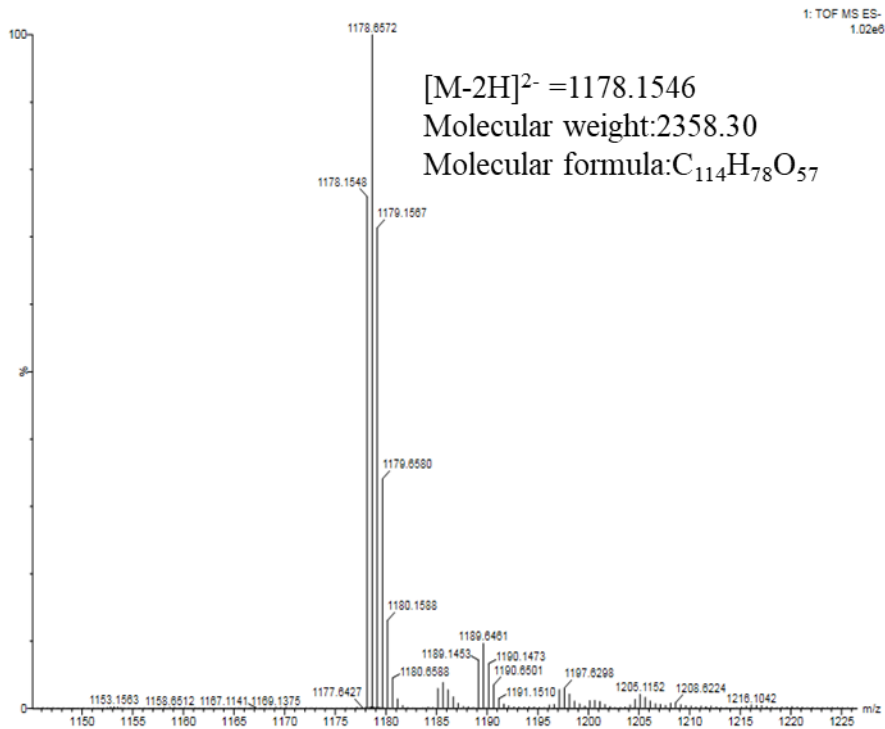


Figure 1-20. MS spectrum analysis of Ishophloroglucin D (IPD), IPD was obtained from ethyl acetate solvent fraction of 50% ethanol extract of brown seaweed *I. okamurae* after through FlashPrep system purification.

Table 5. ¹H, ¹³C and HMQC Data of Ishophloroglucin D (Compound 5)*

No	δ_{H} (mult, J)	δ_{C} (mult)	No	δ_{H} (mult, J)	δ_{C} (mult)	No	δ_{H} (mult, J)	δ_{C} (mult)	No	δ_{H} (mult, J)	δ_{C} (mult)
1		156.1(s)	31		154.1(s)	56	5.85(1H,d)	94.7(d)	86		150.8(s)
2	5.95(1H,s)	94.2(d)	32	5.85(1H,d)	94.7(d)	57		151.1(s)	87	5.59(1H,d, J=1.6Hz)	94.1(d)
3		151.1(s)	33		151.1(s)	58		122.0(s)	88		153.0(s)
4		122.0(s)	34		122.0(s)	59		151.1(s)	89	5.75(1H,dd, J=1.8,1.6Hz)	94.7(d)
5		151.1(s)	35		151.1(s)	60	5.85(1H,d)	122.0(s)	90		152.7(s)
6	5.95(1H,s)	94.2(d)	36	5.85(1H,d)	94.7(d)	61		152.7(s)	91		122.0(s)
7		154.0(s)	37		154.1(s)	62		123.5(s)	92		151.1(s)
8	5.85(1H,d)	94.7(d)	38	5.85(1H,d)	94.7(d)	63		150.8(s)	93	5.85(1H,d)	94.7(d)
9		151.1(s)	39		151.1(s)	64	5.71(1H,d, J=1.8Hz)	94.9(d)	94		154.0(s)
10		122.0(s)	40		122.0(s)	65		152.9(s)	95	5.85(1H,d)	94.7(d)
11		151.1(s)	36	5.85(1H,s)	94.7(d)	66	5.71(1H,dd, J=1.8,1.6Hz)	94.7(d)	96		151.1(s)
12	5.85(1H,d)	94.7(d)	37		154.1(s)	67		122.0(s)	97		152.7(s)
13		154.1(s)	38	5.85(1H,s)	94.7(d)	68		151.1(s)	98		123.5(s)
14	5.85(1H,d)	94.7(d)	39		151.1(s)	69	5.85(1H,d)	94.7(d)	99		150.8(s)
15		151.1(s)	40		122.0(s)	70		154.0(s)	100	5.70(1H,d, J=1.8Hz)	94.9(d)
16		122.0(s)	41		151.1(s)	71	5.85(1H,d)	94.7(d)	101		152.9(s)
17		151.1(s)	42	5.85(1H,d)	94.7(d)	72		151.1(s)	102	5.85(1H,dd, J=1.8,1.6Hz)	94.7(d)
18	5.85(1H,d)	94.7(d)	43		154.1(s)	73		123.5(s)	103		122.0(s)
19		156.1(s)	44	5.85(1H,d)	94.7(d)	74		150.8(s)	104		151.1(s)
20	5.95(1H,s)	94.2(d)	45		151.1(s)	75	5.59(1H,d, J=1.6Hz)	94.0(d)	105	5.85(1H,d)	94.7(d)
21		151.1(s)	46		122.0(s)	76		153.0(s)	106		154.6(s)
22		122.0(s)	47		151.1(s)	77	5.75(1H,dd, J=1.8,1.6Hz)	94.7(d)	107	5.85(1H,d)	94.7(d)
23		151.1(s)	48	5.85(1H,d)	94.7(d)	78		152.7(s)	108		151.1(s)
24	5.95(1H,s)	94.2(d)	49		154.1(s)	79		123.5(s)	109		165.4(s)
25		154.0(s)	50	5.85(1H,d)	94.7(d)	80		152.7(s)	110	6.16(H,s), 6.15(H,s)	94.9(d)
26	5.85(1H,d)	94.7(d)	51		151.1(s)	81	5.75(1H,dd, J=1.8,1.6Hz)	94.7(d)	111		158.7(s)
27		151.1(s)	52		122.0(s)	82		153.0(s)	112	5.95(1H,d, J=1.6Hz)	94.1(d)
28		122.0(s)	53		151.1(s)	83	5.59(1H,d, J=1.6Hz)	94.1(d)	113		158.7(s)
29		151.1(s)	54	5.85(1H,d)	94.7(d)	84		150.8(s)	114	6.17(H,s), 6.16(H,s)	94.9(d)
30	5.85(1H,d)	94.7(d)	55		154.1(s)	85		123.5(s)	-OH*	8.93-9.18 (39H,m)	

*Recorded in DMSO-*d*₆ at 800 MHz for ¹H NMR and 200 MHz for ¹³C NMR; -OH* : all free phenol hydroxyl groups

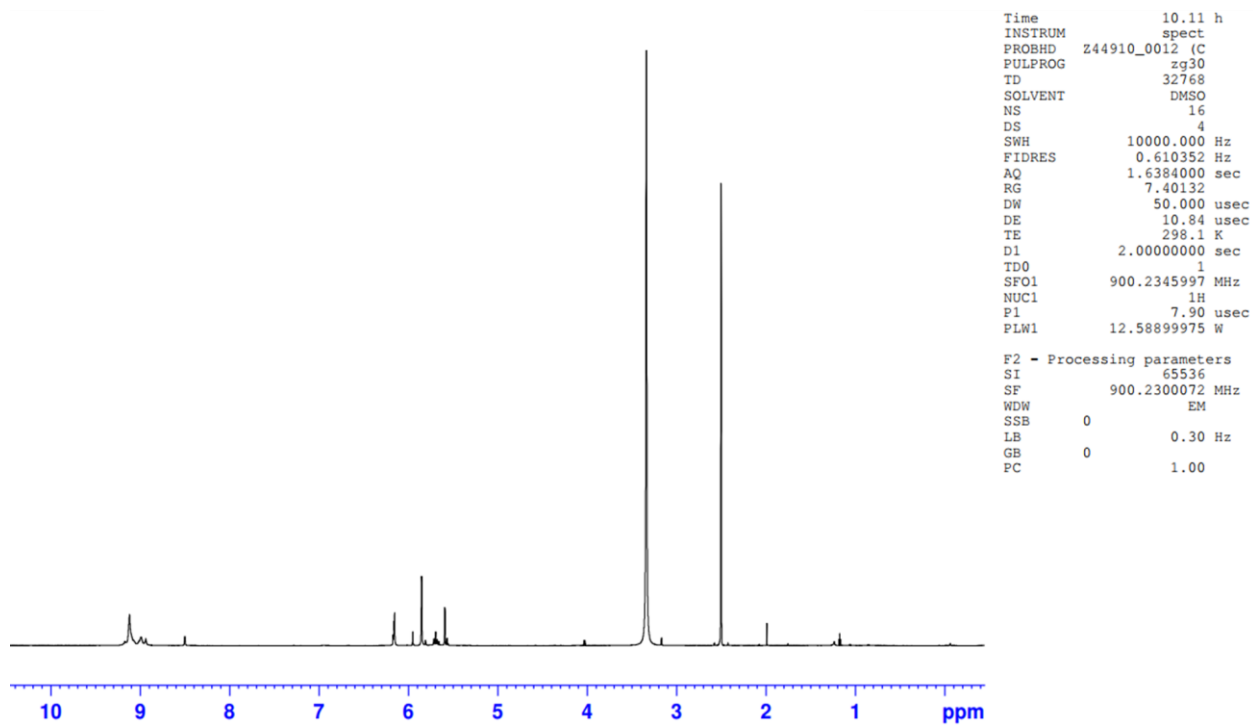


Figure 1-21. ^1H NMR spectroscopy analysis of Ishophloroglucin D (IPD), IPD was obtained from ethyl acetate solvent fraction of 50% ethanol extract of brown seaweed *I. okamurae* after through FlashPrep system purification.

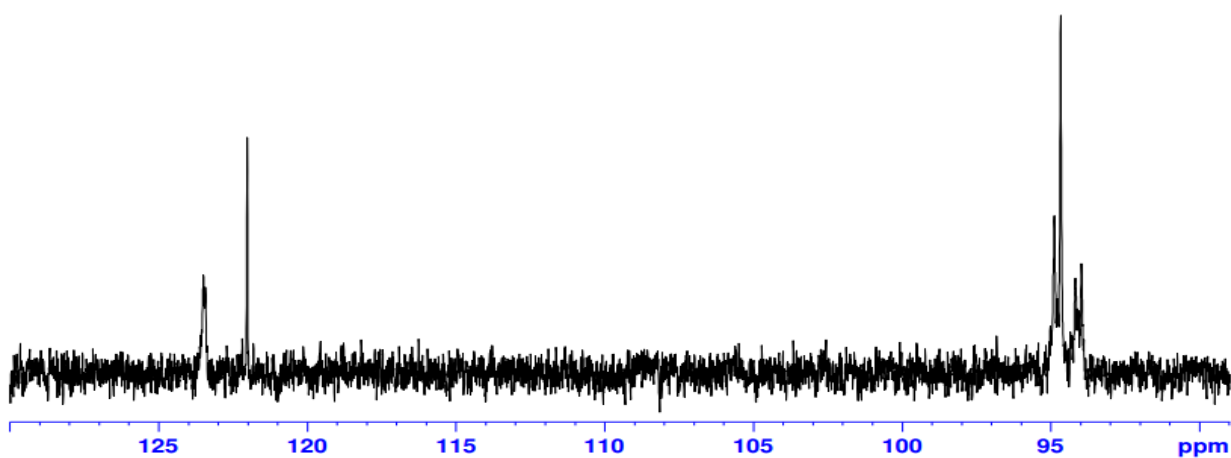
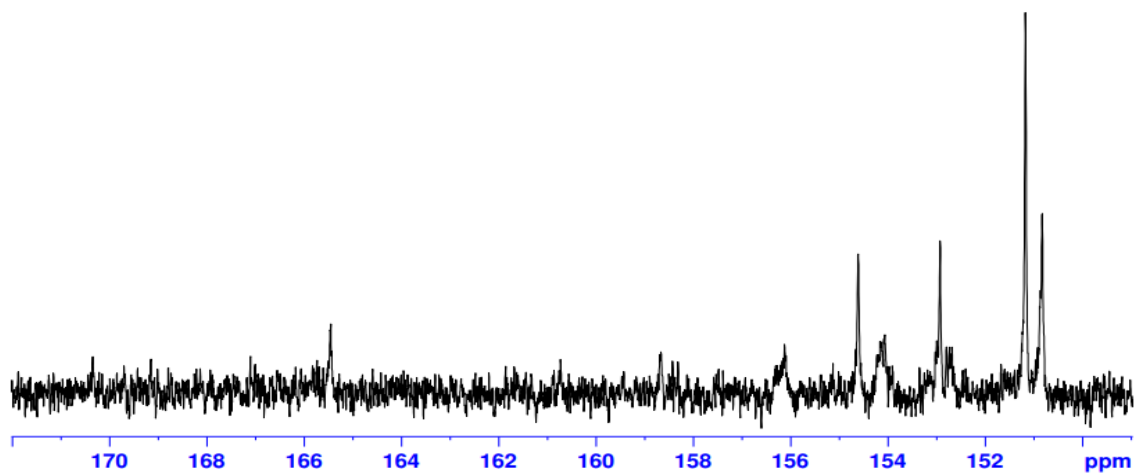


Figure1-22. ¹³C NMR spectroscopy analysis of Ishophloroglucin D (IPD), IPD was obtained from ethyl acetate solvent fraction of 50% ethanol extract of brown seaweed *I. okamurae* after through FlashPrep system purification.

**Section 2: Validation of DPHC by a HPLC method
for the quality control of *Ishige okamurae***

Abstract

This work aimed to develop and validate an analytical method for the quantification of the chemical marker of *I. okamurae*. *I. okamurae* has gained considerable attention as a functional material in industries. In this study, a simple and reliable HPLC method was established and validated for the quantification of DPHC in *I. okamurae*, DPHC was selected as a quantification marker due to it is a remarkable active ingredient and stability in *I. okamurae*. A reversed-phase C18 column was used as a stationary phase and distilled water (0.1% formic acid) and acetonitrile (0.1% formic acid) as the mobile phase. The DPHC were separated in a short run time of 30 min with gradient method of 20-40% acetonitrile (0.1% formic acid) and detected at 230 nm. Peak parameters were acceptable for DPHC. The proposed method has enough linearity with a correlation coefficient > 0.999 within the investigated range for DPHC. Satisfactory precision was achieved with RSD less than 1% for DPHC standards. Reproducibility was also within the acceptable range of RSD $< 1\%$. The limit of detection (LOD) was 0.144 $\mu\text{g/mL}$, and the limit of quantification (LOQ) was 0.435 $\mu\text{g/mL}$ for DPHC. The results show that the proposed method can be used as a readily applicable method for quality control of health functional foods containing the extracts of *I. okamurae*.

1. Introduction

I. okamurae, belongs to the specie of family *Ishige*; it is a kind of brown seaweed as traditional healthy food in Korean and China. previous researches have demonstrated that *I. okamurae* exhibited biological activities such as anti-inflammation, antioxidant, anti-obesity, and anti-diabetes. The current list of compounds found in *I. okamurae* includes the presence of compositions, such as DPHC [9], Ishigoside [10], Fucoxanthin [11], phloroglucinol and 6,6'-Bieckol [12], Methoxylated fatty acid [13]. Previous studies have proven that *I. okamurae* is an important resource of pharmacologically active metabolites with applications in various industries, such as the pharmaceutical, cosmetic, and food industries.

The establishment of method validation is an essential component of Good Manufacturing Practice (GMP) guidelines. HPLC method was established, developed, and validated for the quantification of DPHC in raw materials of *I. okamurae*. To analyze the DPHC from raw materials, the substance or product must be dissolved completely in a solvent. However, the standard maker of DPHC was dissolved in water or methanol, it did not show perfect resolution in HPLC chromatogram, 80% of distilled water is the optimum condition for DPHC. Analytical method validation is an essential component of adherence to current Good Manufacturing Practice guidelines. To quote the US FDA guidelines. The accuracy, sensitivity, specificity, and reproducibility of test methods employed by the firm shall be established and documented.

The purpose of method validation is used to prove that analytical procedures are suitable for their intended use. Analytical test of method validation is performed to ensure that analysis method is accurate, specific, and repeatable that an analyte will be analyzed. The quality control of *I. okamurae* is the determination of the standard marker, which consists of a constituent and present in the seaweed product. The standard marker should be related to their biological activity. Nowadays, several different analytical techniques are applied to identify and quantify these substances, in this study, we used high-performance liquid chromatography (HPLC), which is common method applied to various official standards. This research aimed to develop and validate an HPLC analytical method for the quantification of the standard markers in *I. okamurae*.

2. Materials and methods

2.1. Chemicals

Acetonitrile of HPLC grade and formic acid (FA) were from Honeywell Burdick & Jackson (Ulsan, Korea), the distilled water was obtained from a Milli-Q system (Millipore, Billerica, USA). (DPHC; purity > 95%) and Ishophloroglucin A (IPA; purity > 95%) were produced by You-Jin Jeon professor's lab, Marine life sciences, Jeju National University.

2.2. Analytical instruments and operation conditions

The HPLC analysis was performed using a Waters HPLC system (Millipore, MA, USA) equipped with a separation 2695 module and a 2998 photodiode array (PDA) detector. Chromatography was performed on a reversed-phase Infinity Lab Poroshell 120 EC-C18 (Agilent Technologies) of 4.6×100 mm, 4-Micron. The mobile phase consisted of 0.1% FA in water (solvent A) and 0.1% FA in acetonitrile (solvent B). The gradient method used to follow 0-20 min from 80% to 60% solvent A, the flow rate was 0.3 mL/min. the column temperature was set at 30°C and the sample oven temperature was set at 20°C. The injected volume was 10 µL. The detector was set at 230 nm.

2.3. Sample preparation for HPLC analysis

Stock solutions of DPHC standard prepared at a concentration of 10 mg/mL in 80% aqueous solution of acetonitrile. For powder of *I. okamurae* extract, it was prepared at a concentration of 1 mg/mL in 80% aqueous solution of acetonitrile. the sample solvent was filtered through 0.45 µm membrane filter (Whatman, USA) and injected into the HPLC system.

2.4. Method validation

To establish the validate method, the system suitability testing, and specificity, linearity, precision, and accuracy were evaluated. Six replicate analyses of DPHC of 5 µg/mL were analyzed for system suitability testing. The parameters used for monitoring system suitability which were tailing factor (Tf), plate number (N), % Relative Standard Deviation of peak area (%RSD (pa)), % Relative Standard Deviation of retention time (%RSD (Rt)), resolution (Rs), all calculation equations are following the regulation of United States Pharmacopeia (USP).

System sensitivity was assessed by Limit of Detection (LOD), and Limit of Quantitation (LOQ), Linear regression analysis was assessed for the linearity of the validation method. Specificity was evaluated by comparing the retention times. The precision of the method was evaluated by the repeatability within Intra- and inter-day runs. The relative standard deviation (RSD) of retention time was calculated for the precision. Accuracy was determined using the IOE samples spiked with DPHC (0, 12.5, 25, 50 µg/mL). It was estimated as spike recovery (%), which was calculated using the following equation:

$$\text{spike recovery (\%)} = \frac{(\text{value of spike sample} - \text{value of sample})}{\text{spike amount}} \times 100\%$$

2.5. Statistical analysis

Statistical analysis was conducted using GraphPad Prism 8.30 (GraphPad Software, San Diego, CA, USA). The DPHC contents of the *Lokamurae* samples were compared using one-way analysis of variance (ANOVA), followed by Tukey's test.

3. Results and discussion

3.1. Selection of a quantification marker compound

DPHC and IPA are two major compounds in *I. okamurae*, Figure 2-1 shows the thermal stability of pure DPHC and IPA. According to the thermal analysis of them [17], suggested DPHC as the marker compound in the HPLC quantification method for the *I. okamurae*.

3.2. Method validation

3.2.1. System suitability test and specificity of DPHC

The system suitability testing is used to verify that resolution and system and analysis method are acceptable, The RSD of peak area and retention time for DPHC within 1%. Which proves the suitability of the system and analysis method [18]. As shown in Table 6, the baseline separation expressed as resolution (R_s), the efficiency of the column was expressed by USP tailing factor (T_f), and signal to noise ratio were all within the acceptable range ($R_s > 2.305$, $0.5 < T_f < 2$, and $S/N > 10$). The specificity of DPHC was assessed by comparing the chromatograms of blank (a), DPHC (b), and IOE (c) samples (Figure. 2-2).

3.2.2. The linearity of the method validation for DPHC, LOD, and LOQ

The linearity of the method validation for DPHC was evaluated the amount of eight-point standard curves; with a concentration range of 0.5-100 $\mu\text{g/mL}$, with a correlation coefficient of 0.9999 (R^2), $Y=153.44X - 92.301$. the calculated LOD was 0.144 $\mu\text{g/mL}$, and LOQ value of this method was 0.435 $\mu\text{g/mL}$. all of results were shown in Table 7. Standard curves were constructed triplicate while determining the variability of the slopes and intercepts [19].

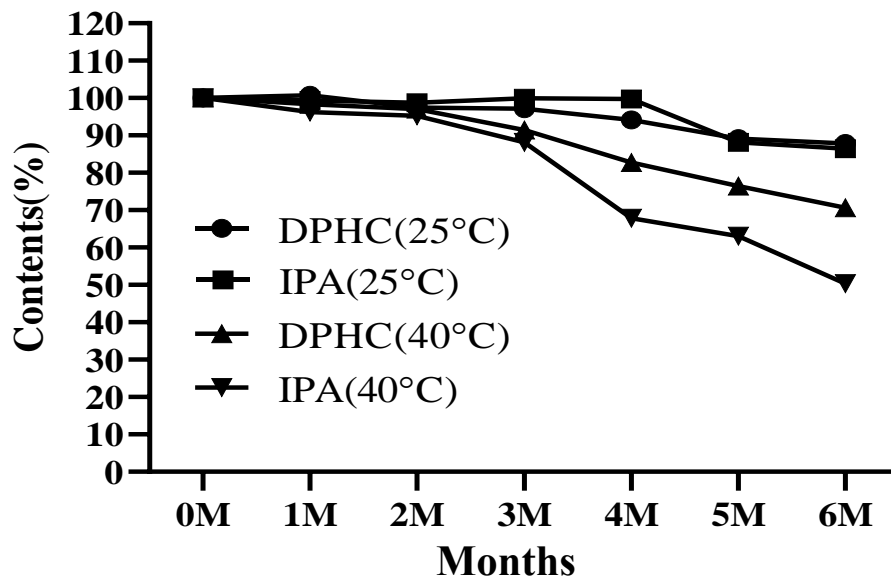


Figure 2-1. Comparison analysis of thermal stability of DPHC and IPA at different temperatures (25 °C and 40°C).

Table 6. Parameters value of system suitability for validation method.

Parameters	Rs	Tf	RSD %(Rt)	RSD %(Pa)	S/N
DPHC	2.305	1.371	0.352<1	0.965<1	116

The values are the average or relative standard deviation (RSD) of DPHC at a concentration of 1 mg/mL using the established method validation parameters calculation for intraday (n = 6). Rs = resolution; Tf = tailing factor; RSD% (Rt) = retention time; RSD% (Pa) = Peak area; S/N = Signal-to-Noise Ratio.

Table 7. Linearity list of the developed high-performance liquid chromatography (HPLC) method for DPHC (n = 3).

Linearity	y=ax+b
Limit of linearity (LOL)	0.5-100 µg/mL
Slope (a)	153.44
Intercept (b)	-92.301
R ²	0.9999
LOQ (µg/ml)	0.435
LOD (µg/ml)	0.144

LOQ: Limit of quantitation, LOD: Limit of detection.

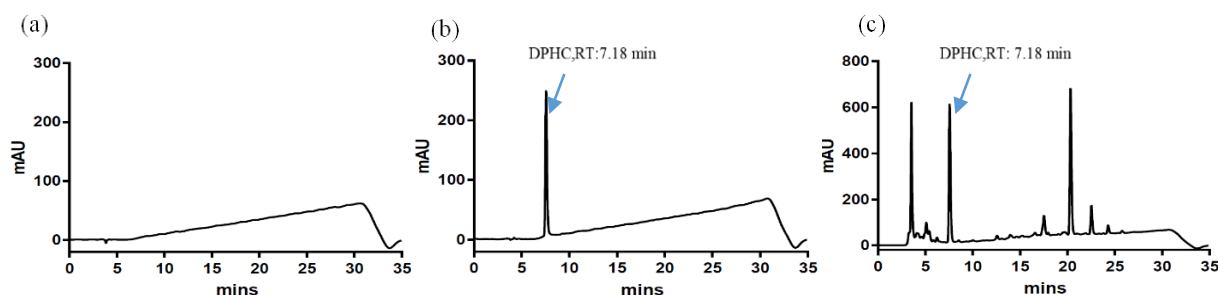


Figure 2-2. The chromatograms showing the specificity of HPLC chromatogram method for DPHC. blank (a), standard DPHC (b), and chromatogram of DPHC (c) in *I. okamurae* extract sample.

3.2.3. The precision and accuracy of DPHC in the method validation

The precision of the validation method was analyzed by analysis of different concentrations of the samples on different days. Precision was determined and shown in Table 8, the percentage relative standard deviation is below 1%, and the accuracy of the method was evaluated by analyzing three spiked samples containing different concentrations of standard DPHC, and accuracy results show in Table 9. Accuracy of method performs is within acceptable limits between 80% and 120% [20]. the accuracy is important to the development of method validation for products. hence all of the validation results well-aligned with FDA regulation.

4. Conclusion

In this study, the reversed-phase HPLC method was established and validated for determination of DPHC in *I. okamurae*. The results have proven that the analysis method is accurate and sensitive for the determination of DPHC in *I. okamurae*. Thus, it is suitable to be used in the quantification of DPHC in seaweed produced with dried extract *I. okamurae*.

Table 8. Results of precision for three analytes at three different concentrations (n = 6).

Batch	0.5 mg/ml	1 mg/ml	2 mg/ml
Day 1	1421.653	3128.062	6247.086
Day 2	1423.549	3143.34	6154.163
Day 3	1432.893	3100.416	6199.332
%RSD(Pa)	0.421	0.696	0.749
Mean %RSD (Pa)	0.622 < 1 % (FDA)		

Table 9. Accuracy of three recoveries with different concentrations to extract of IOE (n =6).

Batch	Sample (µg)	Spike sample (µg)		
#	-	12.5	25	50
1	20.985	34.039	46.804	73.691
2	20.498	34.051	47.625	73.691
3	20.788	33.843	46.670	75.171
Mean % spike Recovery		107.49	106.35	107.82
Mean % spike Recovery		107.2210		
Range % spike Recovery		106.35-107.821		
		FDA: Recovery (100 ± 20%)		

**Section 3: Anti-melanogenesis activity of
Ishophloroglucin A (IPA) from *Ishige okamurae* in
 α -MSH-induced melanoma cells and zebrafish**

Abstract

Ishophloroglucin A (IPA) is a natural product isolated from *Ishige okamurae*; the present study aims to investigate the melanogenesis inhibitory effect of *Ishige okamurae* extract (IOE) and its component of IPA in murine melanoma cells (B16F10), and zebrafish model. IPA significantly inhibited the tyrosinase activity and melanin content dose-dependently in B16F10 cells as well as pigmentation in zebrafish. This polyphenolic compound suppressed the expression of MITF protein expression levels by suppressing the phosphorylation of CREB (cAMP response element-binding protein). Tyrosinase, tyrosinase-related proteins 1 and 2 (TRP1, TRP2) were also evident to be inhibited via IOE and IPA in α -MSH induced melanoma cells. In vivo zebrafish, IOE and IPA significantly attenuated the accumulation of melanin synthesis. According to these results, we suggested that IOE and IPA could be applied in the fields of functional food additives and cosmeceuticals as a skin-whitening agent.

Keywords: *Ishige okamurae*; Anti-melanogenesis; Ishophloroglucin A; Zebrafish model

1. Introduction

Melanin is a dark brown pigment found in the surface, eyes, and hair of humans and animals, it can protect cells from ultraviolet radiation [21]. Melanin is a kind of biological pigment produced by melanocytes, which can be transferred to keratinocytes through the dendritic structure of the cells and rearranged [22]. The melanin particles will also migrate upward into the stratum corneum as the keratinocytes differentiate, and the melanin in the stratum corneum forms pigment deposits on the skin surface [23]. Even though melanin has protective properties, if too much melanin was secreted due to excessive UV irradiation exposure, it will easily lead to abnormal accumulation of pigments, which may cause pigmentation diseases and even increase the risk of malignant melanoma tumors [24]. Previous researches have proven that abnormal accumulation of pigments causes skin diseases including petaloid actinic tanning, solar lentigo, lentigines [25, 26].

In the physiological process of melanogenesis, tyrosinase is a copper ions enzyme, distributed in different organisms of microorganisms, plants, and animals, and it is a crucial enzyme in regulates the metabolic pathway of melanin formation [27]. The enzyme catalyzes melanin synthesis in two distinct reactions in which L-tyrosine is hydroxylated to 3, 4-dihydroxyphenylalanine L-DOPA (monophenolase activity), and the further oxidation of DOPA into dopaquinone [28, 29].

In this study, IOE and IPA from *Ishige okamurae* were investigated in its anti-melanogenic effects, focusing on tyrosinase inhibition activity and their effect on the underlying mechanism, the protein expressions of TYR, MITF, and the phosphorylation of CREB in melanoma cells. Furthermore, we examined the anti-melanogenesis effects of IOE and IPA on in-vivo zebrafish model.

2. Materials and methods

2.1. Chemical and reagents

Dimethylsulfoxide (DMSO), 3-(4,5-dimethylthiazol-2-yl)-2,5-diphenyltetrazolium bromide (MTT), L-DOPA, alpha-melanocyte-stimulating hormone (α -MSH), Arbutin were purchased from Sigma–Aldrich (St. Louis, MO, USA). Primary antibodies including tyrosinase (sc-73244), TRP1 (sc-58438), and TRP2 (sc-74439) were obtained from Santa Cruz Biotechnology (Santa Cruz Biotechnology, CA, USA). MITF (D5G7V), p-CREB (#9198), and CREB (#9197) were purchased from cell signaling. Secondary antibodies (anti-rabbit, anti-mouse IgG) were purchased from Thermo Fisher Scientific (Waltham, MA, USA). All of reagents were analytical grade.

2.2. Preparation of *Ishige okamurae* extract (IOE) and IPA

Ishige okamurae extract (IOE) and IPA were prepared following the method as previously described in section 1. According to our previously validated method of IPA in IOE [30], IOE was used in this study containing $1.81\% \pm 0.362$ of IPA.

2.3. Molecular docking preparation

For docking study, the crystal structure of tyrosinase (PDB: 3NM8) were obtained from Protein Data Bank (PDB, <http://www.pdb.org>) and the docking of the protein-ligand complex, possibility of binding, precise location of binding site and binding energy were examined using Discovery Studio 4.5 software (Accelrys, Inc). Generated the 3D structures of ligands, receptor and optimized the structure by Discovery Studio 4.5 (DS 4.5). IPA and DPHC were evaluated by interaction between receptor (3NM8) and ligands (IPA, DPHC). The comparative analysis

of IPA and DPHC was analyzed according to the CDocker interaction and binding energy (kcal/mol).

2.4. Cell assay

Mouse melanoma cell line B16F10 cells were purchased from ATCC (Washington, DC, USA). Dulbecco's Modified Eagle's Medium (DMEM; Gibco, Carlsbad, CA, USA) supplemented with 10% fetal bovine serum (FBS) and 1% penicillin-streptomycin at 37 °C in a 5% CO₂ a humidified incubator.

2.4.1. Determination of cell viability

Cell survival rate was determined through an MTT assay that measured the mitochondrial activity in viable cells. B16F10 cells were seeded (2×10^4 cells/mL) in 96-well plate, after 24h, the samples were dissolve in DMEM with 1% penicillin-streptomycin, and the cells were treated with various concentrations of IOE and IPA and incubated for another 48h. MTT stock solution (100 μ L; 2 mg/mL in PBS) was added to each well and incubate for 1h, after removing medium, then remove the supernatants gently. The formazan crystals product in each well was dissolved in 200 μ L DMSO. The amount of purple formazan was assessed by measuring the absorbance at 540 nm.

2.4.2. Determination of melanin contents

The melanin contents were determined according to previous published method [31, 32] with slight modifications. In brief, B16F10 cells were plated in a 24-well plate at 2×10^4 cells/mL, the cells were treated with IOE and IPA in presence or absence α -MSH for 48h. Cell pellets were harvested after washing with PBS and then dissolved in 1 N NaOH at 60 °C for 1h and mixed them. Melanin contents were analyzed by measuring absorbance at 450 nm using a

microplate reader (BioTek, United States). For accurate calculation of melanin contents, it was determined by normalizing the absorbance with total protein content. Arbutin (100 μ M) was used as a positive control.

2.4.3. Cellular Tyrosinase activity

The inhibition effect on tyrosinase was measured using previous method with slight modification [33]. Briefly, B16F10 cells were treated with IOE and IPA in presence or absence α -MSH, after 48 h incubation, cells were washed with cold PBS and suspended in a lysis buffer (20 mM Tris, 5 mM EDTA, 10 mM $\text{Na}_4\text{P}_2\text{O}_7$, 100 mM NaF, 2 mM Na_3VO_4 , 1% NP-40, 10 mg/ml Aprotinin, 10 mg/mL leupeptin, and 1 mM PMSF), and Triton-X 100 1.0% in the presence of protease inhibitors (1 μ g/mL leupeptin and 1mM PMSF) and incubated at 4 $^\circ\text{C}$ for 20 min to obtain cell lysates. Then cell lysates were centrifuged at 12,000 rpm and for 10 mins. Protein contents in supernatants were then determined using a bicinchoninic acid (BCA) protein assay kit. Then 90 μ L of cell extract was transferred to a 96-well containing 10 μ L of L-DOPA (final concentration of 1 mmol/L) prepared in 25 mM phosphate buffer (pH 6.8) and incubated at 37 $^\circ\text{C}$ for 20 min. Absorbance was measured at 475 nm by a microplate reader (BioTek, United States).

2.5. In vivo assay

2.5.1. Origin and maintenance of parental zebrafish

Adult zebrafish were purchased from a wholesaler (Seoul Aquarium, Seoul, Korea) and maintained in a temperature-controlled room at 28 $^\circ\text{C}$ with a 14: 10h day/night cycle in each tank. Zebrafish were fed twice per day. Zebrafish were randomly selected for mating in a male-to-female ratio of 2:1. The embryos were collected from the breeding case and washed to

remove any debris lying at the bottom of the tank. The embryos obtained post-spawning were staged and dispensed into embryo media, which contained deionized water with 60 mg/L instant ocean red salts [34].

2.5.2. Zebrafish pigmentation evaluating

The depigmentation effect was determined according to the published method [29, 35], with a slightly modified. Briefly, after 72 h incubated with IOE and IPA, 30 embryos were collected in 1.5 mL eppendorf tubes, placing in -80 °C for 10 min to kill them. Then embryos were sonicated in cold lysis buffer (1% Triton X-100 containing 50 mM PBS with 1 mM PMSF) for 20 min and then lysate was separated by centrifugation at 10,000 rpm for 30 min at 4 °C. The lysate was used to determine the protein content with Bradford assay using BSA as the standard. While the pellet was dissolved in 200 µL of 1 M NaOH at 95 °C for 30 min and the determination of melanin contents was measured by ELISA reader at 450 nm of absorbance.

2.6. Western blot analysis

B16F10 melanoma cells were plated in 60 mm dishes with/without IOE and IPA for 48h and the protein was extracted with Lysis Buffer. An equal amount of protein was electrophoresed in 10% SDS-PAGE. Then the separated proteins were transferred onto PVDF membranes. Then, PVDF membranes were incubated with primary antibody (p-CREB/CREB, MITF, tyrosinase, TRP1, and TRP2, 1:1000 dilution) at cold room for 8h. The membranes were washed two times with tween 20/Tris-buffered saline and incubated with HRP-conjugated rabbit IgG for 120 min (1:3000) at room temperature. The protein bands on PVDF membranes were detected by using an enhanced chemiluminescent substrate. Membranes were captured using a FUSION SOLO Vilber Lourmat system. Signal intensities of protein bands were determined by densitometry using ImageJ (version 1.4).

2.7. Statistical Analysis

The data were analyzed using GraphPad Prism 8 evaluated using two-way ANOVA and Dunnett's multiple range tests. All the experiments were performed three times and expressed as Mean \pm standard deviation (SD). ns; not significant, # $p < 0.05$, ## $p < 0.01$, * $p < 0.05$, ** $p < 0.01$, *** $p < 0.001$, # $p < 0.05$, ## $p < 0.01$.

3. Results

3.1. Molecular Docking analysis of compounds IPA and DPHC

Discovery Studio 4.5 (DS 4.5) program was applied for screening predicted inhibitor candidates from the components of IOE. IPA and DPHC as candidates were docked into the active site of the crystal structure of Tyrosinase from *Bacillus megaterium*(3NM8). IPA and DPHC exert the binding energy is -1359.07 kcal/mol and -391.12. The CDOCKER interaction energy of IPA and DPHC is -195.65 kcal/mol and -80.81 kcal/mol. Therefore, IPA showed the lowest of the binding energy and CDOCKER interaction energy. The molecular docking results demonstrated that IPA was a potent inhibitor of tyrosinase.

3.2. The effects of α -MSH, Arbutin, IOE and IPA on cell viability and melanin synthesis in B16F10 cells

To determine cytotoxic effects α -MSH, Arbutin, IOE, and IPA on B16F10 cells as initial method research, cell viability was measured via the MTT assay. As shown in Figure 3-1. 1nM of α -MSH did not show cytotoxicity and increased the melanin synthesis (Figure 3-1a, c) and 100 μ m of Arbutin were selected as the experiment concentration (Figure.3-1b, d). all of the concentrations of IOE (1,3,10,30 μ g/ml) did not show cytotoxicity (Figure 3-1e) and exhibited an inhibitory effect of melanin synthesis on B16F10 cells (Figure 3-1g), the concentration of IPA (0.5, 1.5, 5 nM) was selected (Figure 3-1f, h) for further research.

3.3. Inhibitory effect of IOE and IPA on Tyrosinase activity and melanin synthesis in α -MSH-induced B16F10 cells

The tyrosinase activity was evaluated in α -MSH-induced B16F10 cells. As shown in Figure 3-2. the tyrosinase activity was significantly increased to 130% compared with control (without α -MSH stimulated) by α -MSH stimulated in B16F10 cells. Arbutin is a kind of commercial whitening agent as a positive control, tyrosinase activity was reduced to 105% compared with α -MSH treatment group. When treated with IOE (3,10, 30 μ g/mL) and IPA (0.5, 1.5, 5 nM) at each concentration, the tyrosinase activities were decreased in a dose depend comparing with α -MSH treatment group in Figure 3-2 a, c. The melanin synthesis was evaluated also, as shown

in Figure.3-2 b, d. Melanin content of arbutin treatment was reduced to 130%, when treated with IOE and IPA at each concentration, the melanin contents were significantly decreased dose-dependently. Those data indicate that IOE and IPA could inhibit melanogenesis in α -MSH-induced B16F10 cells.

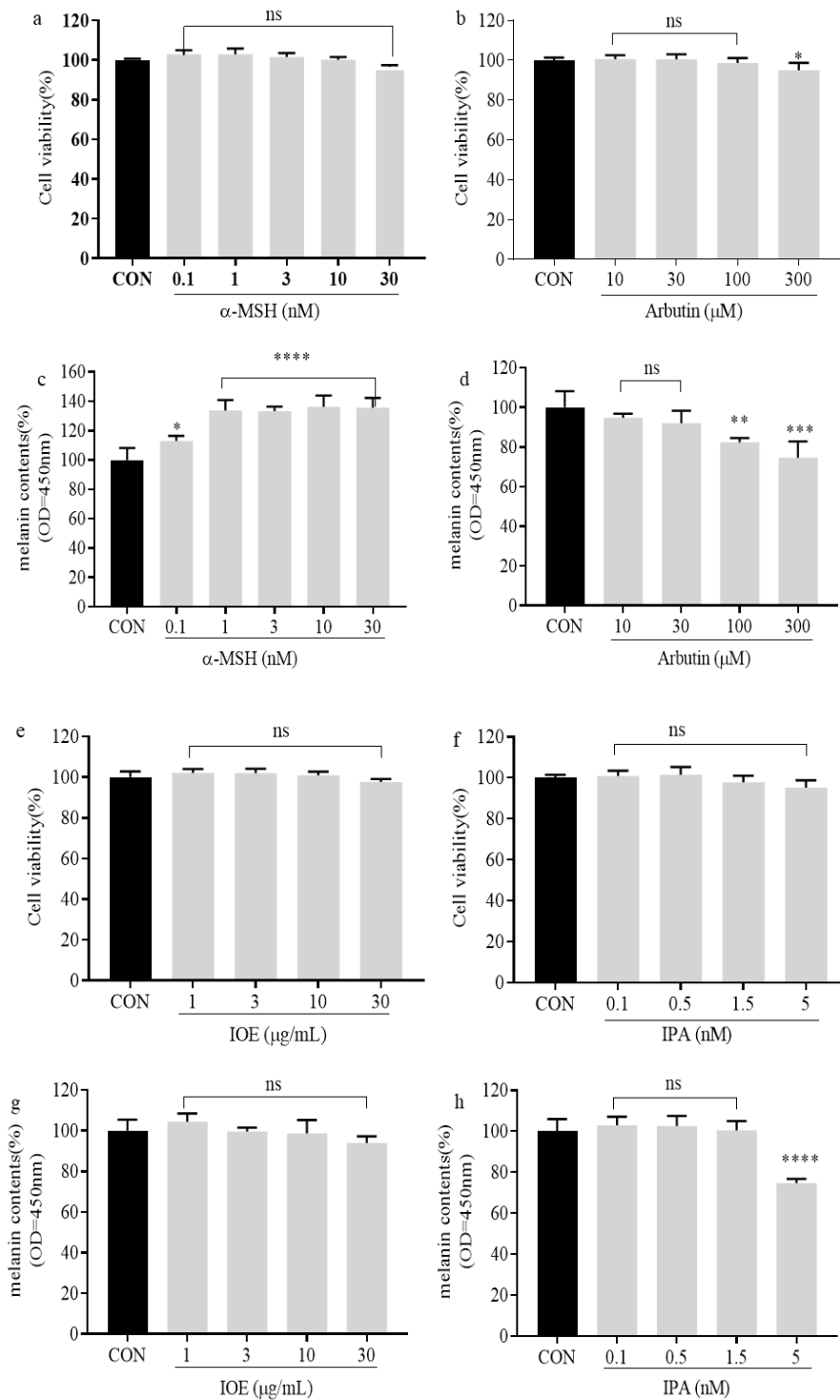


Figure 3-1. The effect of α -MSH, Arbutin, IOE, and IPA on cell viability (a, b, e, and f). Melanin synthesis in B16F10 cells (c, d, g, and h). Each data point represents the mean \pm SE (ns: not significant; * $p < 0.05$, ** $p < 0.01$ by One-Way ANOVA test in GraphPad Prism 8.3.0).

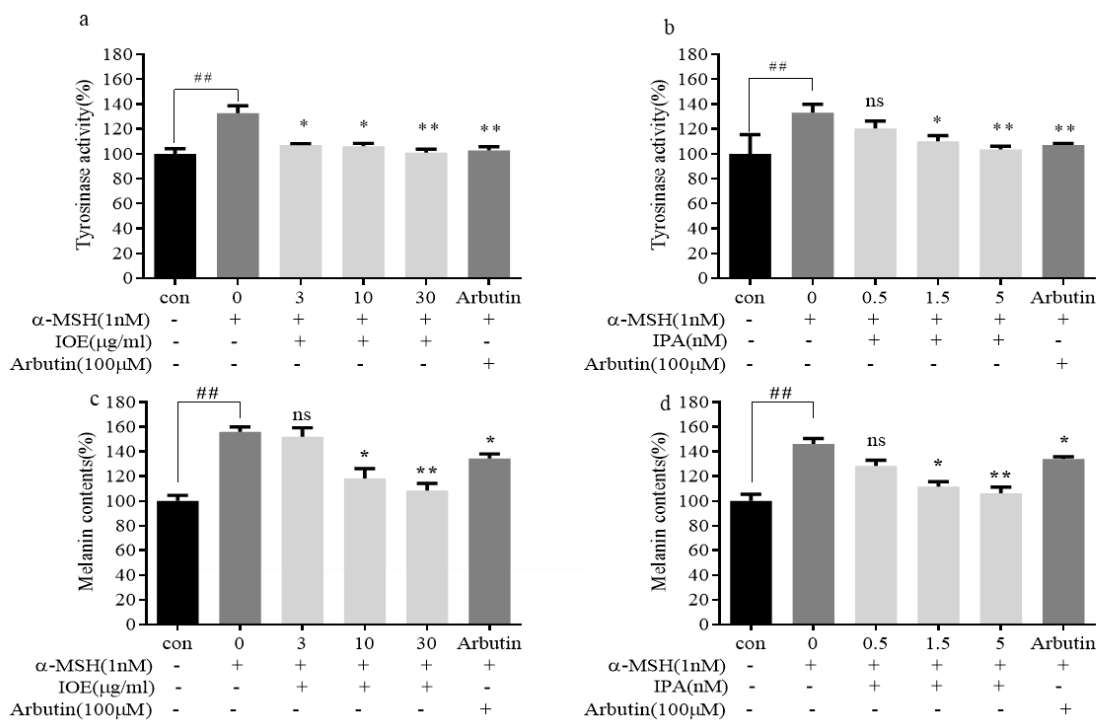


Figure 3-2. IOE and IPA ability for tyrosinase activity inhibition and melanin inhibition on α -MSH-induced B16F10 cells. Cells were treated with various concentrations of IOE and IPA and stimulated with α -MSH. Tyrosinase activity was analyzed using the L-DOPA oxidation assay (a, c). Melanin synthesis was assessed, melanin content is represented compared to the non-treated group as percentage value (b, d). Each data point represents the mean \pm SE (## $p < 0.01$, ### $p < 0.001$, * $p < 0.05$, ** $p < 0.01$, *** $p < 0.001$ by One-Way ANOVA test in GraphPad Prism 8.3.0).

3.4. Western blotting analysis

3.4.1. IPA inhibits melanogenesis through downregulating the expressions of MITF, tyrosinase, TRP1, and TRP2 in α -MSH stimulated B16F10 cells

To examine whether IPA inhibited melanogenesis via regulating the expressions of MITF, tyrosinase family proteins, the effect of IPA on the expression of these enzymes were detected by western blot analysis, as showed in Figure 3-3, the expressions of MITF, tyrosinase, tyrosinase-related protein-1 and 2, were significantly up-regulated by α -MSH treatment, compared with control (without α -MSH treatment). IPA significantly down-regulated the expression levels of melanogenesis-specific proteins MITF, tyrosinase, tyrosinase-related protein 1 and 2 in α -MSH stimulated B16F10 cells in a dose-dependent manner, additionally, the expression levels of MITF, tyrosinase, tyrosinase-related protein 1 and 2 were inhibited more by IPA at 5 nM than by IOE and Arbutin, these results demonstrated that IPA effectively suppressed the expression of MITF, tyrosinase, TRP-1, and TRP-2.

3.4.2. IPA inhibits melanogenesis through downregulating CREB-MITF pathway in α -MSH stimulated B16F10 cells

To examine whether the melanin inhibitory effect of IPA was related to CREB-mediated downregulation of MITF, we investigated the effect of IPA on the expression of phosphorylation CREB, which is a kind of MITF regulator. In Figure 3-4, the expression of phosphorylation CREB was downregulated by IPA in a dose-dependent manner. the expression levels phosphorylation CREB was inhibited more by IPA at nM than by IOE and Arbutin. These results indicate that IPA suppressed melanogenesis through the CREB-mediated transcriptional downregulation of MITF.

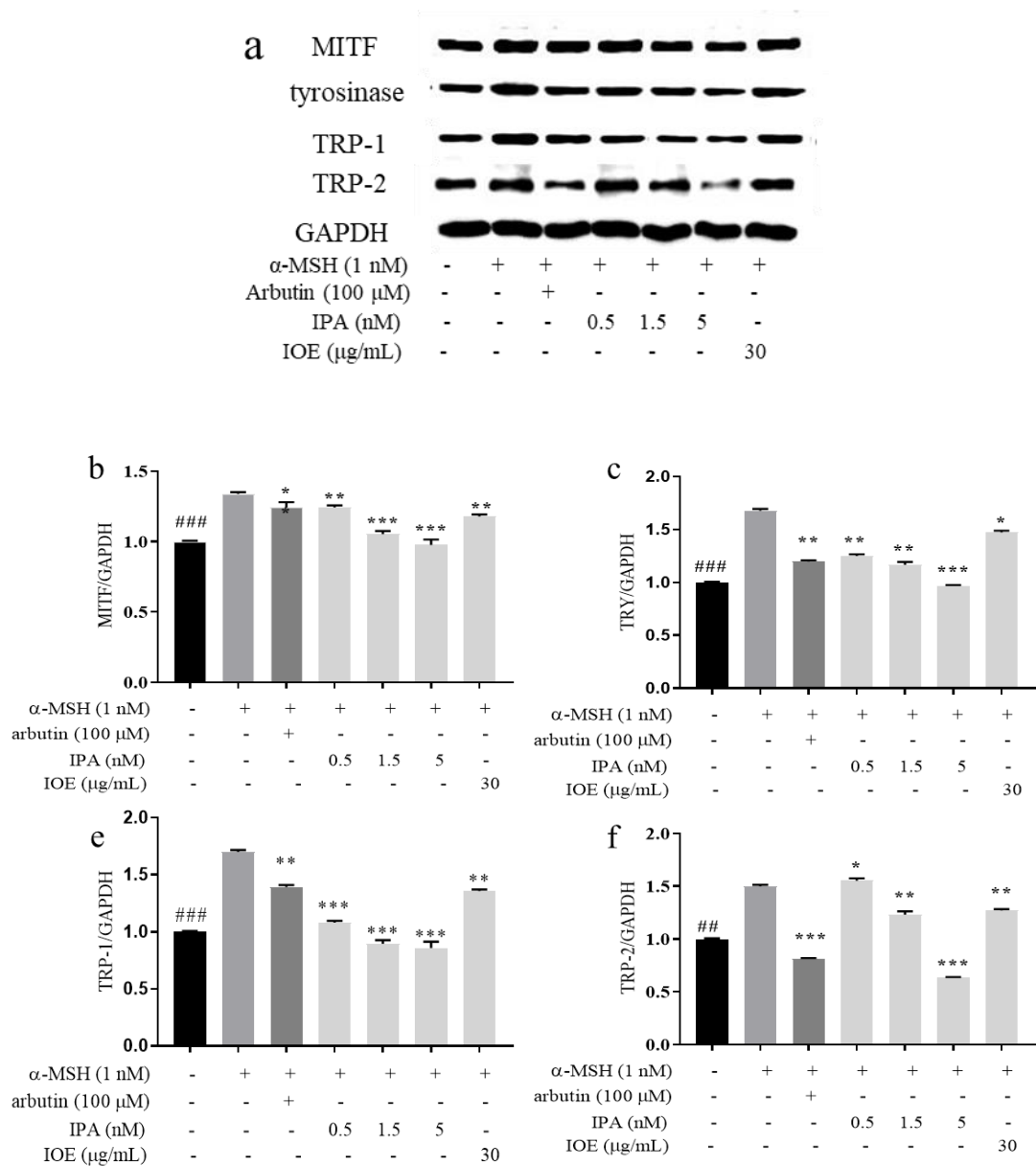


Figure 3-3. IPA inhibits melanogenesis through downregulating the expressions of MITF, tyrosinase, TRP1, and TRP2 in α -MSH stimulated B16F10 cells (a), MITF (b), Tyrosinase (c), TRP1 (d), TRP2 (e). Each data point represents the mean \pm SE (### $p < 0.01$, ### $p < 0.001$, * $p < 0.05$, ** $p < 0.01$, *** $p < 0.001$ by One-Way ANOVA test in GraphPad Prism 8.3.0).

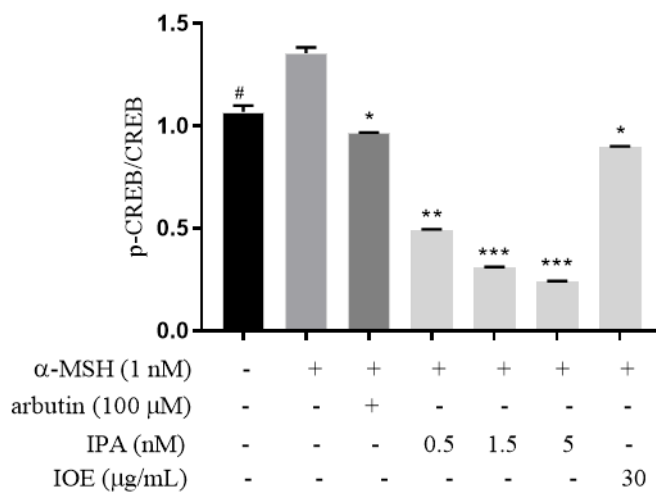
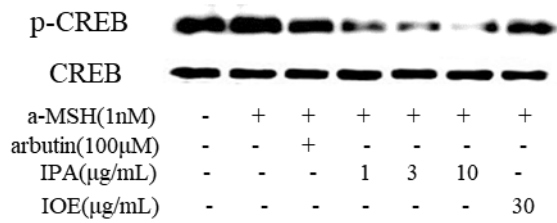


Figure 3-4. IPA inhibits melanogenesis through downregulating the CREB-MITF pathway in α -MSH stimulated B16F10 cells. Each data point represents the mean \pm SE (# $p < 0.01$, * $p < 0.05$, ** $p < 0.01$, *** $p < 0.001$ by One-Way ANOVA test in GraphPad Prism 8.3.0).

3.5. IOE and IPA inhibits melanogenesis in zebrafish

The vivo experiment of depigment effects of IOE and IPA were assessed in α -MSH-induced zebrafish embryos. The toxicity of IOE and IPA was evaluated first, In Figure 3-5(a). 10 μ g/mL of IOE and 1 μ g/mL IPA showed no toxicity significantly in the zebrafish embryos, hence the further experiments were completed following concentrations of 1, 3, 10 μ g/mL of IOE and 0.03, 0.1, 1 μ g/mL IPA in α -MSH-induced zebrafish embryos. Melanin synthesis assay was assessed, as shown in Figure 3-5(b), melanin content was increased to 120 % by α -MSH treatment comparing with control group (without α -MSH treatment), Arbutin treatment reduced melanin formation to 75 % comparing with α -MSH treatment. As for sample treatments of IOE and IPA, the melanin content was significantly decreased in a dose-dependent. These results suggest that IOE and IPA could suppress melanin production significantly and reduced the deposition of the pigment melanin on the whole body.

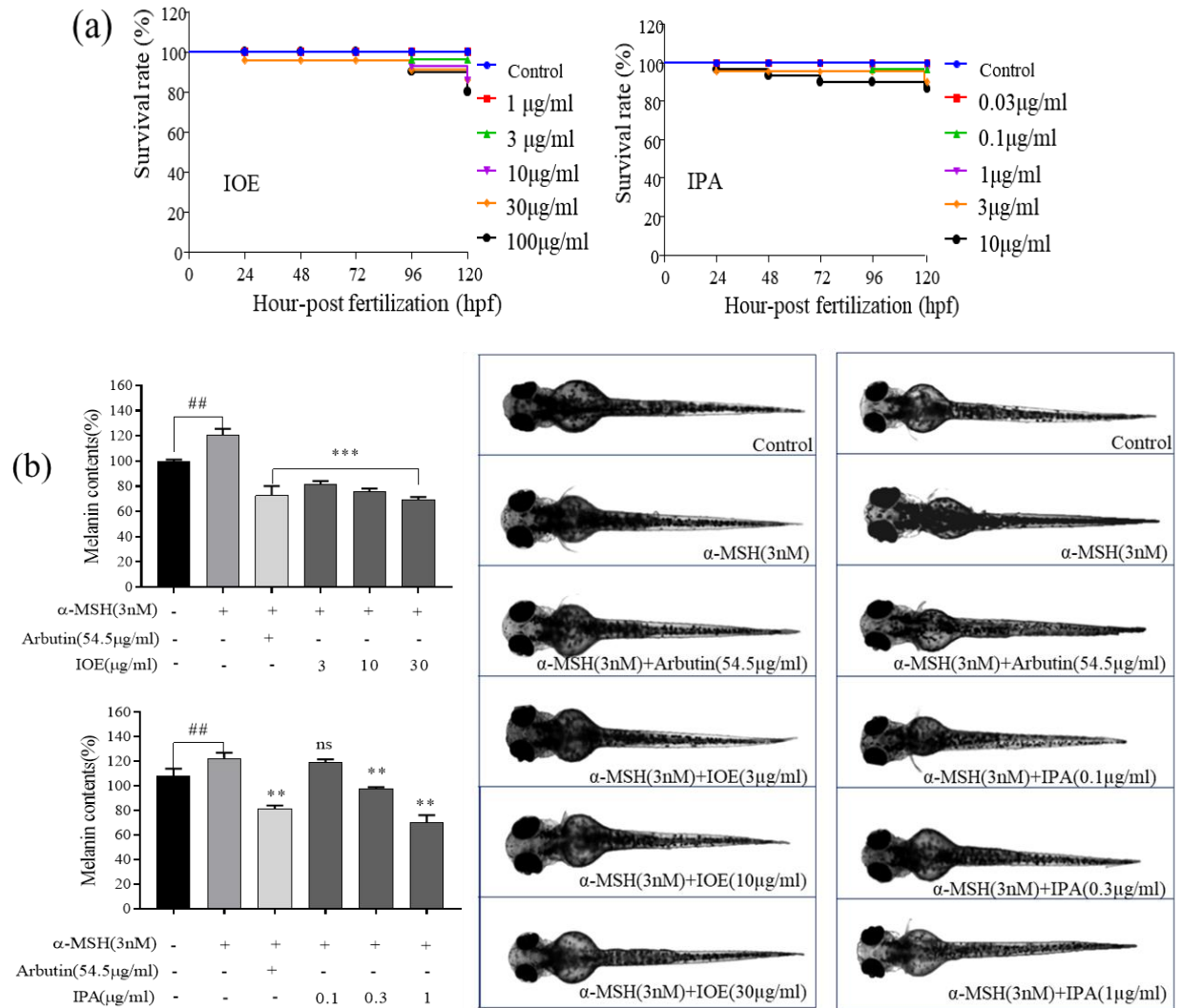


Figure 3-5. The survival rate of IOE and IPA in zebrafish; Inhibitory effect of IOE and IPA on melanin synthesis in zebrafish. (a) The survival rate of IOE and IPA in zebrafish; (b) Inhibitory effect of IOE and IPA on melanin synthesis in α -MSH induced zebrafish. Each data point represents the mean \pm SE (ns; not significant, ## $p < 0.01$, ** $p < 0.01$, *** $p < 0.001$, by One-Way ANOVA test in GraphPad Prism 8.3.0).

4. Discussion

In recent reports have focused on the biological activities and components of marine algae and showed seaweeds compose with a variety of ingredients, including polysaccharides, polyphenols, pigments, and other secondary metabolites [36, 37]. Many of these compositions have been proved to possess diverse biological activities, such as anti-oxidant, anti-inflammation, anti-diabetics, and others [38-40]. In this study, IPA is main active component containing $1.81\% \pm 0.362$ in IOE [30]. IOE and IPA showed inhibition melanin syntheses effects against α -MSH stimulating melanogenesis, to clarify the active compounds and its mechanism of anti-melanogenesis, we examined the inhibitory effects of IOE and IPA on melanogenesis in α -MSH stimulated B16F10 cells and zebrafish model.

MITF regulates the expression of these proteins, a master regulator of melanocyte development, which is revealed as a direct and positive regulator for cell adhesion molecule expression via binding to an M-box motif located in the cell adhesion molecule promoter and subsequently increases the transcription of melanogenic proteins [41]. The expressions of Tyrosinase enzyme, TRP1, and TRP2 were regulated by MITF [42]. We found that IOE and IPA significantly suppressed the expression of MITF. Moreover, the expressions of tyrosinase, TRP-1, and TRP-2 were reduced dose-dependently by increasing the concentration of IPA treatment (Figure 3-3). In the process of melanogenesis, MITF expression was regulated by multiple signaling pathways. Such as MITF gene expression was elevated by activated CREB [43]. In the present study, the expression of phosphorylation CREB was measured (Figure.3-4), IPA significantly attenuated MITF expression through downregulating the expression of phosphorylation CREB [44]. We investigated the effects of IOE and IPA on the pigmentation of zebrafish. Zebrafish is a popular vertebrate model organism with similar organ systems and applied for evaluating the depigmenting activity as a vivo model [45-47]. In the present study, IOE and IPA an inhibitory effect on pigmentation in zebrafish (Figure 3-5). IOE and IPA reduced the melanin formation and inhibited the accumulation of melanocyte on zebrafish.

5. Conclusion

This research suggests that IOE and IPA significantly inhibited tyrosinase activity and melanin synthesis in *in-vitro/in-vivo* models. IOE and IPA suppressed tyrosinase activity and melanin formation. The melanogenesis mechanism is that IPA attenuated the expression of MITF and tyrosinase family proteins through downregulating the expression of p-CREB in α -MSH stimulated B16F10, moreover, the accumulation of melanocyte on zebrafish model was attenuated by IOE and IPA. Therefore, IOE and IPA could be considered to develop as a novel anti-melanogenesis agent to apply in the cosmetics industry.

**Part II. Isolation and identification of α/β adenosine
from *I. okamurae* and its anti-angiogenesis activity**

Abstract

In this study, particulate matter (PM) is becoming a global environmental problem that serious public health. Previous evidence proved that PM correlates to vascular diseases. Their possible effects on angiogenesis remain under-explored. The PM induced angiogenesis was investigated in the vascular endothelial cell line EA.hy926. And the isomers of α and β adenosine were identified from *I. okamurae*, its biological activity was evaluated in PM induced angiogenesis in vascular endothelial cell line EA.hy926 and transgenic zebrafish. The comparative analysis of anti-angiogenesis effect of the mixture α/β -adenosine (1:1) and β -adenosine was investigated, the mixture α/β -adenosine significantly inhibited the cell migration and tube formation in PM-induced EA.hy926 cells. However, β -adenosine did not show significant inhibitory effects on that. Furthermore, the effects of α/β -adenosine and β -adenosine against PM induced angiogenesis was evaluated in zebrafish embryos, the treatment of embryos with α/β -adenosine suppressed PM-induced dilation in the retinal vessel diameter. The results revealed that the mixture of α and β -adenosine (1:1) have potentiality as a treatment for angiogenic.

1. Introduction

Particulate matter (PM) is becoming a global environmental problem that seriously jeopardizes public health. PM can enter the body through various routes when people exposed to air with heavy contamination, including inhalation, eye transport, and skin [48]. PM with potentially toxic metals in aerosols is often present at concentrations well above the natural environmental conditions in Asia [49, 50]. High risk of diseases including lung cancer, chronic respiratory and heart disease, weakening of the immune system, and reduction in lung function is associated with PM [51]. And previous studies have confirmed that PM correlates with multiple systemic injuries, such as inhalation and cardiovascular injuries [52, 53].

The possibility of direct interaction between PM and the target site through blood circulation, PM may seriously harm blood vessels and heart tissue [54]. the cardiovascular system could get further damaged due to PM continuously induce various cytokines in the circulating blood such as inflammatory cytokines or chemokines [55]. Vascular endothelial cells are the first line of the vascular system, the disruption of vascular endothelial function acts as an independent risk factor for cardiovascular diseases. PM-induced oxidative stress increases adhesion molecules expression in human endothelial cells through regulating Akt expression and further promoting monocyte adhesion to endothelial cells [56], these might result in the activation of angiogenesis.

Nucleic acids play an important role in the genetic process of organisms; nucleosides, the building block of nucleic acids, typically exist in nature in α/β configuration, As an isomer of α -nucleoside is extremely rare in nature [57]. Because of their unique and interesting properties such as high stability [58].

Adenosine is an endogenous purine nucleoside present in every cell of the human body [59], It plays an important role in various pathophysiological processes including cardiovascular homeostasis, ischemic pre- and post-conditioning, and inflammation [60, 61]. However, α -nucleosides are extremely rare in nature, with only a few α -isomers of nucleoside or nucleoside derivatives having been reported [62].

In this study, the isomers of adenosine were first time identified from *I. okamurae*, its anti-angiogenesis activity was evaluated in vascular endothelial cell line EA.hy926 and transgenic zebrafish by PM induced.

2. Materials and methods

2.1. Chemicals and reagents

The human vascular endothelial cell line, EA.hy926 was purchased from the American Type Culture Collection (ATCC, Rockville, MD, USA). A CRM certified PM reference material (CRM No. 28 Urban Aerosols) was purchased from the Center for Environmental Measurement and Analysis, National Institute for Environmental Studies, Ibaraki, Japan. Dulbecco's modified Eagle's medium (DMEM) and penicillin, streptomycin was purchased from Gibco Life Technologies, Grand Island, NY, USA. Fetal Bovine Serum (FBS) was purchased from Merck, Sacramento, CA, USA. 3-(4,5-dimethylthiazol-2-yl)-2,5-diphenyltetrazolium bromide (MTT) and Dimethyl sulfoxide (DMSO) were purchased from Sigma, Aldrich, USA. Primary antibodies for Western blot analysis were purchased from Santa Cruz Biotechnology USA. Secondary IgG horseradish peroxidase-linked antibodies were from Santa Cruz Biotechnology (Santa Cruz, CA, USA). All other chemicals and reagents were of analytical grade.

2.2. Plant material

The brown alga *Ishige okamurae* (*I.okamurae*), was collected along the coast of Jeju Island, Korea. The sample was washed three times to remove the salt, and attachment from its surface, after that, seaweeds were kept in a refrigerator at -80 °C. then the frozen sample was lyophilized and grind into powder before extraction.

2.3. Extraction and isolation

I.okamurae powder was extracted three times with 50% ethanol and filtered. The filtrate was evaporated at 37°C to obtain the 50% ethanol extract, which was suspended in distilled water and partitioned with n-Butanol. The n-Butanol fraction was subjected to the ODS cartridge and YMS ODS HPLC column in FlashPrep system (C-850 FlashPrep, BUCHI, Switzerland). The compound B was obtained and purified by high-performance liquid chromatography. And the structure of the target peak was identified the ¹H and ¹³C NMR data and LC-MS/MS, as well as the 2D NMR (HMBC) data.

2.3.1. Identification of α -adenosine and β -adenosine

ESI-MS data revealed that the molecular formula was $C_{10}H_{13}N_5O_4$ at m/z : 268.10 $[M+H]^+$ Molecular weight: 267.10 g/mol, and show that it is a pure compound, however, the 1H and ^{13}C NMR data revealed that it is a mixture of isomer, each signal peaks are double peaks, take the MS data and proton NMR data together (Figure 4-1, 4-2, 4-3, 4-4), compound B was confirmed as an isomer mixture. Therefore, the compound ratios were checked and determined in the mixture using quantitative nuclear magnetic resonance (qNMR), qNMR is based on the fact that the signal intensities of a given NMR resonance are directly proportional to the molar amount of that nucleus in the sample [63], Thus, the calculation of relative peak intensities of NMR plots and relative peak areas of compound pairs in the mixture enables us to determine compound ratios or purity. In the compound B, according to qNMR analysis, the ratio of isomer is 1:1 (Figure 4-3), named compound B as compound B1 and compound B2. According to their coupling constants and reference [64], they were determined to be α adenosine and β adenosine by analyses of HR-ESI-MS, 1DNMR, and 2D-NMR spectral data and comparison with those reported in the literature. This is the first report of these compounds from *I.okamurae*. Its structure is shown in Figure 4-5. 1H and ^{13}C NMR data were designated as below:

α adenosine: Colorless crystal, $C_{10}H_{13}N_5O_4$ at m/z $[M+H]^+=268.10$. 1H -NMR (DMSO-*d*6, 800 MHz), δH (ppm): 8.13 (1H, s, H-2), 8.34 (1H, s, H-8), 7.28 (2H, s, NH_2), 5.96 (1H, d, H-1'), 4.56 (1H, dd, H-2'), 4.27 (1H, dd, H-3'), 4.00 (1H, m, H-4'), 3.96 (1H, dd, H-5').

^{13}C -NMR (DMSO-*d*6, 800 MHz), δC (ppm): 156.1 (C-6), 152.35 (C-2), 149.1(C-4), 139.83 (C-8), 119.19 (C-5), 90.84 (C-1'), 87.66 (C-4'), 81.07 (C-2'), 77.19 (C-3'), 62.53 (C-5'),

β adenosine: Colorless crystal, $C_{10}H_{13}N_5O_4$ at m/z $[M+H]^+=268.10$. 1H -NMR (DMSO-*d*6, 800 MHz), δH (ppm): 8.33 (1H, s, H-8), 8.12 (1H, s, H-2), 7.25 (2H, s, NH_2), 5.95 (1H, d, H-1'), 4.53 (1H, dd, H-2'), 4.26 (1H, dd, H-3'), 3.95 (1H, m, H-4'), 3.66 (1H, dd, H-5').

^{13}C -NMR (DMSO-*d*6, 800 MHz), δC (ppm): 156.0 (C-6), 152.31 (C-2), 149.0 (C-4), 139.80 (C-8), 119.12 (C-5), 90.80 (C-1'), 87.66 (C-4'), 80.57 (C-2'), 76.66 (C-3'), 62.4 (C-5').

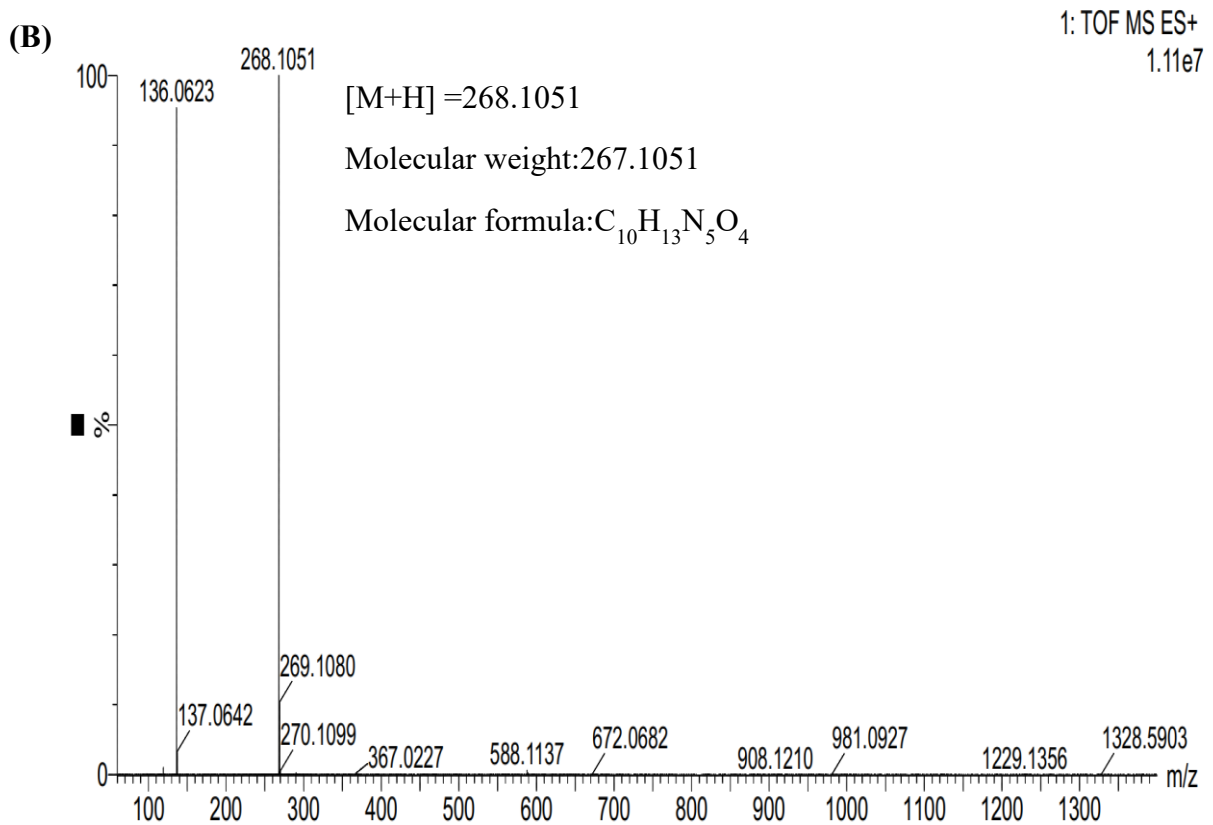
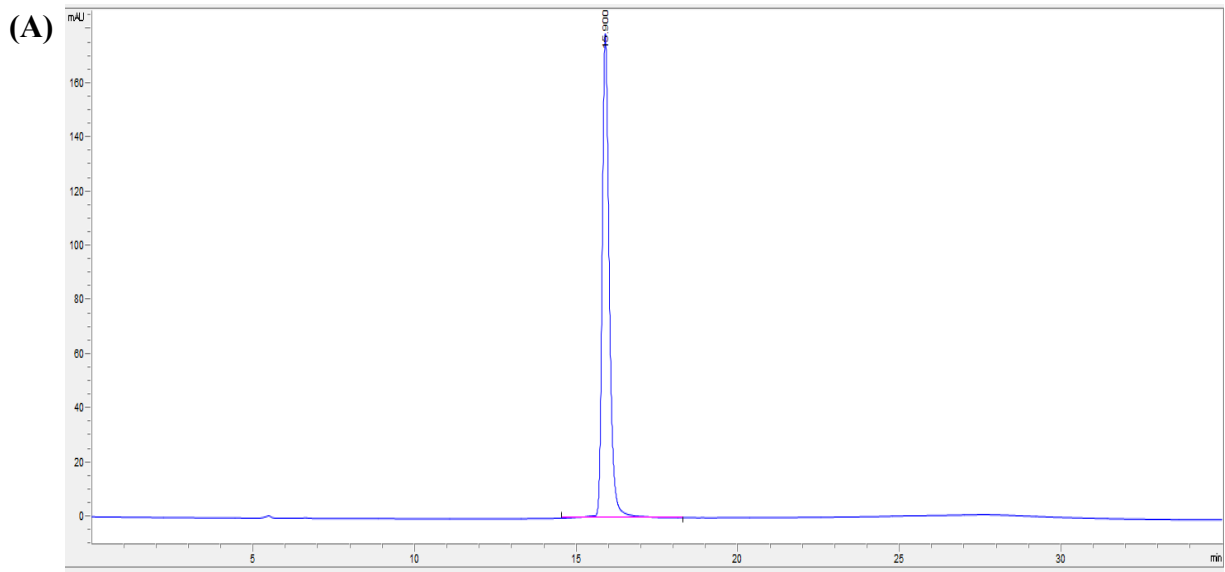


Figure 4-1. HPLC Chromatogram (A) of isomer compound B, and MS chromatogram (B) of the isomer compound B. Compound B was obtained from n-butanol solvent fraction of 50% ethanol extract of brown seaweed *I. okamuræ* after through FlashPrep system purification.

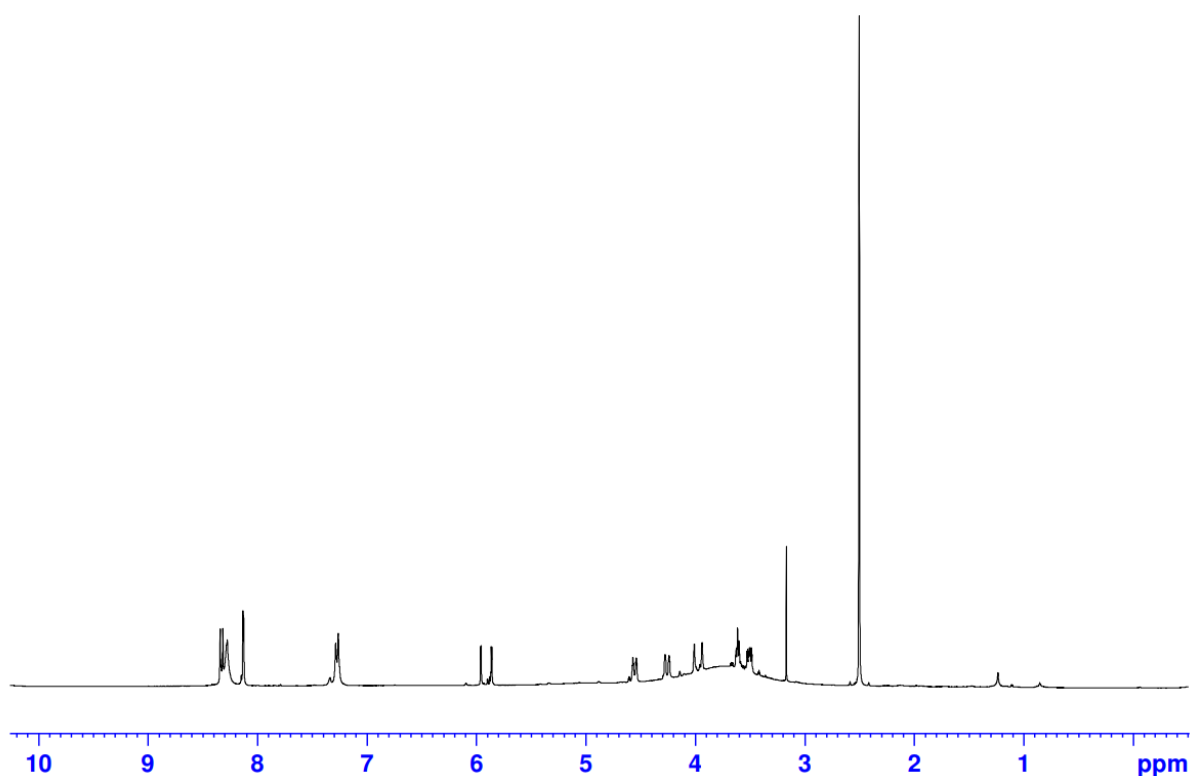


Figure 4-2. ^1H NMR spectroscopy analysis of isomer compound B, compound B was obtained from n-butanol solvent fraction of 50% ethanol extract of brown seaweed *I. okamurae* after through FlashPrep system purification.

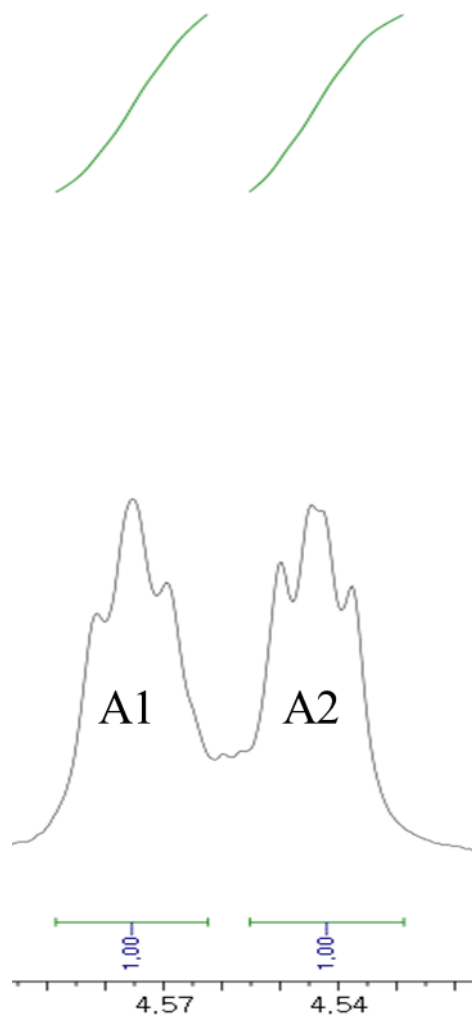


Figure 4-3. qNMR analysis of calculation for the relative percentage of isomer compound B, depending on the signal intensity of NMR, the ratio of isomer was calculated as 1:1.

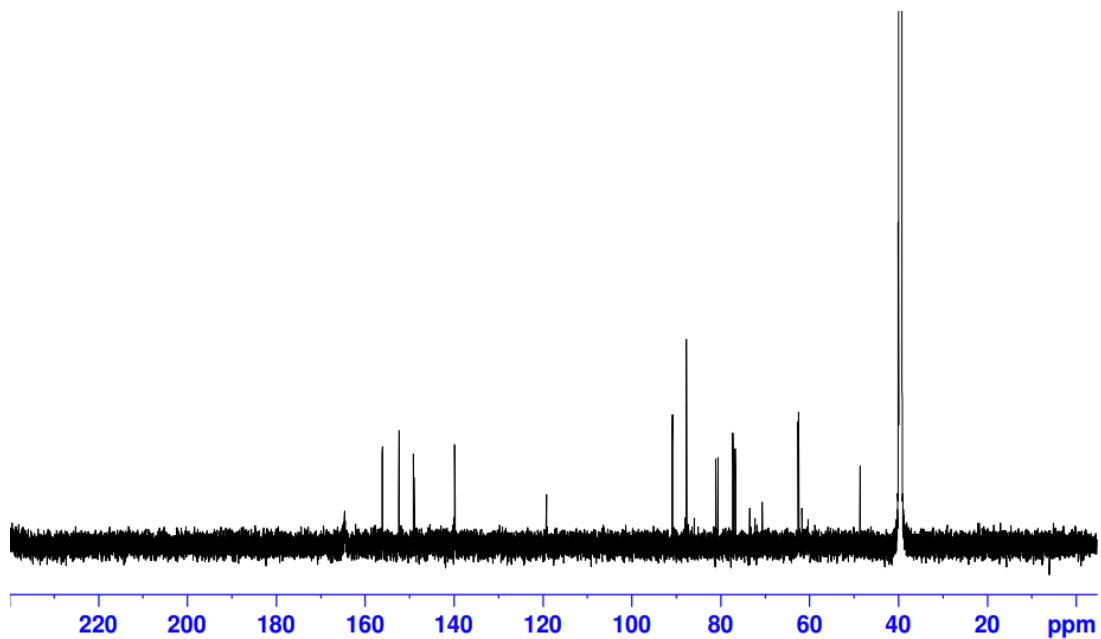


Figure 4-4. ^{13}C NMR spectroscopy analysis of compound B, compound B was obtained from n-butanol solvent fraction of 50% ethanol extract of brown seaweed *I. okamurae* after through FlashPrep system purification.

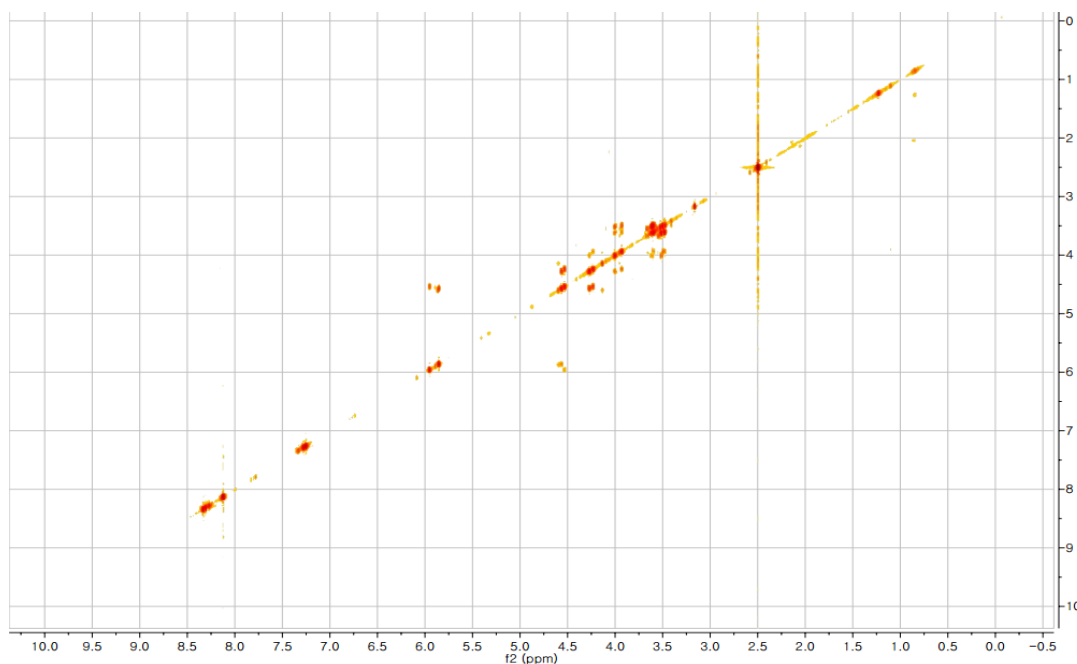


Figure 4-5. Cosy spectroscopy analysis of compound B, compound B was obtained from n-butanol solvent fraction of 50% ethanol extract of brown seaweed *I. okamurae* after through FlashPrep system purification.

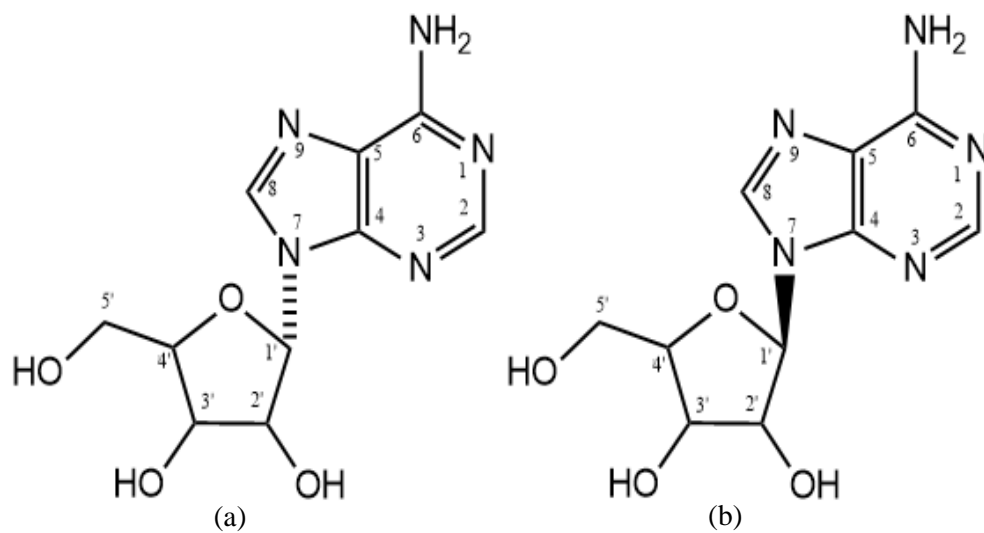


Figure 4-6. The structures of α adenosine (a) and β adenosine (b).

2.4. Cell culture

Vascular endothelial cell line EA.hy926 cells were cultured with DMEM medium supplemented with 10% inactivated fetal bovine serum, penicillin (100 U/ml) and streptomycin (100 µg/mL). Cultures were maintained at 37 °C in a 5% CO₂ incubator.

2.4.1. Cell viability

The cell viability of PM was estimated via a colorimetric MTT method. Cells were seeded into a 96-well plate. After 24 h, the medium was removed and treated with various concentrations (3, 10, 30, and 100 µg/mL) of PM. The cells were incubated for another 24 hours at 37°C. MTT stock solution (50 µL; 2 mg/ml in PBS) was then added to each well. After incubating for 4 h, following removal of MTT, the formazan crystals in each well were dissolved in 100µl DMSO. The amount of purple formazan was determined by measuring the absorbance at 540 nm [65]. The cell viability of samples was evaluated in the same method.

2.4.2. Culture Inserts for the Cell Migration Assay

Cell migration experiment was evaluated following previously method with slight modifications [66]. EA.hy926 cells were equally distributed into Culture-Inserts 2 Well for self-insertion on 6-well plates (1×10^5 cells/well) and given different concentrations of PM (3, 10, 30, or 100 µg/mL). After PM treatment, the cell photos were taken as records and the initial gap length (0h) was measured in the software of Gen 5 3.04 version. After 6h incubation, the final gap length was measured. The gap width was measured at five different places and averaged. To determine the effect of cell migration, the gap closure % was calculated as follows equation [67]. The cell migration assay of samples was evaluated in the same method.

$$\text{Gap closure\%} = \frac{\text{Inihial gap lenth-Final gap lenth}}{\text{Inihial gap lenth}} \times 100\%$$

2.4.3. Tube formation assay

To determine the effect of PM induced capillary formation, according to the previously described method with slight modification [68]. 96 well plates were filled with 75 µL of Matrigel[®] matrix per well and incubated at cell incubator for 30min at 37°C, the harvested

EA.hy926 cells were approximately divided into an equal number of cells (1×10^5) and suspended in different concentrations of PM. After 4h of incubation, each well was taken photos as record and analyzed using the plugin ‘Angiogenesis Analyzer’ of imageJ software. The angiogenic score was calculated as the following equation [69]. The tube formation assay of samples was evaluated in the same method.

$$\text{Angiogenic Score} = \text{Number of braches} \times \text{Total branch length}$$

2.4.4. Western blot analysis

Experiments were performed according to the previous method with slight modification [70]. EA.hy926 cells were seeded, pre-treated for 24h, and then treated with PM (30 $\mu\text{g/mL}$) in the presence of the active compound for the indicated time. After incubation, the cells were collected and washed twice with cold-PBS. The harvested cells were lysed with lysis buffer. Cell lysates were collected by centrifugation, and protein concentrations were determined by using the BCA protein assay kit (Bio-Rad, USA). the lysates were separated on a 12% SDS-polyacrylamide gel and transferred onto a polyvinylidene fluoride (PVDF) membrane (BIO-RAD, HC, USA). After blocking the membranes with 5% skim milk, the membranes were developed with primary antibodies (p-PI3K/PI3K, p-Akt/Akt, eNOS, and β -actin, Santa Cruz Biotechnology) at room temperature for 8 hours. Then membrane was wash with TBST three times, incubated for 2 hours with secondary antibody at room temperature. the Western Blot Chemiluminescent Reagent was used to detect the proteins by a FUSION SOLO Vilber Lourmat system (Paris, France).

2.4.5. Treatments of PM in zebrafish transgenic (flk: EGFP) embryos

Before assessing the vasodilation effect of α/β adenosine and β adenosine on PM induced vasodilation in zebrafish transgenic (flk:EGFP), the survival rate and vasodilation effect of PM were evaluated at first in zebrafish transgenic (flk:EGFP) embryos. 30 embryos were placed in two wells of 12-well plates and maintained in embryo medium water, different concentrations of PM (0.001%, 0.01%, 0.1%), and the survival rate was assessed for 7day post fertilization (dpf). And the vasodilation effect of PM was determined on 7 dpf.

2.4.6. Treatments of α/β -adenosine and β -adenosine in zebrafish transgenic (flk: EGFP) embryos and vasodilation assay

Particulate matter induced vasodilation was developed in zebrafish embryo by maintaining zebrafish transgenic (flk:EGFP) embryos in embryonic water for 3 days. Embryos were treated with various of concentrations of the mixture α/β -adenosine (1, 3, 10 $\mu\text{g}/\text{mL}$) and β -adenosine (1, 3, 10 $\mu\text{g}/\text{mL}$), and stimulated with 0.1% PM, and vessel vasodilation was examined in retinal vessels. After incubated another 4 dpf, images were recorded using a fluorescence microscope (LIONHEART FX automated live-cell imager). Vessel formation in retinal vessels was evaluated by measuring the retinal vessel diameter of the images (10 \times magnification) at 15 different fishes, 10 times in different places using Gen5 3.04 software.

2.5. Statistical Analysis

The data were analyzed using GraphPad Prism 8.30 evaluated using two-way ANOVA and Dunnett's multiple range tests. All the experiments were performed three times and expressed as Mean \pm standard deviation (SD). ns; not significant, # $p < 0.05$, ## $p < 0.01$, * $p < 0.05$, ** $p < 0.01$, *** $p < 0.001$, # $p < 0.05$, ## $p < 0.01$.

3. Results and discussion

3.1. Particulate matter (PM) induced angiogenesis in human endothelial cell line

EA.hy926

Cell viability was determined by the MTT method before check PM induced angiogenic effect. To confirm the concentration of PM that could induce the angiogenesis condition in EA.hy926 cells. EA.hy926 cells were treated with different concentrations of PM (3, 10, 30, 100, 300 $\mu\text{g}/\text{mL}$) for 24 hours, according to the MTT results (Figure 4-7). Its cell viability was decreased at 300 $\mu\text{g}/\text{mL}$, therefore, the concentration of PM (3, 10, 30, 100 $\mu\text{g}/\text{mL}$) was selected to do further confirm whether PM effects on cell migration and tubule formation assay, endothelial cell migration plays an important role in angiogenesis [71], cell migration was expressed as a percentage of gap closure, increased gap closure percentage is indicated that endothelial cell has a higher cell migration [72]. the result is shown in Figure 4-8 that PM treated on EA.hy926 cell significantly increased the gap closure percentage. these results suggested that 30 $\mu\text{g}/\text{mL}$ of PM promotes the cell migration of EA.hy926 cells, thus PM can induce the angiogenic effect. The tube formation assay (capillary-like structure formation) is that endothelial cells retain the ability to migrate rapidly in response to angiogenic signals [73]. To further confirm that PM induced angiogenesis, Tube formation was assessed by growing the cells on Matrigel (Figure 4-9). The angiogenic score was determined for quantitative analysis. The capillary-like tube structure formation was significantly enhanced with 30 $\mu\text{g}/\text{mL}$ of PM treatment. These results suggested that PM conducts the capillary-like structure formation in 30 $\mu\text{g}/\text{mL}$.

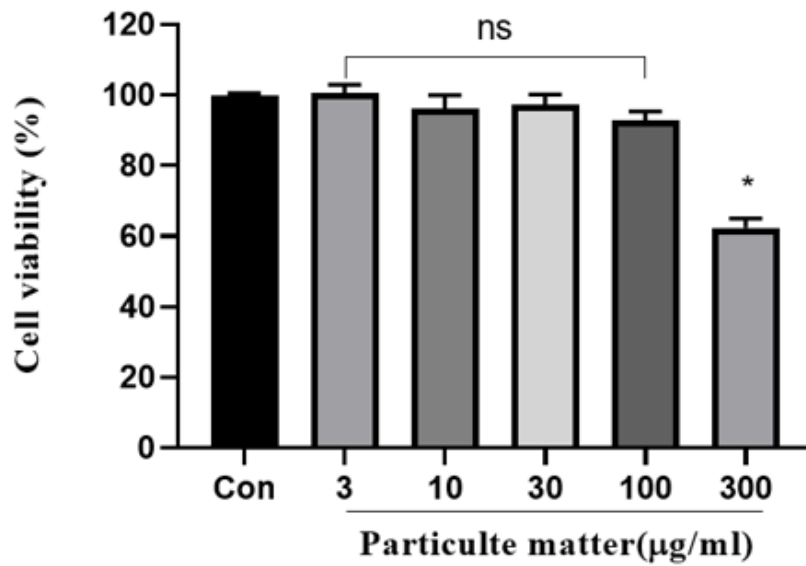


Figure 4-7. Cell viability of particulate matter (PM) in vascular endothelial cell EA.hy926. Cells were exposed to different concentrations of PM for 24 hours, the cell viability was determined by MTT assay. Each data point represents the mean \pm SE (ns: not significant, * $p < 0.05$, by One-Way ANOVA test in GraphPad Prism 8.3.0).

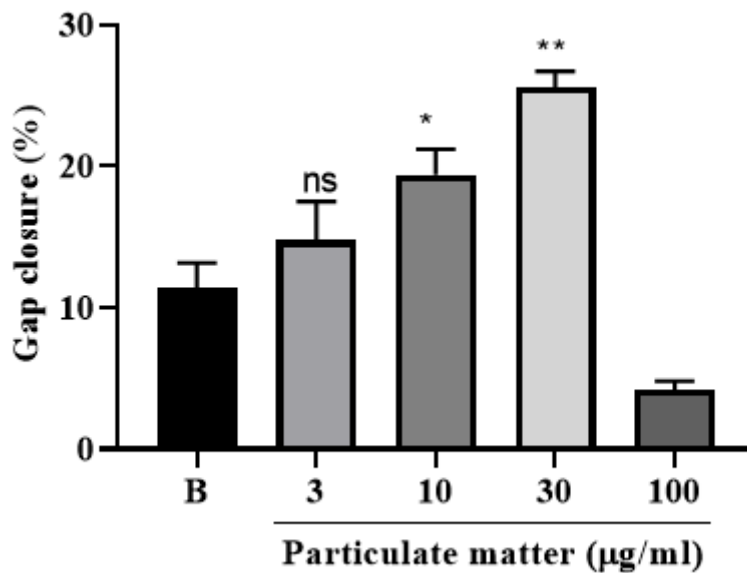
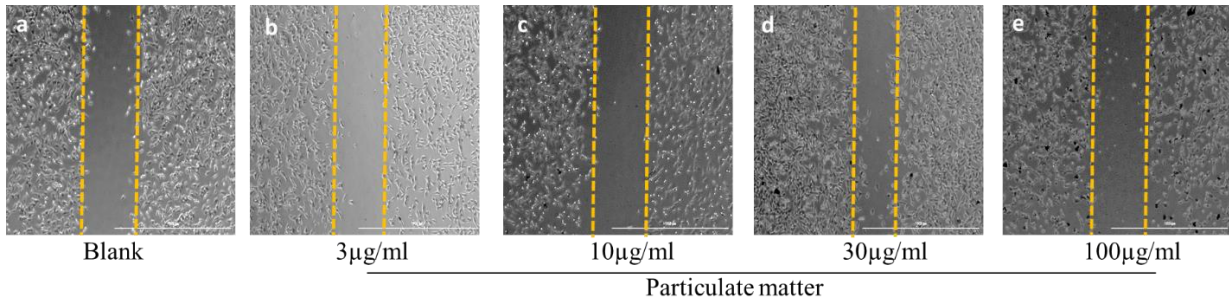


Figure 4-8. The effect of particulate matter induced cell migration on EA.hy926 cells. cells were exposed to PM for 6 hours, the cell photos were taken as records at the initial gap length (0h) and 6h. Cell migration was expressed as a percentage of gap closure. Each data point represents the mean \pm SE (ns: not significant, * $p < 0.05$, ** $p < 0.01$ by One-Way ANOVA test in GraphPad Prism 8.3.0).

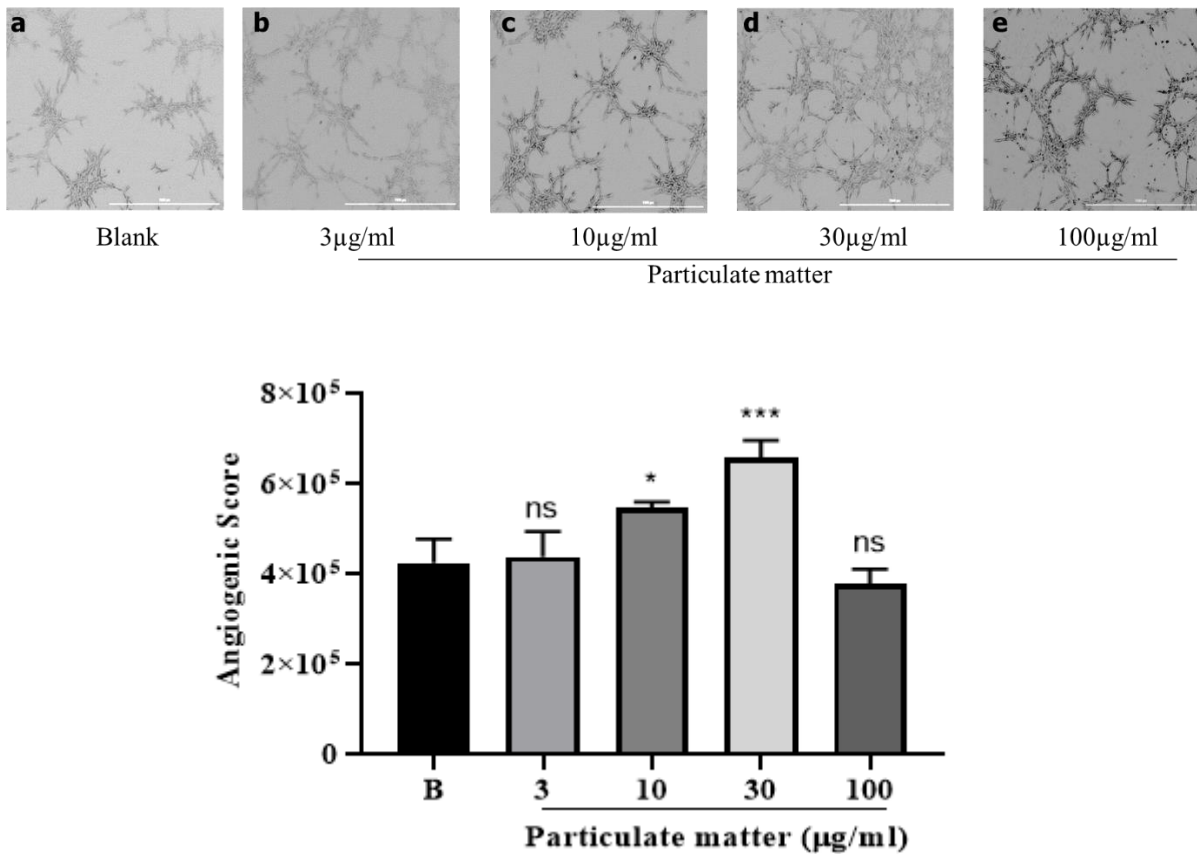


Figure 4-9. The effect of particulate matter induced capillary formation on EA.hy926 cells. the harvest cells were divided into an equal number of cells (1×10^5) and suspended in different concentrations of PM. After 4h of incubation, each well was taken photos as record and analyzed using the plugin ‘Angiogenesis Analyzer’ of imageJ software. The angiogenic score was evaluated the angiogenesis. Each data point represents the mean \pm SE (ns: not significant, * $p < 0.05$, *** $p < 0.001$ by One-Way ANOVA test in GraphPad Prism 8.3.0).

3.2. Cell viability of the mixture of α/β -adenosine and β -adenosine on vascular endothelial cell line EA.hy926

The MTT method was employed to determine the cytotoxicity of the mixture of α/β -adenosine and β -adenosine in EA.hy926. The cells were treated with 0.3, 1, 3, 10 $\mu\text{g}/\text{mL}$ of the mixture of α/β -adenosine and β -adenosine for 24 hours in 96 well plates, separately. Cell viability results shown in Figure 4-9. At 10 $\mu\text{g}/\text{mL}$, both of the mixture of α/β -adenosine and β -adenosine exhibited cytotoxicity. According to this result, the concentrations of 0.3, 1, 3 $\mu\text{g}/\text{mL}$ were selected to evaluate the anti-angiogenesis experiment.

3.3. Inhibitory effect of mixture α/β -adenosine and β -adenosine on PM induced cell migration

To evaluate the angiogenesis effect of the mixture α/β -adenosine and β -adenosine on PM induced angiogenesis, gap closure assay was employed, the results showed in Figure 4-11 and 4-12. Treatment with 30 $\mu\text{g}/\text{mL}$ of PM significantly increased the gap closure percentage (12%), while mixture α/β -adenosine could significantly reduce the gap closure percentage dose-dependently in cells treated with PM, however, β -adenosine did not show the significant inhibition effect on PM-induced cell migration.

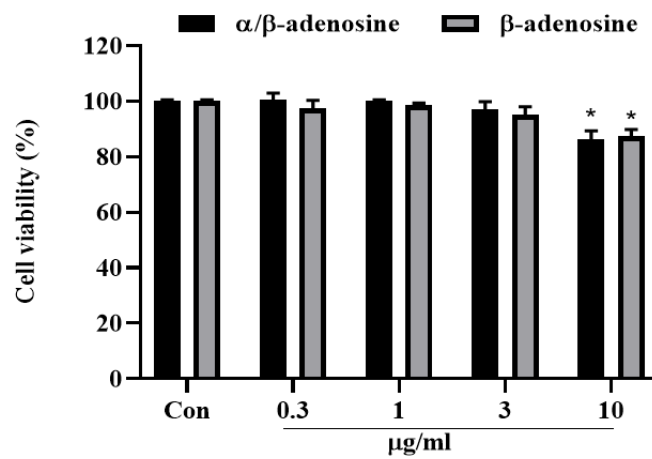


Figure 4-10. Cell viability of the mixture α/β -adenosine and β -adenosine on human endothelial cell line EA.hy926. Each data point represents the mean \pm SE (* $p < 0.05$ by One-Way ANOVA test in GraphPad Prism 8.3.0).

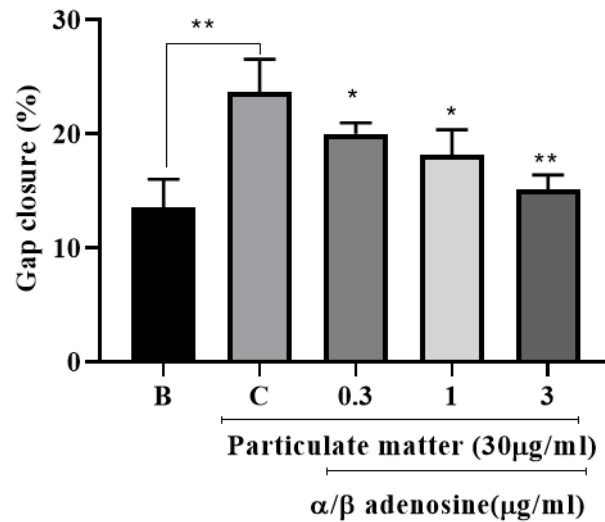
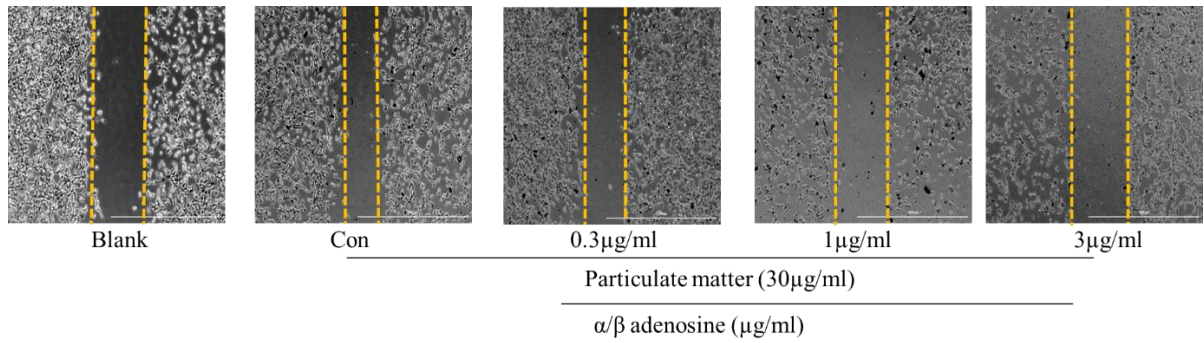


Figure 4-11. The inhibitory cell migration effect of the mixture α/β -adenosine on particulate matter-induced angiogenesis in EA.hy926 cells. Each data point represents the mean \pm SE (* $p < 0.05$, ** $p < 0.01$ by One-Way ANOVA test in GraphPad Prism 8.3.0).

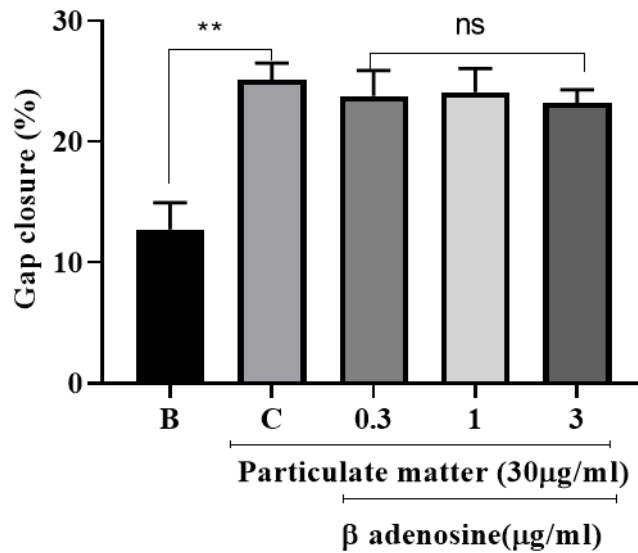
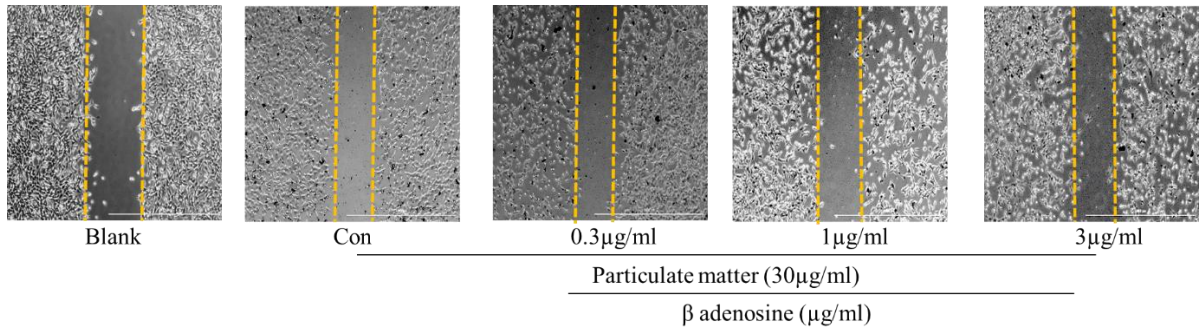


Figure 4-12. The inhibitory cell migration effect of the β -adenosine on particulate matter-induced angiogenesis in EA.hy926 cells. Each data point represents the mean \pm SE (ns: not significant; ** $p < 0.01$ by One-Way ANOVA test in GraphPad Prism 8.3.0).

3.4. Effects of the mixture α/β -adenosine and β -adenosine on capillary formation in PM induced EA.hy926 Cells in Matrigel

To determine whether simulated PM affects the ability of EA.hy926 Cells to form capillary-like tubes, vascular endothelial cells cultured in Matrigel it can differentiate into capillary-like structures. This characteristic feature was used to evaluate the mixture α/β -adenosine and β -adenosine effects on PM-induced capillary-like structure formation (Figure 4-13, and 4-14). The angiogenic score was determined for the quantitative evaluation of capillary formation. An increased angiogenic score is an indicator of higher capillary formation. According to the results, a higher angiogenic score was reported as 1.0×10^6 in the cells treated with $30 \mu\text{g/ml}$ PM. After the mixture α/β -adenosine treatment, the angiogenic score was significantly decreased. However, β -adenosine treatment did not show significant inhibition effect on PM-induced in EA.hy926 Cells, these data suggest that the mixture α/β -adenosine exerts anti-angiogenic effects better than β -adenosine by suppressing capillary formation.

3.5. Effects of the mixture α/β -adenosine on PI3K/Akt/eNOS Signal Pathway

To maintain the integrity of this study, the effect of the mixture α/β -adenosine on the expression of p-PI3K/PI3K, phospho-protein kinase B (p-Akt)/ protein kinase B (Akt), and endothelial nitric oxide synthase (eNOS) was detected by Western blot analysis. As shown in Figure 4-15, PM-induced the expression of p-PI3K/PI3K, p-Akt/Akt, and endothelial nitric oxide synthase (eNOS) was decreased significantly in the cells treated with the mixture α/β -adenosine.

3.6. Particulate matter-induced eyes vessel dilation in zebrafish embryo

The toxicity of PM in transgenic zebrafish (flk:EGFP) embryo was investigated using different concentrations of PM (0.001%, 0.01%, 0.1%). As shown in Figure 4-17a, PM showed no significant toxicity in transgenic zebrafish (flk:EGFP) embryo until 7 dpf. Furthermore, PM treatment significantly increased the retinal vessel diameter. At 0.1% PM, it was selected as a stimulator for zebrafish experiment.

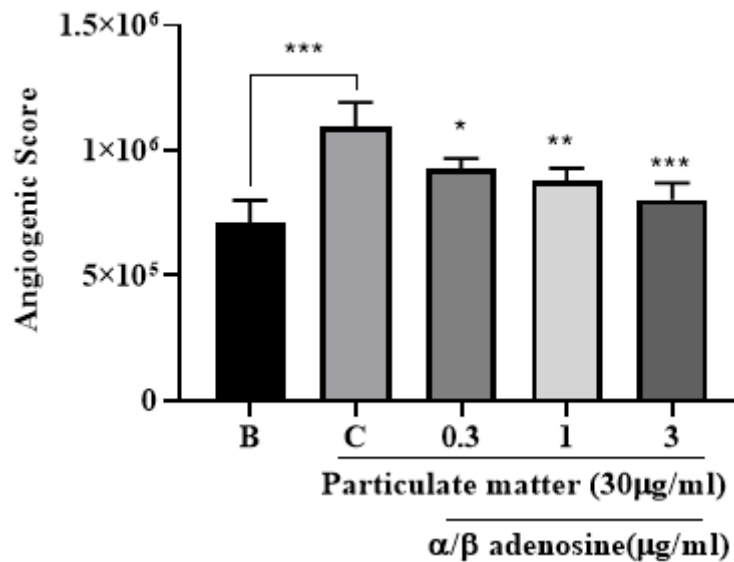
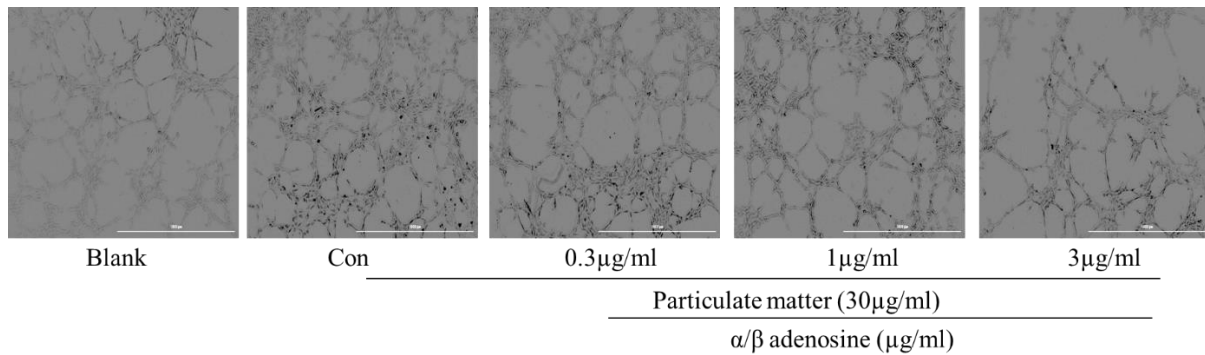


Figure 4-13. Vascular endothelial cells cultured in Matrigel, it can differentiate into capillary-like structures. The angiogenic score was determined for the quantitative evaluation of capillary formation. The inhibitory cell migration effect of the mixture α/β -adenosine on particulate matter-induced angiogenesis in EA.hy926 cells. Each data point represents the mean \pm SE (* $p < 0.05$, ** $p < 0.01$, *** $p < 0.001$ by One-Way ANOVA test in GraphPad Prism 8.3.0).

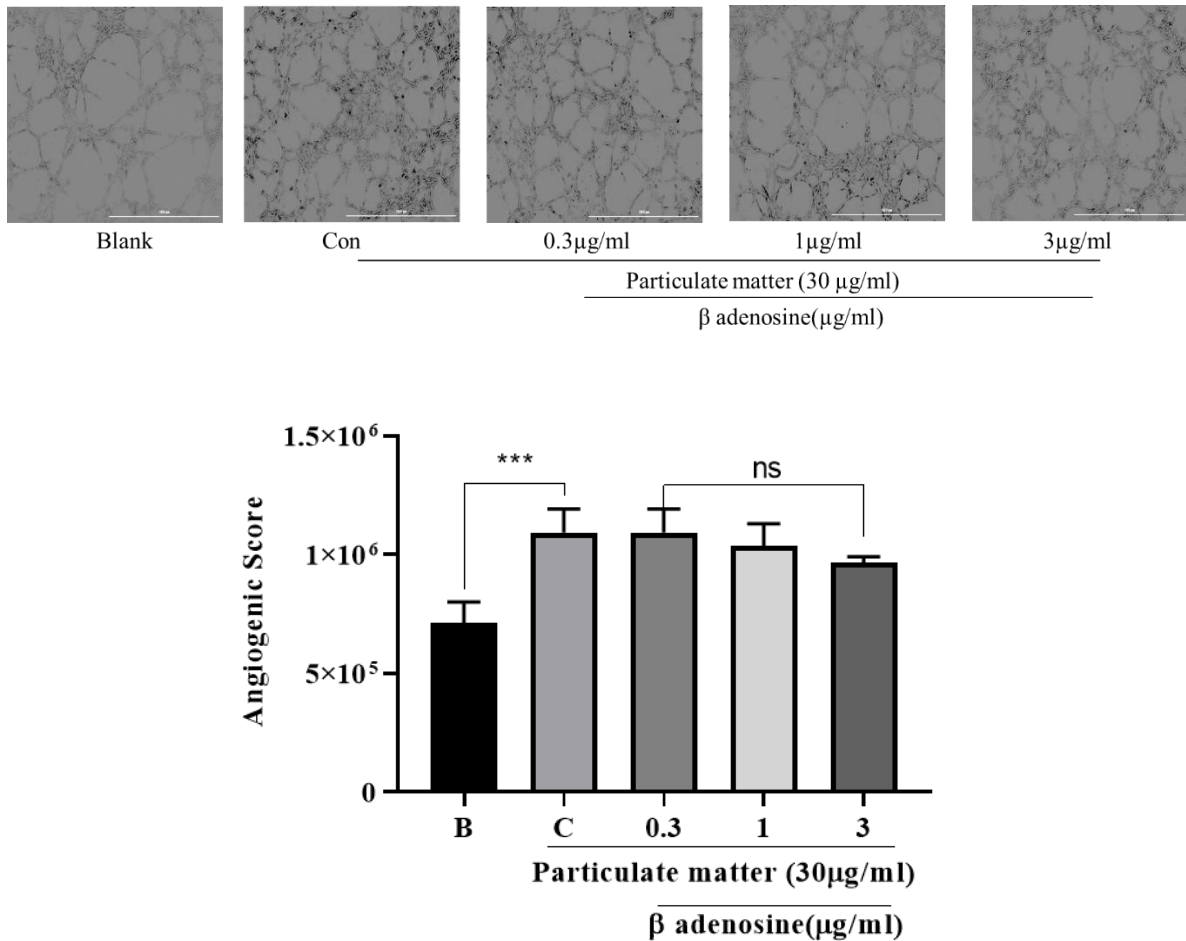


Figure 4-14. Vascular endothelial cells cultured in Matrigel, it can differentiate into capillary-like structures. The angiogenic score was determined for the quantitative evaluation of capillary formation. The inhibitory cell migration effect of β -adenosine on particulate matter-induced angiogenesis in EA.hy926 cells. Each data point represents the mean \pm SE (* $p < 0.05$, ** $p < 0.01$, *** $p < 0.001$ by One-Way ANOVA test in GraphPad Prism 8.3.0).

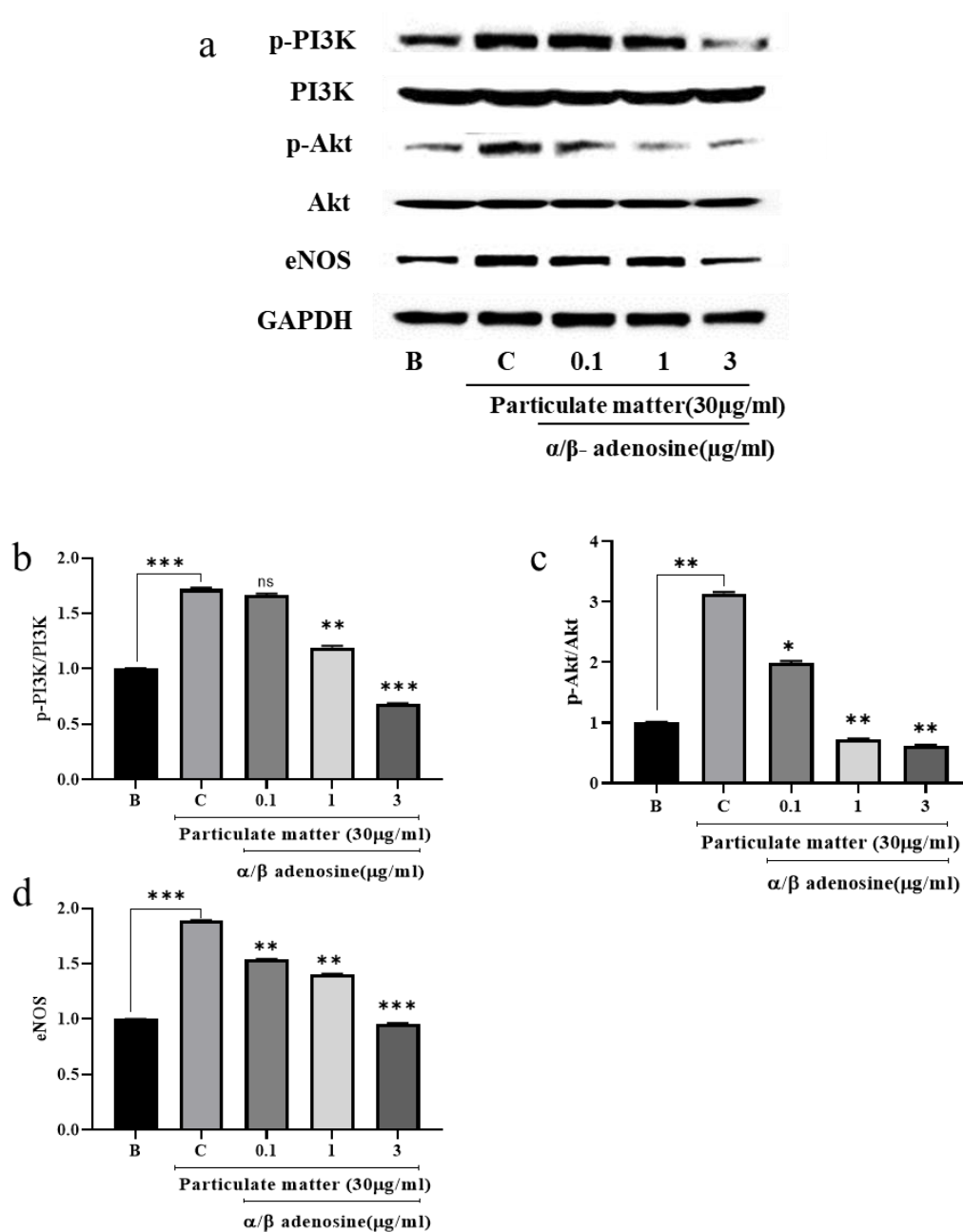


Figure 4-15. The effect of α/β adenosine on particulate matter downstream signaling pathway, b: p-PI3K/PI3K; c: phospho-protein kinase B (pAkt)/ protein kinase B (Akt); d: endothelial nitric oxide synthase (eNOS) were detected by Western blotting. Each data point represents the mean \pm SE (* $p < 0.05$, ** $p < 0.01$, *** $p < 0.001$ by One-Way ANOVA test in GraphPad Prism 8.3.0).

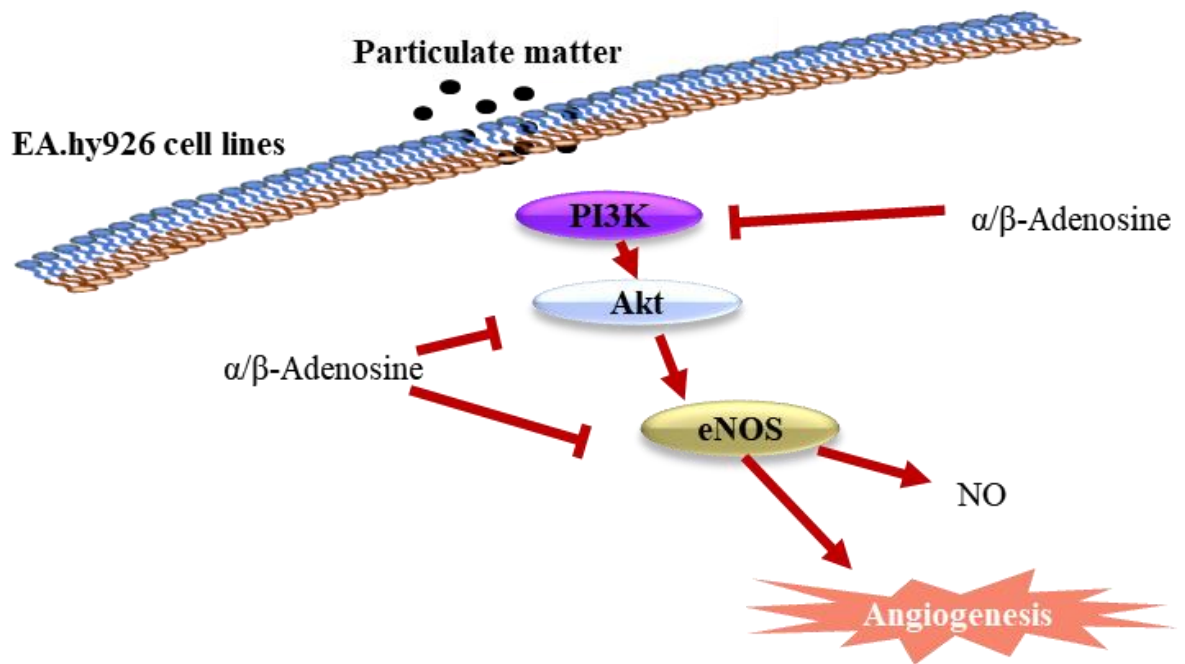


Figure 4-16. Effects of the mixture α/β -adenosine on PI3K/Akt/eNOS Signal Pathway in particulate matter-induced EA.hy926 cells

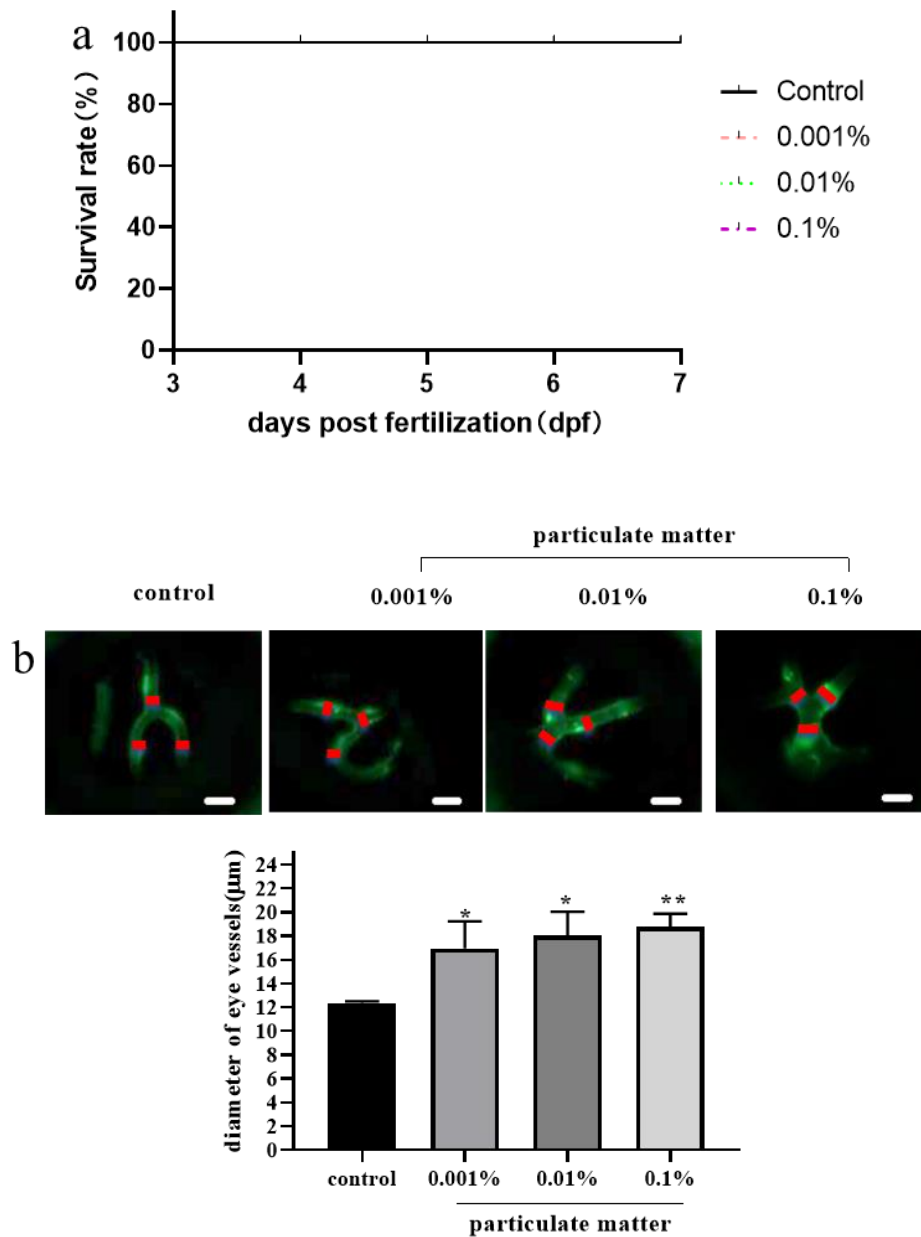


Figure 4-17. *In vivo* evaluation of angiogenesis in PM induced transgenic zebrafish embryos. PM treated to zebrafish embryos at different concentrations, and fluorescence images were taken after 7 dpf. The survival rate of particulate matter in zebrafish (a); The effect of particulate matter induced eyes vasodilation in zebrafish (b). Vessel formation in retinal vessels was evaluated by measuring the retinal vessel diameter of the images (10× magnification) amount of 15 different fishes, 10 times in different places using Gen 5 3.04 software. Each data point represents the mean ± SE (* $p < 0.05$, ** $p < 0.01$ by One-Way ANOVA test in GraphPad Prism8.3.0).

3.7. Effects of the mixture α/β -adenosine and β -adenosine on PM-Treated Zebrafish

Embryo

To evaluate anti-angiogenic effects of the mixture α/β -adenosine and β -adenosine in transgenic zebrafish (flk:EGFP) embryo. The diameter of retinal vessel was increased to 18 μm by 0.1% PM treatment stimulated in transgenic zebrafish (flk:EGFP) embryo. The different concentrations of the mixture α/β -adenosine were treated to transgenic zebrafish (flk:EGFP) embryo, the retinal vessel diameters were decreased in a dose-dependently (Figure 4-17b), however, the treatment of β -adenosine did not show significant inhibition effect on PM-induced Zebrafish Embryo (Figure 4-19). This results illustrated that the mixture α/β -adenosine have the potential to inhibit angiogenesis better than β -adenosine.

4. Conclusion

The α -adenosine and β -adenosine were identified from *I.okamurae*. And the mixture of α/β -adenosine significantly inhibited the cell migration and tube formation in PM-induced EA.hy926 cells. the mixture of α/β -adenosine suppressed PM-induced dilation in the retinal vessel diameter. The results revealed that the mixture of α and β -adenosine (1: 1) have potential as a treatment for angiogenic.

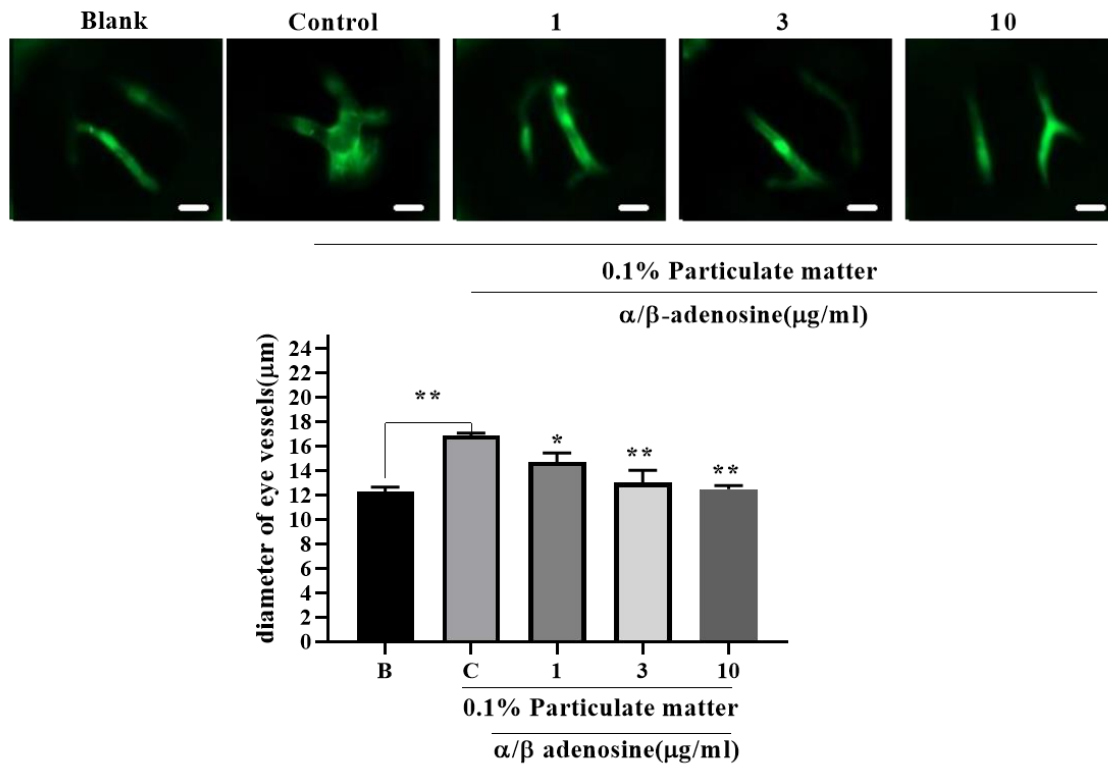


Figure 4-18. *In vivo* evaluation of anti-angiogenesis in PM-induced transgenic zebrafish embryos. the mixture of α/β -adenosine was treated to PM-induced transgenic zebrafish embryos at different concentrations, and fluorescence images were taken after 7 dpf. The mixture of α/β -adenosine inhibits particulate matter-induced eyes vasodilation in zebrafish. Vessel formation in retinal vessels was evaluated by measuring the retinal vessel diameter of the images (10× magnification) amount of 15 different fishes, 10 times in different places using Gen 5 3.04 software. Each data point represents the mean \pm SE (* $p < 0.05$, ** $p < 0.01$ by One-Way ANOVA test in GraphPad Prism8.3.0).

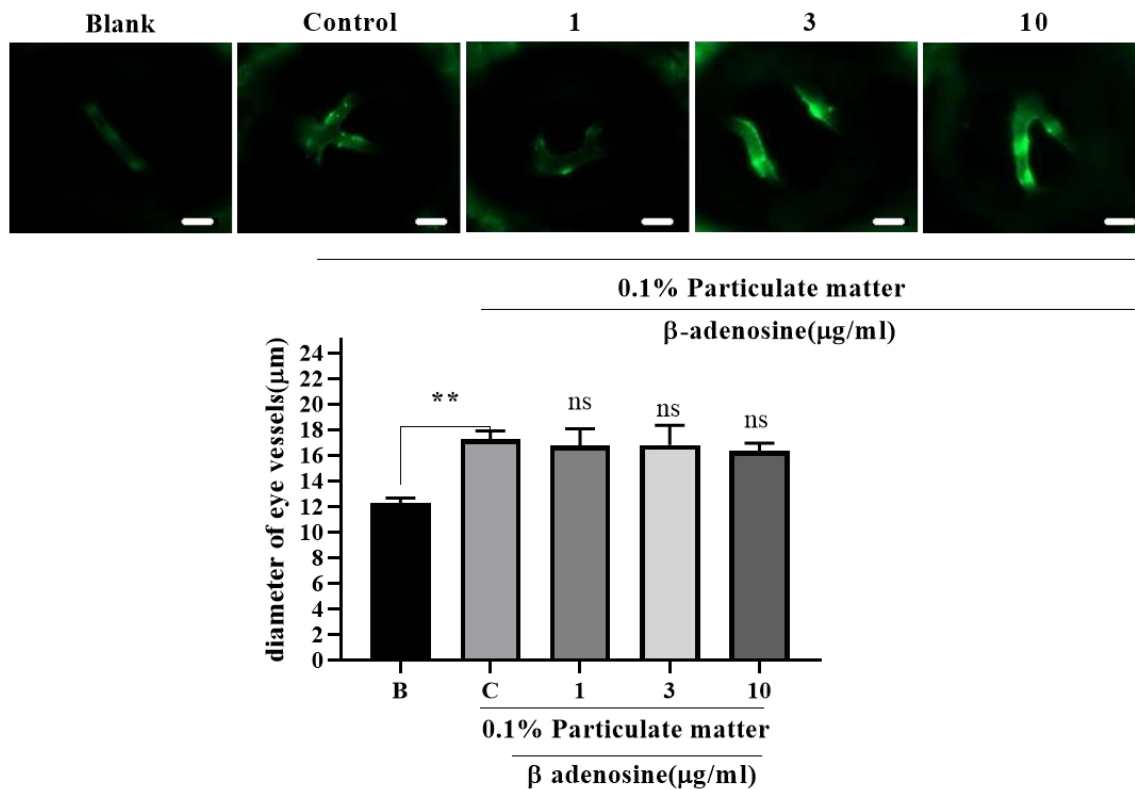


Figure 4-19. *In vivo* evaluation of anti-angiogenesis in PM-induced transgenic zebrafish embryos. β -adenosine was treated to PM-induced transgenic zebrafish embryos at different concentrations, and fluorescence images were taken after 7 dpf. β -adenosine inhibits particulate matter-induced eyes vasodilation in zebrafish. Vessel formation in retinal vessels was evaluated by measuring the retinal vessel diameter of the images (10 \times magnification) amount of 15 different fishes, 10 times in different places using Gen 5 3.04 software. Each data point represents the mean \pm SE (* $p < 0.05$, ** $p < 0.01$ by One-Way ANOVA test in GraphPad Prism8.3.0).

**Part III. Isolation of fucoidan from *Ishige okamurae*
and its anti-inflammatory activity**

Abstract

Fucoidan is a water-soluble polysaccharide containing sulfated and fucose from brown seaweeds, in this study the fucoidan was extracted from the *I. okamurae* using celluclast enzyme-assisted extraction. its anti-inflammatory potential was assessed by *in-vitro* and *in-vivo* studies. Fucoidan structural characterization was analyzed by FTIR, NMR spectroscopy, and HAE-PAD analysis of the monosaccharides content. The purified F4 inhibits nitric oxide (NO) by down-regulating iNOS and COX-2 expression production and the expression of PGE₂ in Lipopolysaccharide (LPS) stimulated RAW 264.7 macrophages. The production of TNF- α , IL1- β , and IL-6 were reduced by F4 treatment in a dose-dependently as well as NO production. F4 exerted a protective effect against cell damage in LPS stimulation in zebrafish embryos, the above of results prove that the potential anti-inflammatory activity of fucoidan from *I. okamurae*.

Keywords: *Ishige okamurae*; anti-inflammatory activity; fucoidan

1. Introduction

Fucoidans belong to polysaccharides, it is a unique group of polysaccharides with a sulfate group, mainly composed of L-fucose [74]. The first discovery of a sulfated polysaccharide from brown algae, named fucoidan because it is mainly composed of fucan, is now known as fucoidan or sulfated fucan according to IUPAC rules [75]. Fucoidans purified from different species of brown algae and some kinds of marine invertebrates [76]. It has been extensively researched due to their biological activity that includes antitumor, antioxidant, anticoagulant, antithrombotic, immunoregulatory, antiviral, and anti-inflammatory effects [77]. Fucoidan is a large molecule containing different types of monosaccharide units (e.g. mannose, glucose, and xylose) [78]. The molecular structure of fucose oligosaccharides is extremely complex and stochastic, depending on species specificity and many other factors, such as harvest season and the number of days to harvest and habitat conditions [79]. Previous research illustrated that the sulfate groups in fucoidan may affect its a range of other biofunctional properties [80].

Ishige okamurae(*I. okamurae*) is a brown alga that distributes along with the coast of the warmer regions of Korean, China, and Japan [81]. Previous studies conducted on *I. okamurae* have focused on crude polysaccharides. The antioxidant and anti-inflammatory properties of crude polysaccharides from *I. okamurae* were investigated. And the *I. okamurae* has been reported

2. Materials and methods

2.1. Materials

Potassium bromide (FTIR grade), 4-Amino-5-methylamino- 2',7'-dichlorofluorescein diacetate (DAF-FMDA), 3-(4,5-dimethylthiazol-2-yl)-2,5-diphenyltetrazolium bromide (MTT), and commercial fucoidan were obtained from Sigma, Aldrich, USA. RAW264.7 macrophages were purchased from the Korean Cell Line Bank (KCLB, Seoul, Korea). Dulbecco's Modified Eagles (DMEM), FBS, penicillin and streptomycin were purchased from GIBCO INC. USA. Primary antibodies of COX-2, and iNOS were purchased from Santa Cruz Biotechnology USA. Adult zebrafish were purchased from a commercial fish trader South Korea. ELISA kits (Mouse IL-1beta, Mouse IL-6, TNF- α , and PGE₂) were purchased from eBioscience, Inc., USA.

2.2. Extraction of polysaccharides

I. okamurae was collected along the coast of Jeju Island, South Korea during April 2019. The sample was washed with tap water to remove salt and was dried by lyophilization and ground into powder. The 100 g powder was de-pigment using 95% ethanol solution three times and kept it for 8 h in a 10% formaldehyde in 95% ethanol solution to remove formaldehyde. After the solvent filtered off, the melt samples were evaporated into total dryness. the depigmented powder was suspended in 1.5L of distilling water and its pH was adjusted to 4.5 using HCl. Celluclast enzyme was added into the extraction medium at a 0.5% of substrate concentration, the extraction process was carried out at 50°C under continuous shaking for 24 h and maintain the pH of the medium at 4.5 during the total digestion period. To deactivate the enzyme activity after extraction, the sample liquid was heated in boiling water (95°C) for 10 min. the extract was centrifuged to clarify the debris and supernatant. The supernatant was filtered and the pH was adjusted to 8.0. after yield was measured, the Alcalase enzyme assisted extraction was introduced by 0.5% of enzyme and kept it shaking for 24 h at 50°C to hydrolyze any proteins, then the enzyme was deactivated again using heat (10 min in 95 °C). The pH was brought down to 5.0 and the alginate contaminants were precipitated by an aqueous solution of CaCl₂. Alginates contaminants were separated by centrifugation, the supernatant was raised the pH to 7.0 and its volume was concentrated to 1/3 of original volume by lyophilization. Then 95% ethanol was added to the supernatant to precipitate polysaccharides, the mixture was maintained at 4 °C for 8 h. The precipitated polysaccharides were separated by centrifugation at 16,000×g for 10 min and were homogenized by dissolving in distilled water. After lyophilization, the *I. okamurae* polysaccharides (IOP) was obtained.

2.3. Separation of the IOP by anion-exchange chromatography

DEAE-cellulose column was applied to separate the IOP, sample was dissolved in water and loaded it into DEAE-cellulose column. The column was equilibrated with 50 mM sodium acetate (pH 5.0). the IOP was separated with gradient elution starting with 50 mM sodium acetate buffer to 1.3M NaCl, four fractions were combined according to polysaccharide content which was measured by phenol-H₂SO₄ assay. Four fractions were lyophilized to reduce its volume, to further remove other contaminants, the dialysis experiment was used to remove

ionic contaminants using dialysis membranes (Spectra.Por USA). This step was done for repeated several times until the conductivity reached the value of distilled water.

2.4. FTIR characterization and monosaccharide analysis of subfraction from IOP

FTIR spectra of each fraction and commercial fucoidan were analyzed FTIR spectrometer (Thermo Scientific Nicolet™ 6700, MA USA). FTIR analysis was equipment with KBr [82]. The monosaccharide analysis of each fraction was degraded by using 4 M trifluoroacetic acid. HPAEC-PAD system (Dionex, USA) was equipment with CarboPac™ PA1 cartridge column (4.5 mm×50 mm), and ED50 Dionex Electrochemical Detector was used. the monosaccharide contents in each fraction was calculated comparing to a standard mixture of monosaccharides, undetected sample constituents such that unhydrolyzed polysaccharides, sulfates, and other possible contaminants were not taken into consideration.

2.5. NMR analysis

NMR spectrum analysis of each fraction was performed on a JEOL JNM-ECX400 (400 MHz spectrometer, Japan). The sample was introduced to the NMR instrument after repeatedly dissolved in deuterium oxide several times for deuterium exchange. 2 mg/ml of each fraction was analyzed. Deuterated methanol was added to the samples as the internal standard [83].

2.6. Cell culture

RAW 264.7 cells was sub-cultured every 2 days, and cells were used for the experiments under the exponential growth phase. MTT assay and Griess assay were used to evaluate the cell viability and NO production [84].

2.7. Determination of the PGE₂ expression and pro-inflammatory cytokines expression

To evaluate the expressions of PGE₂ and the pro-inflammatory cytokines, the RAW 264.7 were treated with LPS (1μg/mL), after 1h, the different concentrations of F4 were treated to the cells. After 24h, the culture media was used from each well for evaluating the expression levels of PGE₂, TNF-α, IL1-β, and IL-6. Commercial enzyme immunoassay kits were applied on this experiment according to the given instructions.

2.8. Western bolt analysis

Experiments were performed according to previous method with slight modification[70]. macrophage cells were seeded culture dish, after 24h, the stimulator of LPS (1 μ g/mL) was treated to RAW 264.7 cell, keep for 1h. the different concentrations of F4 were treated to the cell another 24 hours. And then the cells were washed twice with cold-PBS and harvested. The harvested cells were lysed with lysis buffer. Cell lysates were separated by centrifugation, and protein concentrations were determined by using BCA protein assay kit (Bio-Rad, USA). the lysates were separated on a 12% SDS-polyacrylamide gel and transferred onto a polyvinylidene fluoride (PVDF) membrane (BIO-RAD, HC, USA). After blocking the nonspecific site with 5% skim milk, the membranes were developed with primary antibodies (iNOS, COX-2, and β -actin, Santa Cruz Biotechnology) with 5% skim milk at room temperature for 8 hours. The membrane was further incubated for 2 hours with secondary antibody (1:3000, Vector Laboratories, Burlingame, CA, USA) at room temperature. The immune-active proteins were washed 3 times with TBST before detected using enhanced chemiluminescence (ECL) western blotting detection kit using a FUSION SOLO Vilber Lourmat system (Paris, France).

2.9. In vivo zebrafish experiment

2.9.1 Evaluation of the inhibition of NO production, and protective effects against cell death in LPS induced zebrafish embryo model

To detect LPS-induced NO production and cell death in zebrafish embryos, zebrafish embryos were transferred to 12-well plates, at the 7 hours of post fertilization (7 hpf) embryos were treated with F4 at different concentration of 12.5, 25, and 50 μ g/mL. At the 3 dpf, each well of zebrafish embryos were incubated with DAF-FM DA solution (10 μ M) until 3h in the dark room at room temperature for detecting NO production, and zebrafish embryos were incubated with acridine orange (7 μ g/mL) until 1h for the determination of cell death [85].

2.10. Statistical analysis

All the data values are expressed as mean \pm SD based on at least three independent experiments. Statistical analysis for comparing the data was performed using GraphPad Prism 8.3.0 software

using one-way ANOVA by Duncan's multiple range test. p -values less than 0.05 ($p < 0.05$) were considered significant.

3. Results and discussion

3.1. Extraction, separation and monosaccharide analysis of IOP fractions

As shown in Figure 5-1, it demonstrates the variation of polysaccharide content in the DEAE-cellulose anion exchange column. Four fractions (F1, F2, F3, and F4) were separately identified from eluates according to the polysaccharide content. Sulfated polysaccharides have several key molecular features that are relative with biological functionality, such as the monosaccharide composition, structure sequence, branching pattern, and the substitution pattern of sulfate groups, hence, the monosaccharide composition of IOP was analyzed using HPAE-PAD chromatography, the chromatography was show in Figure 5-4. And the Table 10. illustrates that the amounts of fucose and sulfate contents were increasing with the order of $F1 < F2 < F3 < F4$. In the F4 fraction, which is highly rich in sulfate content (19.54%) and fucose (80.65%). This implies a successful separation of F1, F2, F3, and F4 from the IOP.

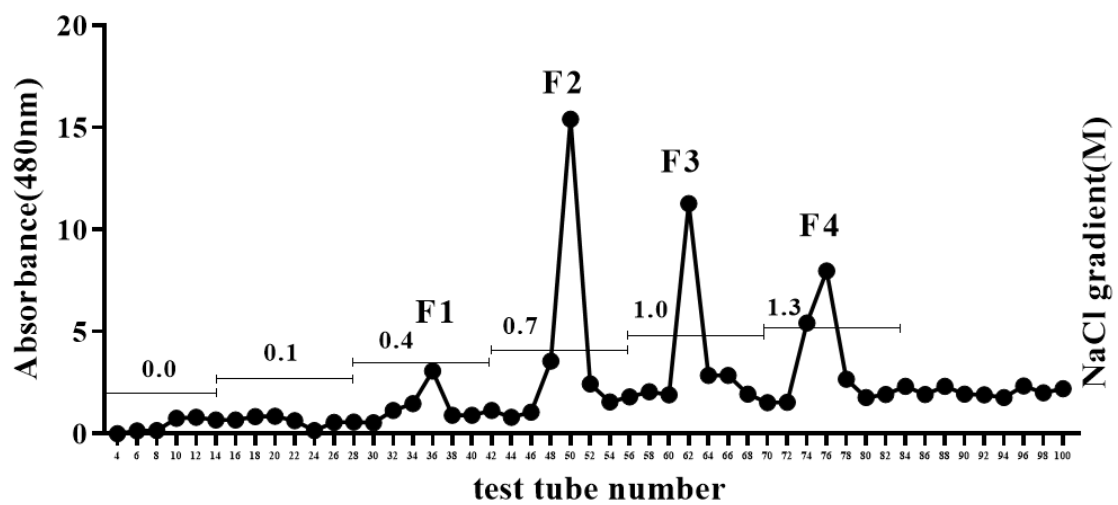


Figure 5-1. Isolation of IOP using DEAE-cellulose anion exchange chromatography. Column pre-equilibrated with 50.0 mM acetate buffer (pH 5.0). Increasing gradient of NaCl (0.0-1.3 M in the same buffer) was used as the mobile phase. Phenol-sulfuric method was used to measure the polysaccharide content.

3.2. FT-IR spectroscopic and ^1H NMR analysis of structural features of the polysaccharides

FTIR was used to identify the functional groups of the F1-F4 fractions. The range of scanned wavelength is $500\text{-}2000\text{ cm}^{-1}$. Figure 5-2. shows the FTIR spectrums of F1-F4 and commercial fucoidan. The observed peaks at 1270, 1035, and 845. The peak of 1270 cm^{-1} is S=O stretching vibrations. [86]. Figure 5-3. shows the proton ^1H NMR analysis of four fractions with characteristic peaks of fucoidan as previously reported [87], chemical shift between 1.1 and 1.8 ppm, which of them were corresponded to methyl proton of fucose. Moreover, an observed shift at 3.5-4.0 ppm corresponded to Ring proton. Sulfated polysaccharides have complex and heterogeneous structures.

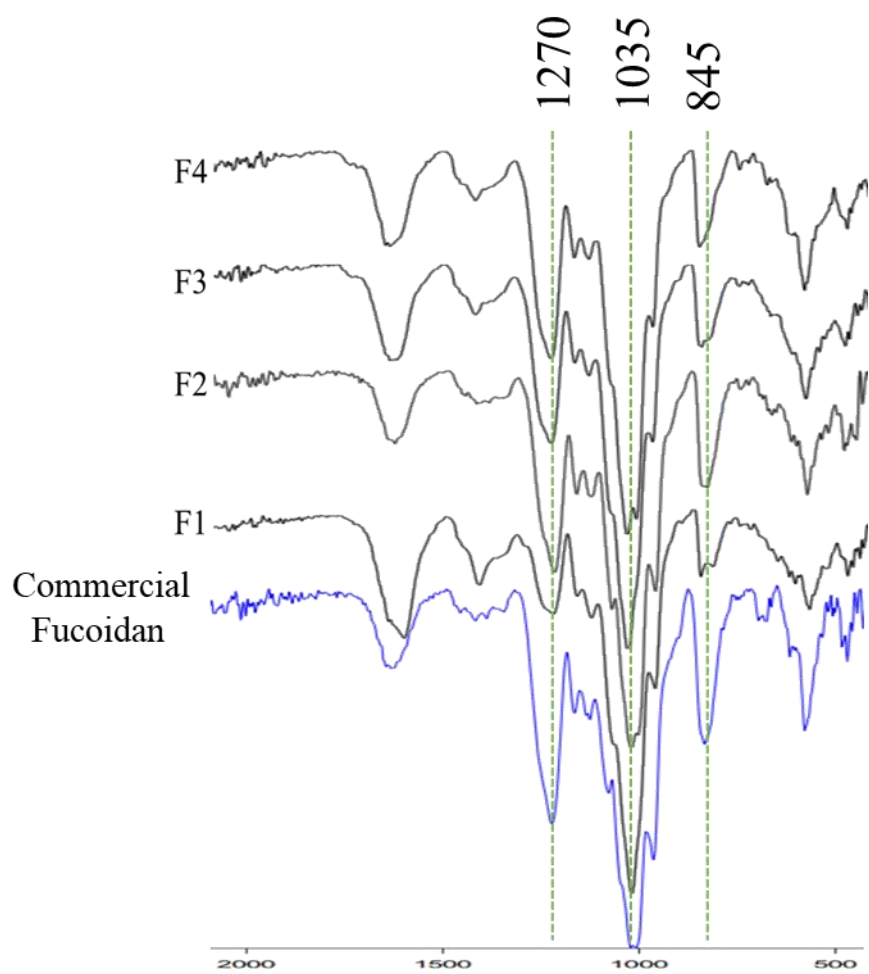


Figure 5-2. FTIR spectra of all subfractions (F1-F4) compared with commercial fucoidan.

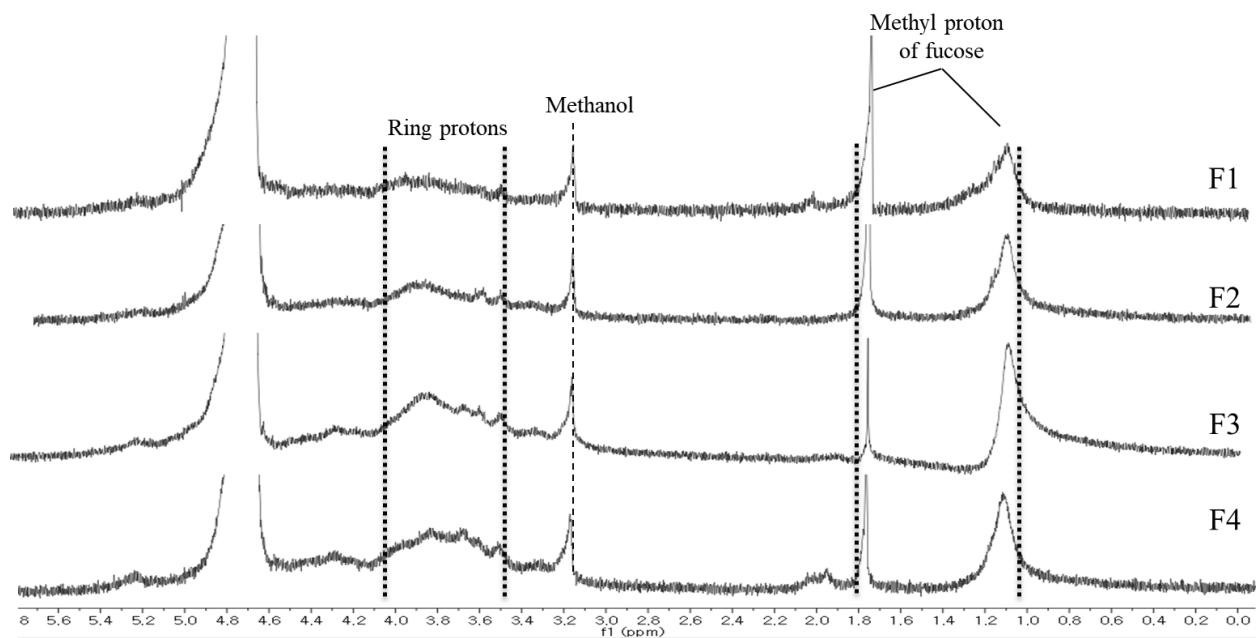


Figure 5-3. ¹H NMR spectrum of the all subfractions in D₂O solution-analyzed at 400 MHz.

Table 10. Monosaccharide composition and sulfate content of F1, F2, F3 and F4 from IOP.

	IOP	F1	F2	F3	4
Fucose (%)	71.98	55.62	65.7	68.05	80.65
Galactose (%)	8.15	2.24	23.76	19.7	4.45
Xylose (%)	18.32	32.09	8.76	9.25	14.9
Other (%)	1.54	10.05	1.78	2.97	0
Sulfate content (%)	17.57± 0.54	4.57± 0.24	10.35± 0.13	16.78 ± 0.32	19.54± 0.36

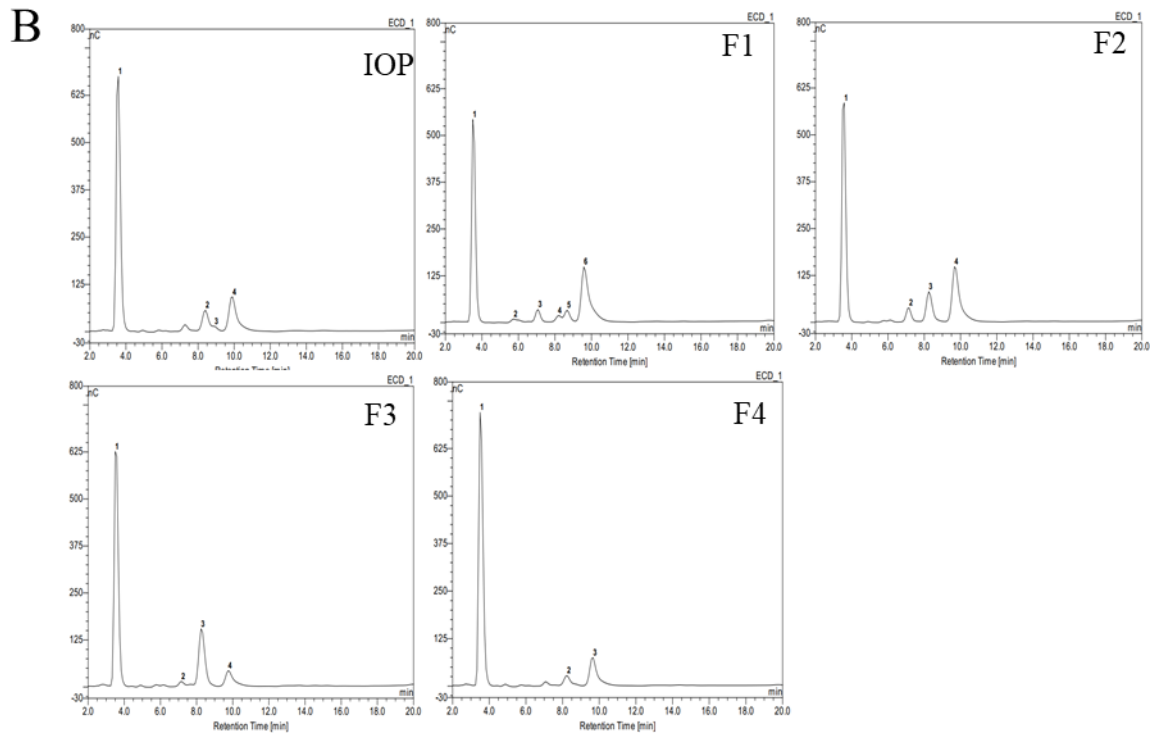
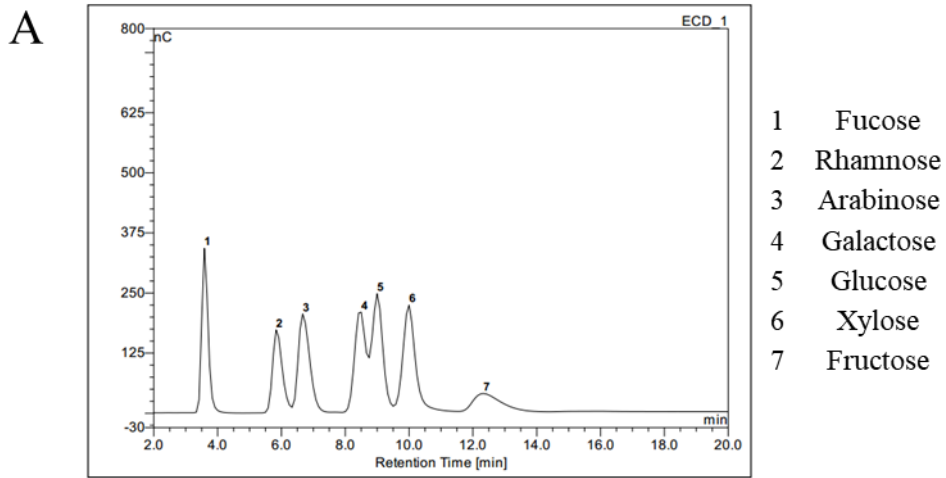


Figure 5-4. A: HPAE-PAD spectrum analysis of mixture standard monosaccharid. B: HPAE-PAD spectrum analysis of all subfractions.

3.4. Cytotoxicity of each fraction from IOP in RAW 264.7 macrophages

To determine cytotoxicity effects of each fraction from IOP in RAW 264.7 macrophages as initial method research, cell viability was measured by MTT assay. As shown in Figure 5-5, 100 µg/mL of F1-F4 showed cytotoxicity. the concentration of F1-F4 (12.5, 25, 50 µg/mL) was selected to do sample treatment on LPS-induced RAW 264.7 macrophages.

3.5. The anti-inflammatory effect of F1-F4 fractions from IOP on the inhibition of NO in LPS stimulated RAW 264.7 macrophages

Raw 264.7 macrophage cell line releases cytokines in response to LPS stimulation. This experiment has been used to determine the anti-inflammatory activities of compounds by studying cytokine production, marked by increased production of NO. NO is a key inflammatory mediator important in defending the body against inflammation. However, NO generated by activated macrophages has been shown to mediate host defense functions such as antimicrobial and anti-tumor activities, but excess NO production induces tissue damage associated with acute and chronic inflammation [88]. As indicated in Figure 5-6, RAW 264.7 macrophages were stimulated with LPS (1 µg/mL) for 24 h, NO production was stimulated by LPS in RAW 264.7 macrophages, which was significantly inhibited by the F1, F2, F3, F4 treatment at 12.5, 25, 50 µg/mL. LPS-induced NO production was decreased by the fractionated fucoidans in a dose-dependent manner. In particular, the F4 fraction exhibited a maximum inhibitory effect on NO production. Moreover, the results indicated an ordered pattern of NO inhibitory activities (F4 > F3 > F2 > F1).

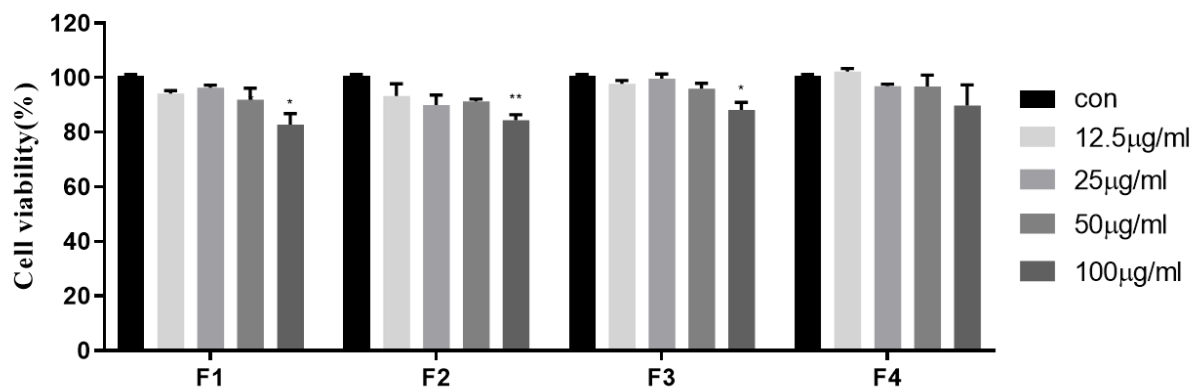


Figure 5-5. The cytotoxicity of each fraction (F1, F2, F3, and F4) on RAW 264.7 cells. Cells were treated with different sample concentrations, after 24h, MTT assay was determined for cytotoxicity. Each data point represents the mean \pm SE (* $p < 0.05$, ** $p < 0.01$ by One-Way ANOVA test in GraphPad Prism 8.3.0).

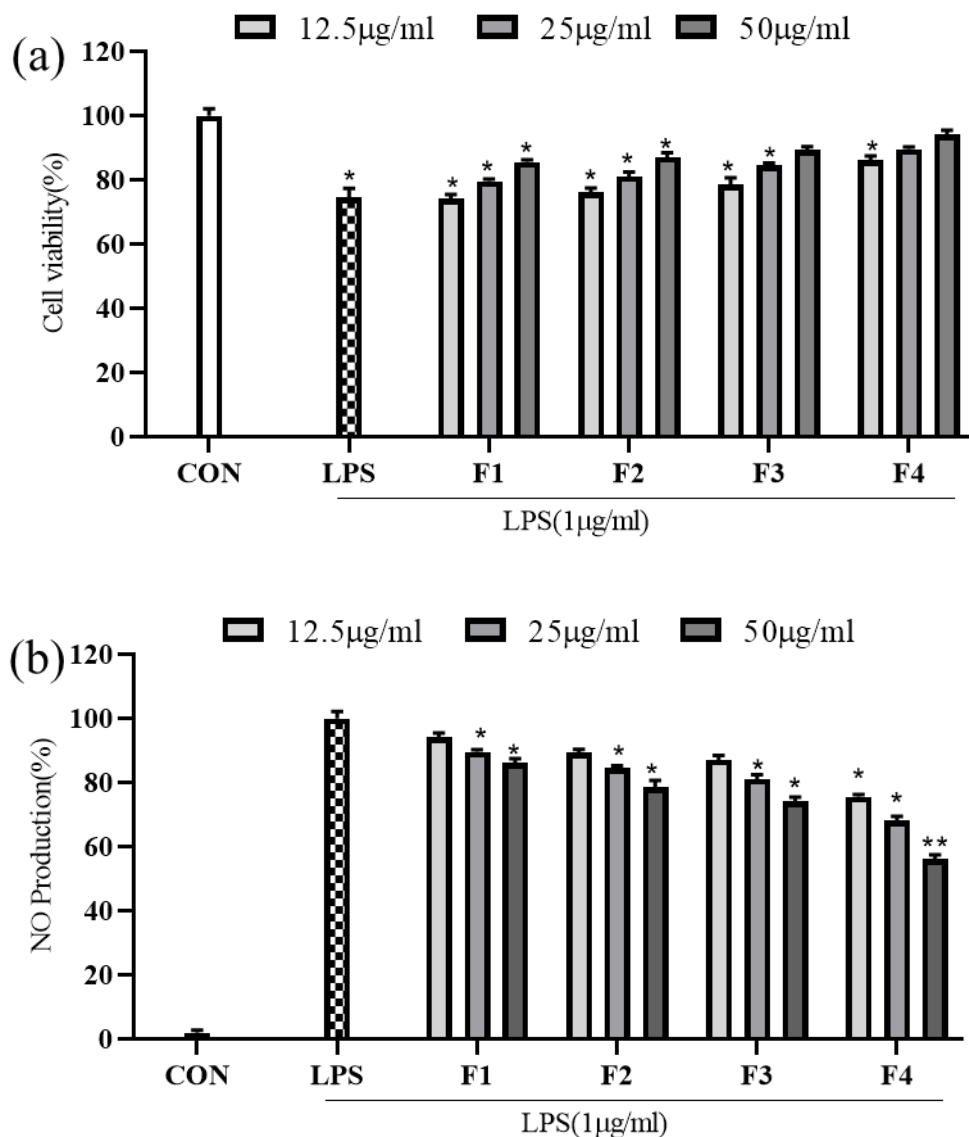


Figure 5-6. The inhibition of NO production and its protective effects against LPS induced cytotoxicity was evaluated in RAW 264.7 cells. cells were treated with LPS (1 µg/ml) and different concentrations of each fraction (F1, F2, F3, and F4). After 24h, the cytotoxicity was determined for cell viability (a), and culture media was used to analyze the NO production using Griess assay (b). Data points and bars represent the arithmetic means \pm SE (n = 3). Each data point represents the mean \pm SE (* $p < 0.05$, ** $p < 0.01$ by One-Way ANOVA test in GraphPad Prism 8.3.0).

3.6. Pro-inflammatory cytokines production against F4 in LPS-stimulated RAW 264.7 macrophages

Several immune cells including neutrophils, macrophages are involved in the pathogenesis of inflammation through the production of inflammatory cytokines. Prostaglandin E₂ (PGE₂) is an important lipid mediator in inflammatory and immune responses during acute and chronic infections [89], TNF- α elicits some physiological effects, including inflammation [90], IL-6 is a well-known pro-inflammatory cytokine and is regarded as an endogenous mediator of LPS-induced fever [91], IL-1 β is also considered a pivotal pro-inflammatory cytokine, primarily released by macrophages, which is believed to play an important role in the pathophysiology of rheumatoid arthritis [92]. Thus, inhibition of cytokine production or function is a key mechanism to control inflammation, according to the results Figure 5-7, LPS treatment significantly increased the PGE₂ and pro-inflammatory cytokine production (TNF- α , IL1- β , and IL-6) in macrophage cells. However, treatment of F4 reduced the LPS-induced pro-inflammatory cytokine production and PGE₂ production in a dose-dependent manner.

3.7. Effects of F4 on the mediation of iNOS, COX-2 in LPS-stimulated RAW 264.7 macrophages

iNOS and COX-2 are the key inflammatory mediators, which could be used to evaluate the anti-inflammatory activity, and several types of human tumors[93]. Inflammatory mediators derived from iNOS and COX-2 were observed in Western blot analysis (Figure 5-8). The expression of iNOS and COX-2 was downregulated by F4 treatment dose-dependently in LPS stimulated RAW 264.7 cells. The iNOS is relative to the NO production, the down-regulation of iNOS expression has resulted in the suppression of NO production in RAW 264.7 macrophages.

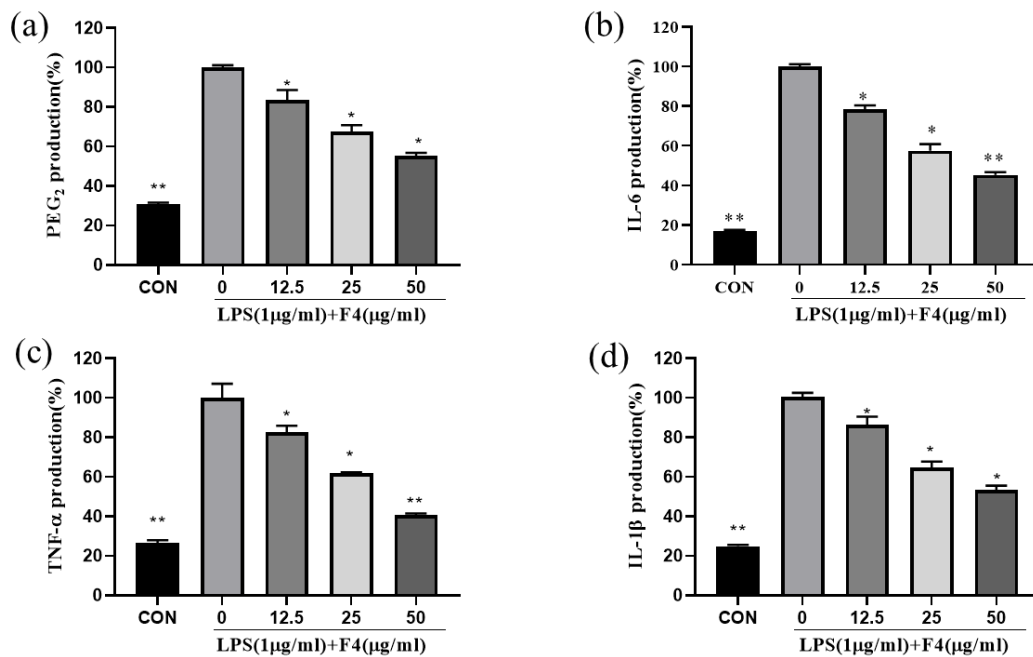


Figure 5-7. Evaluation of the expression of PGE₂ and pro-inflammatory cytokines. PGE₂(a) and pro-inflammatory mediators including IL-6 (b); TNF-α (c); IL1-β (d) in LPS stimulated RAW 264.7 macrophages. RAW 264.7 cells were pretreated with different concentrations of F4 and co-treated with LPS (1μg/ml). After 24 h, culture media was used to analyze the productions of PGE₂, TNF-α, IL1-β, and IL-6. Each data point represents the mean ± SE (* $p < 0.05$, ** $p < 0.01$ by One-Way ANOVA test in GraphPad Prism 8.3.0).

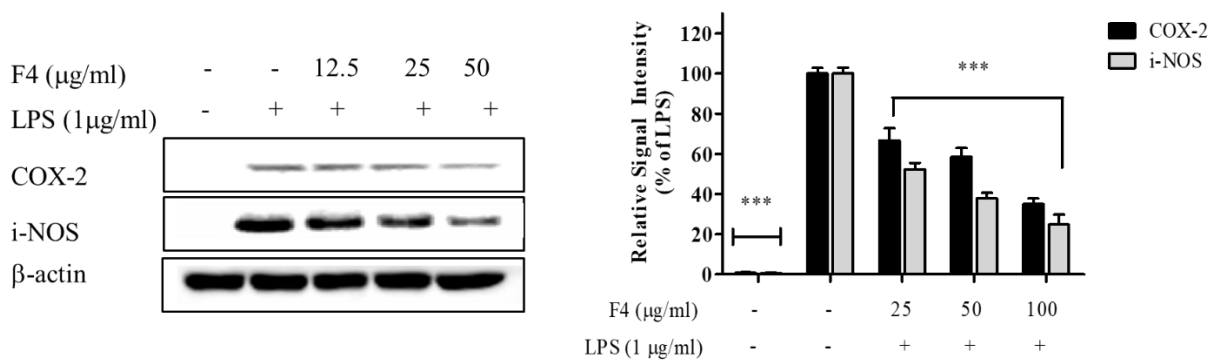


Figure 5-8. Western blotting analysis of the expression of inflammatory regulators of COX-2 and i-NOS against F4 in RAW 264.7 macrophages induced by LPS. RAW 264.7 cells were pretreated with different concentrations of F4 and co-treated with LPS (1μg/ml). After 24 h, cells were harvested to analyze the expression of COX-2 and i-NOS. Each data point represents the mean ± SE (** $p < 0.01$, *** $p < 0.001$ by One-Way ANOVA test in GraphPad Prism 8.3.0).

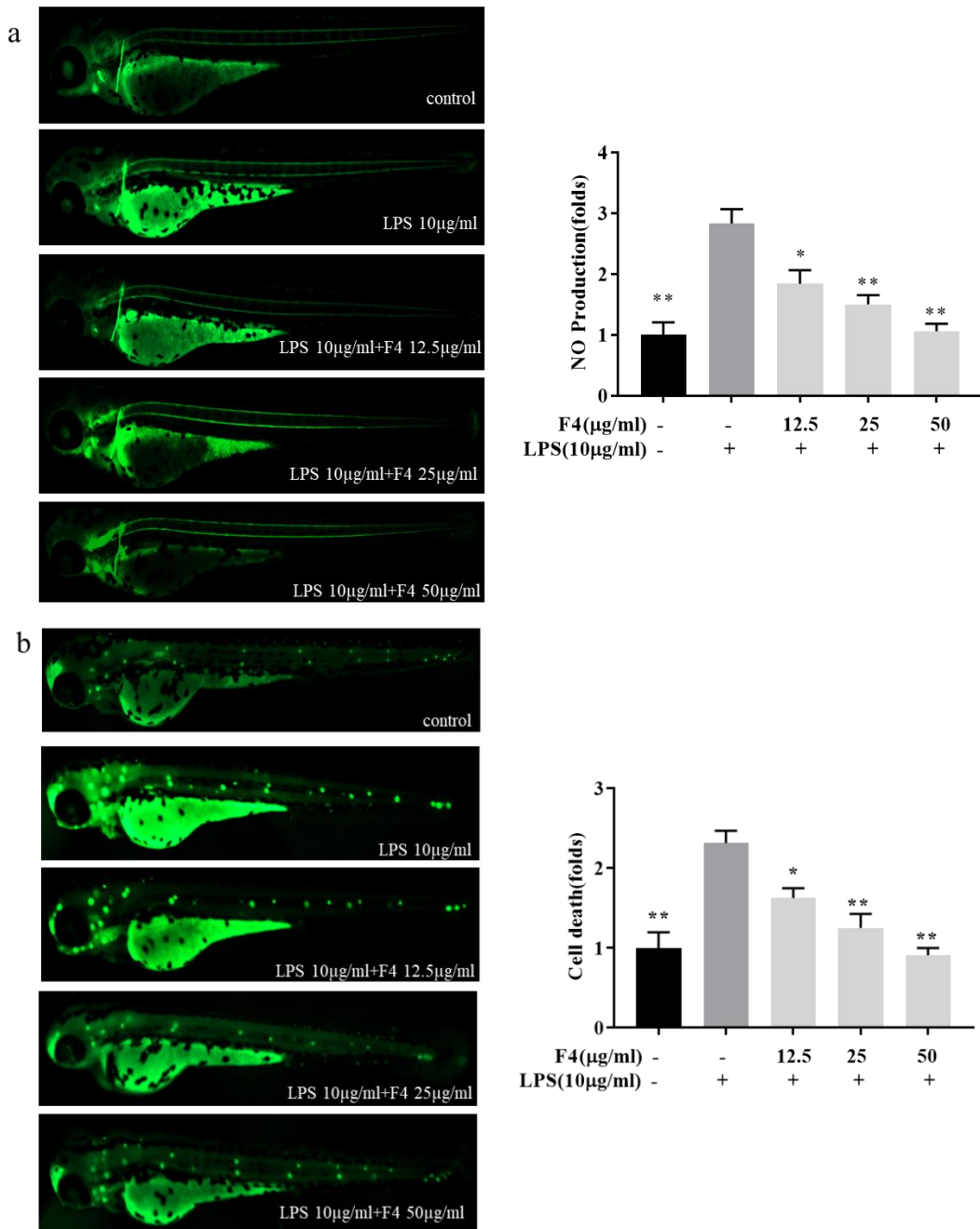


Figure 5-10. *In vivo* evaluation of anti-inflammatory potential of F4 using zebrafish embryos. zebrafish embryos were treated with F4 and stimulated with LPS (10 µg/mL). After 168 hpf, Fluorescence images of the zebrafish embryos of NO production (a), and Cell death (b) were calculated according to the intensity of green fluorescence. Each data point represents the mean \pm SE (* $p < 0.05$, ** $p < 0.01$ by One-Way ANOVA test in GraphPad Prism 8.3.0)

3.8. In vivo evaluation of anti-inflammatory potential of F4 using zebrafish embryos

Before we evaluated the protective effect of F4 against LPS-induced cell death and NO production of zebrafish embryos. In Figure 5-10a, we determined the protective effect of F4 against LPS-induced NO production in zebrafish embryos. F4 significantly inhibited NO production in dose-dependently. The results show in Figure 5-10c that F4 could significantly protect zebrafish embryos against LPS-induced cell death.

4. Conclusion

In the present study, we illustrated that the fucoidan containing high content of sulfated was separated from *I. okamurae*. it has exhibited a significant ability to reduce NO production under both in vitro and in vivo conditions. However, further studies are warranted to find out underlying mechanisms responsible for these anti-inflammatory effects observed both in in vitro and in vivo experiments.

References

1. Wijesinghe WAJP, Jeon Y-J: **Enzyme-assistant extraction (EAE) of bioactive components: A useful approach for recovery of industrially important metabolites from seaweeds: A review.** *Fitoterapia* 2012, **83**(1):6-12.
2. Hussain T, Tan B, Yin Y, Blachier F, Tossou MCB, Rahu N: **Oxidative Stress and Inflammation: What Polyphenols Can Do for Us?** *Oxid Med Cell Longev* 2016, **2016**:7432797-7432797.
3. Singh A, Holvoet S, Mercenier A: **Dietary polyphenols in the prevention and treatment of allergic diseases.** *Clinical & Experimental Allergy* 2011, **41**(10):1346-1359.
4. **Antibacterial Activity of Ecklonia cava Against Methicillin-Resistant Staphylococcus aureus and Salmonella spp.** *Foodborne Pathogens and Disease* 2010, **7**(4):435-441.
5. Benjamin MM, Khalil RA: **Matrix metalloproteinase inhibitors as investigative tools in the pathogenesis and management of vascular disease.** *Exp Suppl* 2012, **103**:209-279.
6. Niedzwiecki A, Roomi MW, Kalinovsky T, Rath M: **Anticancer Efficacy of Polyphenols and Their Combinations.** *Nutrients* 2016, **8**(9):552.
7. Heo S-J, Jeon Y-J: **Radical scavenging capacity and cytoprotective effect of enzymatic digests of Ishige okamurae.** *Journal of Applied Phycology* 2008, **20**(6):1087-1095.
8. Kim K-N, Heo S-J, Yoon W-J, Kang S-M, Ahn G, Yi T-H, Jeon Y-J: **Fucoxanthin inhibits the inflammatory response by suppressing the activation of NF- κ B and MAPKs in lipopolysaccharide-induced RAW 264.7 macrophages.** *European Journal of Pharmacology* 2010, **649**(1):369-375.
9. Kim H-S, Wang L, Jayawardena TU, Kim E-A, Heo S-J, Shanura Fernando IP, Lee J-H, Jeon Y-J: **High-performance centrifugal partition chromatography (HPCPC) for efficient isolation of diphlorethohydroxycarmalol (DPHC) and screening of its antioxidant activity in a zebrafish model.** *Process Biochemistry* 2020, **88**:189-196.
10. Zou Y, Li Y, Kim M-M, Lee S-H, Kim S-K: **Ishigoside, a new glyceroglycolipid isolated from the brown alga Ishige okamurae.** *Biotechnology and Bioprocess Engineering* 2009, **14**(1):20-26.
11. Kang M-C, Lee S-H, Lee W-W, Kang N, Kim E-A, Kim SY, Lee DH, Kim D, Jeon Y-J: **Protective effect of fucoxanthin isolated from Ishige okamurae against high-glucose induced oxidative stress in human umbilical vein endothelial cells and zebrafish model.** *Journal of Functional Foods* 2014, **11**:304-312.
12. Yoon NY, Lee S-H, Yong L, Kim S-K: **Phlorotannins from Ishige okamurae and their acetyl- and butyrylcholinesterase inhibitory effects.** *Journal of Functional Foods* 2009, **1**(4):331-335.
13. Cho J-Y, Gyawali YP, Ahn S-H, Khan MNA, Kong I-S, Hong Y-K: **A methoxylated fatty acid isolated from the brown seaweed Ishige okamurae inhibits bacterial phospholipase A2.** *Phytotherapy Research* 2008, **22**(8):1070-1074.
14. Zou Y, Qian Z-J, Li Y, Kim M-M, Lee S-H, Kim S-K: **Antioxidant Effects of Phlorotannins Isolated from Ishige okamurae in Free Radical Mediated Oxidative Systems.** *Journal of Agricultural and Food Chemistry* 2008, **56**(16):7001-7009.
15. Toume K, Miyata M, Egawa K, Nose K, Hayashi M, Komiyama K, Ishibashi M: **Isolation of Diphlorethohydroxycarmalol from a Brown Alga Ishige okamurae.** *Natural medicines* 2004, **58**(2):79-80.
16. Ryu B, Jiang Y, Kim H-S, Hyun J-M, Lim S-B, Li Y, Jeon Y-J: **Ishophloroglucin A, a novel phlorotannin for standardizing the anti- α -glucosidase activity of Ishige okamurae.** 2018, **16**(11):436.
17. Yang X-X, Zhang X-X, Chang R-M, Wang Y-W, Li X-N: **Simultaneous quantification of five major active components in capsules of the traditional Chinese medicine 'Shu-Jin-Zhi-Tong' by high performance liquid chromatography.** *Journal of Pharmaceutical Analysis* 2011, **1**(4):284-290.

18. Overhage S, Skroch O, Turowski K: **A Method to Evaluate the Suitability of Requirements Specifications for Offshore Projects.** *Business & Information Systems Engineering* 2010, **2**(3):155-164.
19. Guideline IHT: **Validation of analytical procedures: text and methodology Q2 (R1).** In: *International conference on harmonization, Geneva, Switzerland: 2005.*
20. Al-Rimawi F: **Development and validation of a simple reversed-phase HPLC-UV method for determination of oleuropein in olive leaves.** *Journal of food and drug analysis* 2014, **22**(3):285-289.
21. Jayawardena TU, Sanjeewa KKA, Kim H-S, Lee HG, Wang L, Lee D-S, Jeon Y-J: **Padina boryana, a brown alga from the Maldives: inhibition of α -MSH-stimulated melanogenesis via the activation of ERK in B16F10 cells.** *Fisheries and Aquatic Sciences* 2020, **23**(1):8.
22. Ali SA, Naaz I: **Biochemical aspects of mammalian melanocytes and the emerging role of melanocyte stem cells in dermatological therapies.** *Int J Health Sci (Qassim)* 2018, **12**(1):69-76.
23. Joly-Tonetti N, Wibawa JID, Bell M, Tobin DJ: **Basis of melanin distribution in the human skin epidermis.** *British Journal of Dermatology* 2018, **179**(5):e209-e209.
24. Brenner M, Hearing VJ: **Modifying skin pigmentation - approaches through intrinsic biochemistry and exogenous agents.** *Drug Discov Today Dis Mech* 2008, **5**(2):e189-e199.
25. Gillbro JM, Olsson MJ: **The melanogenesis and mechanisms of skin-lightening agents – existing and new approaches.** *International Journal of Cosmetic Science* 2011, **33**(3):210-221.
26. Hseu Y-C, Chen X-Z, Vudhya Gowrisankar Y, Yen H-R, Chuang J-Y, Yang H-L: **The Skin-Whitening Effects of Ectoine via the Suppression of α -MSH-Stimulated Melanogenesis and the Activation of Antioxidant Nrf2 Pathways in UVA-Irradiated Keratinocytes.** *Antioxidants* 2020, **9**(1):63.
27. Khaled M, Larribere L, Bille K, Ortonne J-P, Ballotti R, Bertolotto C: **Microphthalmia Associated Transcription Factor Is a Target of the Phosphatidylinositol-3-Kinase Pathway.** *Journal of Investigative Dermatology* 2003, **121**(4):831-836.
28. Kang SM, Heo SJ, Kim KN, Lee SH, Yang HM, Kim AD, Jeon YJ: **Molecular docking studies of a phlorotannin, dieckol isolated from Ecklonia cava with tyrosinase inhibitory activity.** *Bioorg Med Chem* 2012, **20**(1):311-316.
29. Chen YM, Su WC, Li C, Shi Y, Chen QX, Zheng J, Tang DL, Chen SM, Wang Q: **Anti-melanogenesis of novel kojic acid derivatives in B16F10 cells and zebrafish.** *Int J Biol Macromol* 2019, **123**:723-731.
30. Ryu B, Jiang Y, Kim H-S, Hyun J-M, Lim S-B, Li Y, Jeon Y-J: **Ishophloroglucin A, a Novel Phlorotannin for Standardizing the Anti- α -Glucosidase Activity of Ishige okamurae.** *Mar Drugs* 2018, **16**(11):436.
31. Hosoi J, Abe E, Suda T, Kuroki T: **Regulation of Melanin Synthesis of B16 Mouse Melanoma Cells by $1\alpha,25$ -Dihydroxyvitamin D₃ and Retinoic Acid.** *Cancer Research* 1985, **45**(4):1474-1478.
32. Azam MS, Kwon M, Choi J, Kim HR: **Sargaquinoic acid ameliorates hyperpigmentation through cAMP and ERK-mediated downregulation of MITF in alpha-MSH-stimulated B16F10 cells.** *Biomed Pharmacother* 2018, **104**:582-589.
33. Peng L-H, Liu S, Xu S-Y, Chen L, Shan Y-H, Wei W, Liang W-Q, Gao J-Q: **Inhibitory effects of salidroside and paeonol on tyrosinase activity and melanin synthesis in mouse B16F10 melanoma cells and ultraviolet B-induced pigmentation in guinea pig skin.** *Phytomedicine* 2013, **20**(12):1082-1087.
34. Ma Y, Zhang C, Gao XB, Luo HY, Chen Y, Li HH, Ma X, Lu CL: **Folic acid protects against arsenic-mediated embryo toxicity by up-regulating the expression of Dvr1.** *Sci Rep* 2015, **5**:16093.

35. Kim KN, Yang HM, Kang SM, Ahn GN, Roh SW, Lee W, Kim DK, Jeon YJ: **Whitening Effect of Octaphlorethol A Isolated from *Ishige foliacea* in an In Vivo Zebrafish Model.** *J Microbiol Biotechnol* 2015, **25**(4):448-451.
36. Pomin VH: **Review: An overview about the structure–function relationship of marine sulfated homopolysaccharides with regular chemical structures.** *Biopolymers* 2009, **91**(8):601-609.
37. Priyan Shanura Fernando I, Kim K-N, Kim D, Jeon Y-J: **Algal polysaccharides: potential bioactive substances for cosmeceutical applications.** *Critical Reviews in Biotechnology* 2019, **39**(1):99-113.
38. Ha JW, Song H, Hong SS, Boo YC: **Marine Alga *Ecklonia cava* Extract and Dieckol Attenuate Prostaglandin E2 Production in HaCaT Keratinocytes Exposed to Airborne Particulate Matter.** *Antioxidants* 2019, **8**(6):190.
39. Yang C-f, Lai S-s, Chen Y-h, Liu D, Liu B, Ai C, Wan X-z, Gao L-y, Chen X-h, Zhao C: **Anti-diabetic effect of oligosaccharides from seaweed *Sargassum confusum* via JNK-IRS1/PI3K signalling pathways and regulation of gut microbiota.** *Food and Chemical Toxicology* 2019, **131**:110562.
40. Ahn M, Moon C, Yang W, Ko E-J, Hyun JW, Joo HG, Jee Y, Lee NH, Park JW, Ko RK *et al*: **Diphloretohydroxycarmalol, isolated from the brown algae *Ishige okamurae*, protects against radiation-induced cell damage in mice.** *Food and Chemical Toxicology* 2011, **49**(4):864-870.
41. Vachtenheim J, Borovanský J: **“Transcription physiology” of pigment formation in melanocytes: central role of MITF.** *Experimental Dermatology* 2010, **19**(7):617-627.
42. Kim H-E, Ishihara A, Lee S-G: **The effects of Caffeoylserotonin on inhibition of melanogenesis through the downregulation of MITF via the reduction of intracellular cAMP and acceleration of ERK activation in B16 murine melanoma cells.** *BMB Rep* 2012, **45**(12):724-729.
43. Wan P, Hu Y, He L: **Regulation of melanocyte pivotal transcription factor MITF by some other transcription factors.** *Molecular and Cellular Biochemistry* 2011, **354**(1):241-246.
44. Su T-R, Lin J-J, Tsai C-C, Huang T-K, Yang Z-Y, Wu M-O, Zheng Y-Q, Su C-C, Wu Y-J: **Inhibition of Melanogenesis by Gallic Acid: Possible Involvement of the PI3K/Akt, MEK/ERK and Wnt/ β -Catenin Signaling Pathways in B16F10 Cells.** 2013, **14**(10):20443-20458.
45. Veldman MB, Lin S: **Zebrafish as a Developmental Model Organism for Pediatric Research.** *Pediatric Research* 2008, **64**(5):470-476.
46. Dooley K, Zon LI: **Zebrafish: a model system for the study of human disease.** *Current Opinion in Genetics & Development* 2000, **10**(3):252-256.
47. Lin VC-H, Ding H-Y, Kuo S-Y, Chin L-W, Wu J-Y, Chang T-S: **Evaluation of in Vitro and in Vivo Depigmenting Activity of Raspberry Ketone from *Rheum officinale*.** 2011, **12**(8):4819-4835.
48. Geiger A, Cooper J: **Overview of airborne metals regulations, exposure limits, health effects, and contemporary research.** *US Environmental Protection Agency Accessed Accessed on August 2010*, **25**:2015.
49. Hu X, Zhang Y, Ding Z, Wang T, Lian H, Sun Y, Wu J: **Bioaccessibility and health risk of arsenic and heavy metals (Cd, Co, Cr, Cu, Ni, Pb, Zn and Mn) in TSP and PM_{2.5} in Nanjing, China.** *Atmospheric Environment* 2012, **57**:146-152.
50. Charlesworth S, De Miguel E, Ordóñez A: **A review of the distribution of particulate trace elements in urban terrestrial environments and its application to considerations of risk.** *Environmental geochemistry and health* 2011, **33**(2):103-123.
51. Zhang J, Smith KR: **Household air pollution from coal and biomass fuels in China: measurements, health impacts, and interventions.** *Environmental health perspectives* 2007, **115**(6):848-855.

52. Wang Y, Kong L, Wu T, Tang M: **Urban particulate matter disturbs the equilibrium of mitochondrial dynamics and biogenesis in human vascular endothelial cells.** *Environmental Pollution* 2020, **264**:114639.
53. de Oliveira BFA, Chacra APM, Frauches TS, Vallochi A, Hacon S: **A curated review of recent literature of biomarkers used for assessing air pollution exposures and effects in humans.** *Journal of Toxicology and Environmental Health, Part B* 2014, **17**(7-8):369-410.
54. Wang C, Chen R, Shi M, Cai J, Shi J, Yang C, Li H, Lin Z, Meng X, Liu C: **Possible mediation by methylation in acute inflammation following personal exposure to fine particulate air pollution.** *American journal of epidemiology* 2018, **187**(3):484-493.
55. Yang J, Huo T, Zhang X, Ma J, Wang Y, Dong F, Deng J: **Oxidative stress and cell cycle arrest induced by short-term exposure to dustfall PM 2.5 in A549 cells.** *Environmental Science and Pollution Research* 2018, **25**(23):22408-22419.
56. Rui W, Guan L, Zhang F, Zhang W, Ding W: **PM2.5-induced oxidative stress increases adhesion molecules expression in human endothelial cells through the ERK/AKT/NF- κ B-dependent pathway.** *Journal of Applied Toxicology* 2016, **36**(1):48-59.
57. Pal AJDAI: **Synthesis of nucleoside analogues: Glycosylation, rigid nucleosides and Janus Wedge derivatives.** In., vol. 73; 2012.
58. Ni G, Du Y, Tang F, Liu J, Zhao H, Chen QJRa: **Review of α -nucleosides: from discovery, synthesis to properties and potential applications.** 2019, **9**(25):14302-14320.
59. Haskó G, Cronstein BNJTii: **Adenosine: an endogenous regulator of innate immunity.** 2004, **25**(1):33-39.
60. Kumar V, Sharma AJEjop: **Adenosine: an endogenous modulator of innate immune system with therapeutic potential.** 2009, **616**(1-3):7-15.
61. Ghiardi GJ, Gidday JM, Roth SJVr: **The purine nucleoside adenosine in retinal ischemia-reperfusion injury.** 1999, **39**(15):2519-2535.
62. Hirschhorn RJPr: **Overview of biochemical abnormalities and molecular genetics of adenosine deaminase deficiency.** 1993, **33**(4):S35-S41.
63. Malz F, Jancke H: **Validation of quantitative NMR.** *Journal of Pharmaceutical and Biomedical Analysis* 2005, **38**(5):813-823.
64. Anh NQ, Yen TT, Hang NT, Anh DH, Viet PH, Van Doan V, Van Kiem P: **1H-Indole-3-acetonitrile glycoside, phenolic and other compounds from Stixis suaveolens.** 2019, **57**(5):558-561.
65. Fernando KHN, Yang H-W, Jiang Y, Jeon Y-J, Ryu B: **Diphlorethohydroxycarmalol Isolated from Ishige okamurae Represses High Glucose-Induced Angiogenesis In Vitro and In Vivo.** 2018, **16**(10):375.
66. Chen J-M, Chen P-Y, Lin C-C, Hsieh M-C, Lin J-T: **Antimetastatic Effects of Sesamin on Human Head and Neck Squamous Cell Carcinoma through Regulation of Matrix Metalloproteinase-2.** 2020, **25**(9):2248.
67. Grada A, Otero-Vinas M, Prieto-Castrillo F, Obagi Z, Falanga V: **Research Techniques Made Simple: Analysis of Collective Cell Migration Using the Wound Healing Assay.** *Journal of Investigative Dermatology* 2017, **137**(2):e11-e16.
68. Aisha AFA, Ismail Z, Abu-Salah KM, Siddiqui JM, Ghafar G, Abdul Majid AMS: **Syzygium campanulatum korth methanolic extract inhibits angiogenesis and tumor growth in nude mice.** *BMC Complementary and Alternative Medicine* 2013, **13**(1):168.
69. Fernando KHN, Yang H-W, Jiang Y, Jeon Y-J, Ryu B: **Ishige okamurae Extract and Its Constituent Ishophloroglucin A Attenuated In Vitro and In Vivo High Glucose-Induced Angiogenesis.** 2019, **20**(22):5542.
70. Ko E-Y, Cho S-H, Kang K, Kim G, Lee J-H, Jeon Y-J, Kim D, Ahn G, Kim K-N: **Anti-inflammatory activity of hydrosols from Tetragonia tetragonoides in LPS-induced RAW 264.7 cells.** *EXCLI J* 2017, **16**:521-530.

71. Lamalice L, Le Boeuf F, Huot JJC: **Endothelial cell migration during angiogenesis.** 2007, **100**(6):782-794.
72. Ashton AW, Yokota R, John G, Zhao S, Suadicani SO, Spray DC, Ware JAJJoBC: **Inhibition of endothelial cell migration, intercellular communication, and vascular tube formation by thromboxane A2.** 1999, **274**(50):35562-35570.
73. DeCicco-Skinner KL, Henry GH, Cataisson C, Tabib T, Gwilliam JC, Watson NJ, Bullwinkle EM, Falkenburg L, O'Neill RC, Morin A *et al*: **Endothelial cell tube formation assay for the in vitro study of angiogenesis.** *J Vis Exp* 2014(91):e51312-e51312.
74. Li B, Lu F, Wei X, Zhao R: **Fucoidan: structure and bioactivity.** *Molecules* 2008, **13**(8):1671-1695.
75. Cunha L, Grenha A: **Sulfated Seaweed Polysaccharides as Multifunctional Materials in Drug Delivery Applications.** *Mar Drugs* 2016, **14**(3):42.
76. Wang Y, Xing M, Cao Q, Ji A, Liang H, Song S: **Biological Activities of Fucoidan and the Factors Mediating Its Therapeutic Effects: A Review of Recent Studies.** *Mar Drugs* 2019, **17**(3):183.
77. Fernando IPS, Sanjeeva KKA, Samarakoon KW, Lee WW, Kim H-S, Kang N, Ranasinghe P, Lee H-S, Jeon Y-J: **A fucoidan fraction purified from Chnoospora minima; a potential inhibitor of LPS-induced inflammatory responses.** *International Journal of Biological Macromolecules* 2017, **104**:1185-1193.
78. Kopplin G, Rokstad AM, Mérida H, Bulone V, Skjåk-Bræk G, Aachmann FL: **Structural Characterization of Fucoidan from Laminaria hyperborea: Assessment of Coagulation and Inflammatory Properties and Their Structure–Function Relationship.** *ACS Applied Bio Materials* 2018, **1**(6):1880-1892.
79. Houser J, Komarek J, Kostlanova N, Cioci G, Varrot A, Kerr SC, Lahmann M, Balloy V, Fahy JV, Chignard M *et al*: **A Soluble Fucose-Specific Lectin from Aspergillus fumigatus Conidia - Structure, Specificity and Possible Role in Fungal Pathogenicity.** *PLOS ONE* 2013, **8**(12):e83077.
80. Fernando IPS, Kim D, Nah J-W, Jeon Y-J: **Advances in functionalizing fucoidans and alginates (bio)polymers by structural modifications: A review.** *Chemical Engineering Journal* 2019, **355**:33-48.
81. Lee KM, Yang EC, Coyer JA, Zuccarello GC, Wang W-L, Choi CG, Boo SM: **Phylogeography of the seaweed Ishige okamurae (Phaeophyceae): evidence for glacial refugia in the northwest Pacific region.** *Marine Biology* 2012, **159**(5):1021-1028.
82. Zayed A, Dienemann C, Giese C, Krämer R, Ulber R: **An immobilized perylene diimide derivative for fucoidan purification from a crude brown algae extract.** *Process Biochemistry* 2018, **65**:233-238.
83. Bilan MI, Grachev AA, Ustuzhanina NE, Shashkov AS, Nifantiev NE, Usov AI: **A highly regular fraction of a fucoidan from the brown seaweed Fucus distichus L.** *Carbohydrate Research* 2004, **339**(3):511-517.
84. Fernando IPS, Sanjeeva KKA, Kim H-S, Kim S-Y, Lee S-H, Lee WW, Jeon Y-J: **Identification of sterols from the soft coral Dendronephthya gigantea and their anti-inflammatory potential.** *Environmental Toxicology and Pharmacology* 2017, **55**:37-43.
85. Sanjeeva KKA, Fernando IPS, Kim S-Y, Kim H-S, Ahn G, Jee Y, Jeon Y-J: **In vitro and in vivo anti-inflammatory activities of high molecular weight sulfated polysaccharide; containing fucose separated from Sargassum horneri: Short communication.** *International Journal of Biological Macromolecules* 2018, **107**:803-807.
86. Palanisamy S, Vinosha M, Manikandakrishnan M, Anjali R, Rajasekar P, Marudhupandi T, Manikandan R, Vaseeharan B, Prabhu NM: **Investigation of antioxidant and anticancer potential of fucoidan from Sargassum polycystum.** *International journal of biological macromolecules* 2018, **116**:151-161.

87. Monsur HA, Jaswir I, Simsek S, Amid A, Alam Z: **Chemical structure of sulfated polysaccharides from brown seaweed (*Turbinaria turbinata*)**. *International Journal of Food Properties* 2017, **20**(7):1457-1469.
88. Kang S-M, Kim K-N, Lee S-H, Ahn G, Cha S-H, Kim A-D, Yang X-D, Kang M-C, Jeon Y-J: **Anti-inflammatory activity of polysaccharide purified from AMG-assistant extract of *Ecklonia cava* in LPS-stimulated RAW 264.7 macrophages**. *Carbohydrate Polymers* 2011, **85**(1):80-85.
89. Agard M, Asakrah S, Morici L: **PGE2 suppression of innate immunity during mucosal bacterial infection**. 2013, **3**(45).
90. Kim M-S, Bae G-S, Park K-C, Koo BS, Kim B-J, Lee H-J, Seo S-W, Shin YK, Jung W-S, Cho J-H *et al*: **Myrrh inhibits LPS-induced inflammatory response and protects from cecal ligation and puncture-induced sepsis**. *Evid Based Complement Alternat Med* 2012, **2012**:278718-278718.
91. Kany S, Vollrath JT, Relja B: **Cytokines in Inflammatory Disease**. *Int J Mol Sci* 2019, **20**(23):6008.
92. Wojdasiewicz P, Poniatowski ŁA, Szukiewicz D: **The role of inflammatory and anti-inflammatory cytokines in the pathogenesis of osteoarthritis**. *Mediators Inflamm* 2014, **2014**:561459-561459.
93. Cianchi F, Perna F, Masini E: **iNOS/COX-2 Pathway Interaction: A Good Molecular Target for Cancer Treatment**. *Current Enzyme Inhibition* 2005, **1**(2):97-105.